UNIVERSITI TEKNOLOGI MALAYSIA

DECLARATION OF THESIS AND COPYRIGHT

Author's full name : ROSYIDA PERMATASARI

Date of birth : 27 SEPTEMBER 1966

Title : EXPERIMENTAL AND NUMERICAL STUDY OF FLUIDIZED BED COMBUSTION WITH AIR STAGING USING PALM SHELL

Academic Session : 2011/2012-1

I declare that this thesis is classified as :

☐	**CONFIDENTIAL**	(Contains confidential information under the Official Secret Act 1972)*
☐	**RESTRICTED**	(Contains restricted information as specified by the organization where research was done)*
☑	**OPEN ACCESS**	I agree that my thesis to be published as online open access (full text)

I acknowledged that Universiti Teknologi Malaysia reserves the right as follows:

1. The thesis is the property of Universiti Teknologi Malaysia.
2. The Library of Universiti Teknologi Malaysia has the right to make copies for the purpose of research only.
3. The Library has the right to make copies of the thesis for academic exchange.

Certified by :

Rosyida

SIGNATURE

S400687

Date : 17.4.2013

SIGNATURE OF SUPERVISOR

PROF. DR. MOHAMMAD NAZRI MOHD. JAAFAR

Date : 17.4.2013

NOTES : * If the thesis is CONFIDENTAL or RESTRICTED, please attach with the letter from the organization with period and reasons for confidentiality or restriction.

"We hereby declare that I have read this thesis and in our opinion this thesis is sufficient in terms of scope and quality for the award of the degree of Doctor of Philosophy (*Mechanical Engineering*)"

Signature : 

Name of Supervisor I : Prof. Dr. Mohammad Nazri Mohd. Jaafar

Date : 17.4.2018

Signature : 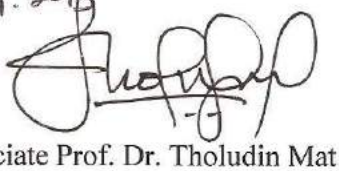

Name of Supervisor II : Associate Prof. Dr. Tholudin Mat Lazim

Date : 17.4.2013

BAHAGIAN A – Pengesahan Kerjasama*

Adalah disahkan bahawa projek penyelidikan tesis ini telah dilaksanakan melalui kerjasama antara _____ dengan _____

Disahkan oleh:

Tandatangan : ..... Tarikh : .....

Nama : .....

Jawatan : .....
(Cop rasmi)

* *Jika penyediaan tesis/projek melibatkan kerjasama.*

BAHAGIAN B – Untuk Kegunaan Pejabat Sekolah Pengajian Siswazah

Tesis ini telah diperiksa dan diakui oleh:

Nama dan Alamat Pemeriksa Luar : **Prof. Dr. Zainal Alimudin bin Zainal Alauddin**
School of Mechanical Engineering,
Engineering Campus,
Universiti Sains Malaysia,
Seri Ampangan,
14300 Nibong Tebal, Pulau Pinang

Nama dan Alamat Pemeriksa Dalam : **Prof. Dr. Mohd Rozainee bin Taib**
Fakulti Kejuruteraan Kimia,
UTM, Johor Bahru

Nama Penyelia lain (jika ada) : -

Disahkan oleh Timbalan Pendaftar di Sekolah Pengajian Siswazah:

Tandatangan : ---------- Tarikh : ----------

Nama : **ZAINUL RASHID BIN ABU BAKAR**

EXPERIMENTAL AND NUMERICAL STUDY OF FLUIDIZED BED COMBUSTION WITH AIR STAGING USING PALM SHELL

ROSYIDA PERMATASARI

A thesis submitted in fulfilment of the
requirements for the award of the degree of
Doctor of Philosophy (Mechanical Engineering)

Faculty of Mechanical Engineering
Universiti Teknologi Malaysia

APRIL 2013

I declare that this thesis entitled "*Experimental and Numerical Study of Fluidized Bed Combustion with Air Staging*" is the result of my own research except as cited in the references. The thesis has not been accepted for any degree and is not concurrently submitted in candidature of any other degree.

Signature : .....

Name : Rosyida Permatasari

Date : 17.4.2013

Dedicated to

My beloved parents:
Muhammad Rosyidin
Ida Zubaidah

My beloved parents in law:
Imamoeddin Noer Ganda Saputra
Rochanah

My lovely husband:
Syahrul Maulana

My lovely children:
Mutiara Nurul Faadhilah
Muhammad Azmi Taqiuddin
Muhammad Zaidan Ammar

My brother and sisters:
Luddy, Intan, Dewi and their families

ACKNOWLEDGEMENT

Alhamdulillah. I praise and glorify be only to **Allah SWT** the Almighty, the Most Beneficent, and the Most Merciful, whose blessings and guidance have helped me to be able to finish this thesis. In particular, I wish to express my sincere appreciation to my supervisors, Prof. Dr. Mohammad Nazri Mohd. Jaafar and Associate Prof. Dr. Tholudin Mat Lazim for encouragement, guidance, critics, advices, motivation, and friendship. Without their support and interest, this thesis would not have been the same as presented here.

I am also indebted to Trisakti University and Research Management Centre Universiti Teknologi Malaysia for their financial support during the term of this study. Many thanks to my colleague Mrs. Ernie Mat Tokit, Dr. Bambang Supriyo and his wife Mrs. Nurmayanti, Dr. Yehia Eldrainy, Mr. Wan Zaidi Wan Omar, Hanafi and also full thanks to Nazar, Sayuti, Kang Kin Hui, Fong, Sukri, Shaiful, Amin, and Shalini for their supports in my experimental works. Thanks to for providing Combustion and Aeronautics Laboratory for its facilities and its technicians: Mr. Basid, Mr. Rosli, Mr. Ibrahim, and Mr Johari. Jazakumullah khairan katsir to my sisters and my brothers in IKMI for their supporting and praying for me. Gratefully acknowledge to Department of Mechanical Engineering of Trisakti University for the opportunity to pursue Ph.D. program at UTM. This thesis will not be completed without their full encouragement and support as a solid team.

My sincere appreciation also extends to all my friends: Dr. Irma, Dr. Yani, Dr. Tuti, Rela, Budi, Ismail, Emilia, Amir and Mazuriah and the others who have provided assistance at various occasions. Their views and tips are useful indeed. Unfortunately, it is not possible to list all of them in this limited space. I am grateful to all my family members, especially my husband Syahrul Maulana, my mothers, my fathers, my children, my sisters and my brothers.

ABSTRACT

The objectives of this research are to study the characteristics of the gaseous emissions due to combustion of palm shell in an Atmospheric Bubbling Fluidized Bed Combustor (ABFBC) and to study the flow and mixing characteristics of granulation material in the ABFBC. In the first part of this work, experiments were conducted with staged air at 2 m of the combustor, using palm shell fuel (diameter, Ø = 3mm) with B Geldart silica sand (diameter, Ø = 300 – 425 µm) as the inert bed material. The sand was used to ensure sustained combustion of the fuel in ABFBC. The emissions due to the combustion were found to be very dependent on a number of operating conditions, namely, the combustion temperature, amount of staged and excess air, fuel feed rate and fuel properties. Gaseous emission concentrations of NO_x, CO, CO_2, and axial temperature distribution along the combustor height were measured. The experimental results show that air staging reduces NO_x and CO emission significantly as the proportion of secondary air (SA) is increased at 0% and 60% excess air (EA). The combustion efficiency increases with increasing SA for 60% EA at 20% and 40% SA. Increasing the fuel feed rates decreases the CO and NO_x concentrations and increases the combustion efficiency. In the second part of work, the fluidization behavior of a non-reactive gas-solid in the ABFBC was studied. Experiments were conducted using laser based Particle Imaged Velocimetry (PIV) with B Geldart silica sand (diameter, Ø = 300 – 425 µm) in 2 m high cylindrical combustion chamber. The PIV was used to determine the particle velocity distribution in the combustion chamber. The experiments established the distribution of the sand along the height of the combustion chamber. Consequently, 3D CFD simulations were conducted for both parts of the research using ANSYS FLUENT 13.0 software, of which their results were compared with the experimental counterpart. The comparison between the results of the developed CFD models and the experimental data showed very close agreement.

ABSTRAK

Objektif penyelidikan ini adalah untuk mengkaji ciri pelepasan gas disebabkan oleh pembakaran bahan api tempurung sawit dalam Sistem Pembakar Terbendalir Menggelembung Atmosfera (ABFBC) dan mengkaji ciri aliran serta pencampuran bahan granul dalam ABFBC. Dalam bahagian pertama kerja-kerja penyelidikan ini, eksperimen dijalankan dengan masukan udara tambahan pada ketinggian 2 m dari pembakar, menggunakan bahan api tempurung kelapa sawit (garis pusat, Ø = 3 mm) dengan pasir silica B Geldart (garis pusat, Ø = 300 - 425 μm) sebagai bahan lengai. Pasir telah digunakan untuk memastikan pembakaran bahan api dalam ABFBC yang berterusan. Pelepasan gas disebabkan oleh pembakaran didapati sangat bergantung kepada keadaan operasi, iaitu suhu pembakaran, jumlah udara terperingkat dan lebihan, kadar suapan bahan api dan sifat bahan api. Kepekatan pelepasan gas NO_x, CO, CO_2 dan taburan suhu sepanjang ketinggian pembakar diukur. Keputusan ujikaji menunjukkan bahawa pemeringkatan udara mengurangkan pelepasan NO_x dan CO dengan ketara apabila nisbah udara sekunder (SA) dinaikkan pada 0% dan 60% udara lebihan (EA). Kecekapan pembakaran meningkat dengan peningkatan SA untuk EA 60% pada 20% dan 40% SA. Meningkatkan kadar suapan bahan api mengurangkan kepekatan CO dan NO_x dan meningkatkan kecekapan pembakaran. Dalam bahagian kedua kerja penyelidikan, kelakuan pembendaliran suatu gas-pepejal tak-reaktif dalam ABFBC dikaji. Ujikaji telah dijalankan menggunakan sistem ukuran halaju imej zarah berasaskan laser (PIV) dengan pasir silica B Geldart (garis pusat, Ø = 300 – 425 μm) dalam kebuk pembakaran silinder setinggi 2 m. PIV digunakan untuk menentukan taburan halaju zarah dalam kebuk pembakaran. Ujikaji ini menghasilkan taburan pasir sepanjang ketinggian kebuk pembakaran. Simulasi 3D CFD telah dilaksanakan bagi kedua-dua bahagian penyelidikan menggunakan perisian ANSYS FLUENT 13.0, yang mana keputusannya telah dibandingkan dengan hasil ujikaji. Perbandingan antara keputusan model CFD yang dibangunkan dengan data ujikaji menunjukkan keserupaan yang sangat rapat.

TABLE OF CONTENTS

LIST OF TABLES

LIST OF FIGURES

LIST OF ABREVIATIONS

2D	-	Two Dimensional
3D	-	Three Dimensional
ABFB	-	Atmospheric Bubbling Fluidized Bed
ABFBC	-	Atmospheric Bubbling Fluidized Bed Combustor
ACFB	-	Atmospheric Circulating Fluidized Bed
AFBC	-	Atmospheric Fluidized Bed Combustor
AFR	-	Air Fuel Ratio
BFB	-	Bubbling Fluidized Bed
BM	-	Bed Material
C	-	Carbon
CaO	-	Calcium Oxide
CaSO4	-	Calcium Sulfate
CCD	-	Charged Couple Device
CFB	-	Circulating Fluidized Bed
CFD	-	Computational Fluid Dynamics
CH4	-	Methane
Cl	-	Chlorine
CO	-	Carbon Monoxide
CO2	-	Carbon Dioxide
COmax	-	Carbon Monoxide maximum
CPO	-	Crude Palm Oil
CxHy	-	the general *chemical* formula of a hydrocarbon
EA	-	Excess Air
EE	-	Eulerian-Eulerian
EFB	-	Empty Fruit Bunches
EIA	-	Energy Information Administration
EL	-	Eulerian-Lagrangian

EPA	-	Environmental Protection Agency
FBC	-	Fluidized Bed Combustion
FC	-	Fixed Carbon
Fe2O3	-	Ferric Oxide or Iron Oxide
FFB	-	Fibre Fruit Bunches
FG	-	Flue Gas
GHG	-	Green House Gas
H	-	Hydrogen
H2O	-	Hydrogen Oxide
HC	-	Hydro Carbon
HCl	-	Hydrogen Chloride
HHV	-	Higher Heating calorific Value
LDA	-	Laser Doppler Anemometry
LPG	-	Liquid Petroleum Gas
N	-	Nitrogen
N2O	-	Nitrous Oxide
NO	-	Nitrogen Monoxide
NO2	-	Nitrogen Dioxide
NO2	-	Nitrous Dioxide
NOx	-	Nitrogen Oxides
O	-	Oxygen
PA	-	Primary Air
PAH	-	Polycyclic Aromatic Hydrocarbons
PBFB	-	Pressurized Bubbling Fluidized Bed
PCFB	-	Pressurized Circulating Fluidized Bed
PDA	-	Phase Doppler Anemometry
PFBC	-	Pressurized Fluidized Bed Combustor
PIC	-	Products of Incomplete Combustion
PIV	-	Particle Image Velocimetry
PM	-	Particulate Matter
POME	-	Palm Oil Mill Effluent
PVC	-	Polyvinyl Chloride
RDF	-	Reused Derived Fuel

S	-	Sulphur
SA	-	Secondary Air
SO2	-	Sulfur Dioxide
SOx	-	Sulphur Oxide
TA	-	Tertiary Air
VM	-	Volatile Matter

LIST OF SYMBOLS

d_p	-	Particle mean size
$\dot{m}$	-	Mass flow rate
$\dot{m}_{air}$	-	Air mass flow rate
ϕ	-	Equivalence ratio
Q	-	Calorific value
Q_{gr}	-	Gross calorific value
Q_{net}	-	Net calorific value
Re	-	Reynolds number
Re_{mf}	-	Reynolds number of particle at minimum fluidization
T	-	Temperature
T_f	-	Flue temperature
T_i	-	Inlet temperature
T_{net}	-	Net temperature
U	-	Velocity
U_{mb}	-	Minimum bubbling velocity
U_{mf}	-	Superficial velocity at minimum fluidization
η	-	Efficiency
η_{gr}	-	Gross efficiency
η_{net}	-	Net efficiency
ρ	-	Density
ρ_{air}	-	Air density
ρ_f	-	Fluid density
ρ_p	-	Particle density
ρ_s	-	Solid density
ρ_g	-	Gas density

Φ	-	Sphericity of sand
s	-	Solid phase
α	-	volume fraction
v	-	Real velocity
g	-	Gravitational acceleration
τ_s	-	Solid tensor
T_g	-	Gas tensor

LIST OF APPENDICES

CHAPTER 1

INTRODUCTION

1.1 Research Background

Air pollution occurs due to the presence of large quantities of undesirable materials in atmosphere causing harmful effects for human and environment. The undesirable materials may damage human health, human property, vegetation, global environment and create aesthetic insults in the forms of brown or hazy air or unpleasant smell. Most of the harmful materials enter the atmosphere from sources currently beyond human control.

Energy represents the ability to do work. About fifty years ago, energy demands are relatively low hence its price was very cheap. But now engineering and technology have recognized that the earth is a finite eco-sphere having limited terrestrial resources and a delicately balanced environment. Nowadays, energy sources may be divided into two categories, i.e.:

i. Exhaustible sources, e.g. fossil fuels such as coal, crude oil, natural gas, etc. But atomic or nuclear energy may be also considered as exhaustible sources since the uranium and thorium deposits could be completely consumed.

ii. Inexhaustible or continuous sources, e.g. hydraulic, wind, solar, oceans, waste and synthetic fuels, etc [1-3].

Fossil fuels continue to dominate energy usage of the world even though there is also significant expansion in the utilization of renewable energy sources of

energy and electricity generation. In terms of energy uses and consumptions, the most striking feature is dramatically increased in the energy demand of developing countries. The developments in energy consumption patterns of the world have resulted in many environmental, economic, and institutional problems such as: depletion of fossil fuel resources, uncertainties of energy prices and availability, significant climate changes due to greenhouse gas emissions from energy generation, increase in local and regional pollution due to acid rains, ozone layer depletion, etc.

To meet the growing needs of high efficiency, sustainable and environmentally friendly energy, the development and implementation of newer and cleaner energy conversion system are essential [4-8]. The major sources of air pollutant like CO, NO_x, SO_2 and particulate matter (PM) are from waste of combustion process in industry, even though tremendous efforts have been developed to reduce those emissions. The increased concentration of greenhouse gases in the atmosphere, in particular CO_2, is changing the Earth's climate. According to the Kyoto protocol, where the international community agreed on binding emission targets, developed countries committed to reduce their greenhouse gas emissions. Increasing use of biomass in energy systems is an important strategy to reduce the pollutant emissions concentration [8-13].

Some studies implied that biomass energy appears to be the most important renewable energy resource in terms of technical and economic feasibility during the next few decades [2, 12-41]. Biomass which is one of the renewable energy sources is defined as the biodegradable fraction of products, waste and residues from agriculture including vegetable and animal substances, forestry and related industries [40, 42]. Biomass residues from palm oil are very potential resources because many palm oil plantation areas are found in Southeast Asia countries, such as Malaysia, Thailand, and Indonesia [8, 25, 31, 34, 36, 43-48].

The fluidized bed technology is one of the technologies that have been identified for future energy and electricity generation, and has been used successfully in numerous industrial processes. The fluidized bed technology was originally used in the chemical industry, metallurgy and other industries, but not in power

engineering. There are two essential factors why the fluidized bed technology is applied in power engineering. Firstly, the fluidized bed efficiently burns low grade fuels, including mining industry enrichment wastes, chemical industry and household wastes and other combustible waste. Secondly, it decreases the harmful emissions of the burnt fuel without using an expensive cleaning equipment of flue gases. Fluidized Bed Combustion (FBC) has emerged as an environmentally attractive method for burning coal, biomass and wastes [10, 49-71]. In addition, fluidized bed combustion uses a continuous stream of air to create turbulence in a mixed bed of fuel, inert material and fuel particles. It occurs at temperature typically between 850 and 900^{o}C. Constant mixing of particles encourages rapid heat transfer and complete combustion [62].

An air staging technique is applied in FBC to reduce the resulted emission of combustion, especially for NO emission in fluidized bed coal combustor. The extended of NO reduction for staged operation increases with the proportion of secondary air injection and with bed temperature [53]. The emissions of NO_2 of coal combustion in FBCs are very dependent on a number of operating conditions (temperature, sorbent addition, excess oxygen, etc.), fuel characteristics and many homogeneous and heterogeneous reactions [72-73].

Some researchers have done the experiment and modeling works about the emission generated by the combustor. Mathematical modeling of FBC can optimize and predict the performance of the combustors and save a tremendous amount of operating costs incurred from parametric studies. However, biomass combustion modeling and its emissions in a FBC, especially for palm oil wastes, received much less attention and therefore much less understood. Studying about modeling of NO_x, SO_x and CO_2 emission of palm shell combustion in FBC is still less. However, in recent years, enormous mathematical modeling in FBC applications using several resources have been researched extensively, such as straw [74-75], coal [76-77], rice husk [78-79], Greek lignite [80], olive cake, peat, and wood [79]. Also, a stochastic particle system as a model for transport of particulate matter in the air and ash formation model during pulverized coal combustion was studied [81].

The flow and mixing of granular materials is also important in a wide range of industrial, agricultural, and geophysical situations. Granular flows exhibit a wide range of phenomena including convection, particle size segregation, heaping, waves, fluidization, and pattern formation. The fluidization attempts to overcome the problems in handling granular solids and to improve the heat transfer properties.

Fluidized beds are common and important reactors in process engineering because of good mass and heat transfer rate between fluid and particles, and between particles and sidewall. It is well known that there are non-uniform flow structures such as bubbles and slugs in fluidization. Large bubbles and slugs are undesirable for efficient operations, because they reduce the contact efficiency.

A new technique has been introduced for the measurement of average particle displacements in granular flows using laser based in Particle Image Velocimetry (PIV). The illumination uses a strobe, and then the resulted images are recorded and analyzed using PIV techniques [82-84].

There are some difficulties inherent in model fluidized beds i.e.: multiphase system, dynamics which are very dependent on operating conditions, particle gas interactions within beds which are not fully understood, difficulty in selecting a suitable measure to describe bed, difficulty in interpreting data from real beds, problems in scaling experimental results to real systems [85]. One of the current solutions is Computational Fluid Dynamics (CFD) approach. The CFD modeling is well known and widely used in major research projects [86-88].

1.1.1 History of Fluidized Bed Combustion (FBC)

Combustion and its control are essential to our daily life needs. Almost all sources of energy are resulted from combustion sources. Heat for our room or home comes directly from combustion (either a gas or oil fired furnace or boiler), or

indirectly through electricity that was generated by burning a fossil fuel. Combustion or burning is a complex sequence of exothermic chemical reactions between a fuel and an oxidant accompanied by the production of heat or both heat and light in the form of either a glow or flames.

Combustion of solids involves the simultaneous processes of heat and mass transport, progressive pyrolysis, gasification, ignition, and burning, with no intermediate steps and with unsteady, sometimes turbulent, fluid flow. Normally, combustion employs an excess of oxidizer to ensure maximum fuel conversion, but it can also occur under fuel-rich conditions. Products of combustion processes include heat, oxidized species (e.g. carbon dioxide (CO_2), water (H_2O)), products of incomplete combustion and other reaction products (mostly as pollutants), and ash. Other processes, such as supercritical water oxidation and electrochemical oxidation can produce similar products at lower temperatures but higher pressures.

'Getting rid of waste' was the ultimate goal when the FBC technology was introduced. FBC suddenly became of interest at the end of the 1970s as a result of the efforts to find energy resource alternatives to replace fossil-fuel based oil due to the increase in oil price. Also, FBC becomes an environmentally friendly technology because of its promising ability for in-bed desulphurization. This goal evolves over time to 'clean energy for the future'.

The technology becomes competitive with conventional coal combustion technologies, and in some aspects shows significant advantages over conventional technology. Moreover, it is the only coal combustion technology originating from the beginning of the first world energy crisis that is actually available in the commercial market as an economic, efficient, and ecologically acceptable technology which is fully competitive with conventional oil and gas burning technologies.

Since its introduction in the 1970s the technology has gained acceptance in various industrial applications, such as reactors, heat exchanger, drying operations, coating (example: metals with polymer), solidification / granulation, etc. This

technology has ability to burn low-grade fuels with low calorific value, high ash content and high moisture content.

1.1.2 Basic Principles of Fluidized Bed Combustion

FBC systems use a heated bed of sand-like material suspended (fluidized) within a rising column of air to burn many types and classes of fuel. This technique results in a vast improvement in combustion efficiency of high moisture content fuels, and is adaptable to a variety of waste type fuels. The scrubbing action of the bed material on the fuel particle enhances the combustion process by stripping away the carbon dioxide and char layers that normally form around the fuel particle. This allows oxygen to reach the combustible material much more readily and increases the rate and efficiency of the combustion process. The main components of a Atmospheric Bubbling Fluidized Bed Combustor (ABFBC) are air distributor, bed and freeboard as shown in Figure 1.1. The freeboard is for disengaging the particles that blow up above the bed.

FBC uses a continuous stream of air to create turbulence in a mixed bed of fuel, inert material and coarse fuel ash particles. It occurs at temperatures typically between 850 and 900°C. Constant mixing of particles encourages rapid heat transfer and complete combustion.

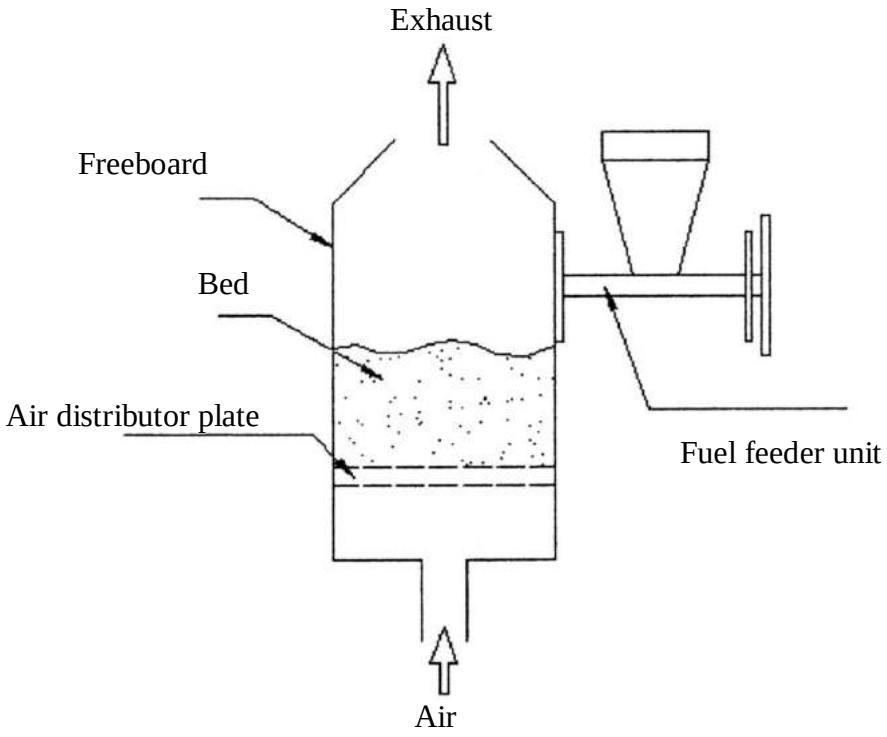

Figure 1.1 Schematic diagram of ABFBC [89]

1.2 Problem Statement

Biomass waste is a promising fuel because of its abundance and cheap source; however stringent emission regulations require lower emissions from the combustion of this biomass. In addition, burning of solid fuel is so problematic such that complete combustion is difficult to attain.

In order to reduce emissions from biomass combustion, many methods were applied, such as recirculation exhaust gas, pre-heating, swirling air and fuel staging fluidized bed combustor. But, those methods are mostly complicated and costly to implement. Thus this research introduced a method based on air staging with variable ratio of secondary to primary air for reducing the emissions.

1.3 Research Objectives and Scopes of Work

The main objective of this research is to lower the emission level of palm shell combustion in ABFBC using air-staging method. To achieve this objective, the following sub-objectives are as follow:

i. Design and fabricate an air staging system, for the ABFBC capable of varying the air mass flow ratios to obtain optimum mass flow ratio for lowest emission.
ii. Construct a numerical model able to predict the flow aerodynamics and the combustion performance within the ABFBC.

Meanwhile the scopes of work in the research are as follows:

i. Utilize an available CFD software package (ANSYS FLUENT 13.0) for simulation
ii. Apply Eulerian Multiphase Model for two phases flow simulation.
iii. Utilize PIV as laser based measurement to measure velocity magnitude of bed material (B Geldart silica sand) granulation, for cold flow experiment.
iv. Apply staged air method to reduce emission in the ABFBC using palm shell.

1.4 Contributions of the Research

This research has contributed to the field of combustion engineering through:

i. Validated 3D model of solid-gas multiphase flow in ABFBC.
ii. Validated 3D model of palm shell combustion in ABFBC.
iii. Experimental test rigs for the multiphase cold flow and for palm shell combustion in ABFBC.

Since the researches in this field are scarce, these contributions have increased the knowledge in the area of the combustion of palm shell.

1.5 Thesis Overview

The background theories and concepts related to the present resesarch works are discussed in Chapter 2. This includes the ABFBC characteristics, fluidization and the numerical modeling of the ABFBC. In addition, it discusses about the palm shell fuel and the other biomass.

Chapter 3 describes the experimental and numerical methodology used in the research. The chapter starts by cold flow study and then hot flow (combustion) study.

The experimental and the numerical results of cold flow are discussed in Chapter 4. The numerical models were then validated by previous experimental work.

The experimental and the numerical results of hot flow (combustion) are discussed in Chapter 5. The numerical models were then validated by previous experimental work.

Finally in Chapter 6, proposed summarized the general conclusions and recommendations for further work.

CHAPTER 2

LITERATURE REVIEW

There are combustion technologies available for biomass combustion such as fixed bed combustion, fluidized bed combustion (FBC) and pulverized bed combustion. FBC burns fuel with low quality, high ash and low calorific values. The other two combustions are limited and techno-economically incapable of meeting the challenge from the nature of biomass fuel.

FBC technology converts alternative solid fuels to energy and the possibility to achieve an efficient and clean operation. FBC of renewable solid fuels is becoming attractive alternative as an impact of the increasing price and depletion of fossil fuels, the presence of high quantities of wastes to be disposed of and global warming issues. By alternative fuels, some researches indicate a wide range of non-fossil solid materials, ranging from biomass and peat to municipal, agricultural and industrial wastes burned alone or in combination with fossil fuels. A development which makes FBC an attractive technology for burning solid fuel is its fuel flexibility and high efficiency [90].

During the past three decades, FBC burnt all types of coals, coal wastes and a wide variety of other fuels, either separately or together with coal [91-94]. Nowadays, the solid fuel has a substituted potential to improve the environmental impact of coal utilization [40].

The background theories and concepts related to the present research works are discussed in this chapter. This includes the ABFBC characteristics, fluidization

and the numerical modeling of the ABFBC. In addition, it discusses about the palm shell fuel and the other biomass.

2.1. Atmospheric Bubbling Fluidized Bed Combustor (ABFBC)

Fluidized bed combustion has significant advantages over conventional combustion systems in terms of compact boiler design, fuel flexibility, higher combustion efficiency and reduction of harmful gas emissions pollutants such as SO_x and NO_x. Fuel burnt in the boiler including coal and biomass. Fluidized bed boiler has a wide capacity range of 0.5T/h to more than 100T/hr [32].

Fluidized bed combustion systems fit into essentially three major groups, bubbling fluidized bed (BFB), circulating fluidized bed (CFB) and a variant of BFB and CFB, namely atmospheric systems (AFB) and pressurized systems (PFB), as shown in Figures 2.1 and 2.2. In BFB, most of the fluidizing bed material remains in the bottom of the furnace, whereas in CFB, most of the fluidizing bed material is carried upwards with the flue gas and separated in a hot cyclone, or U-beam separator, which then finally fed back into the combustion chamber.

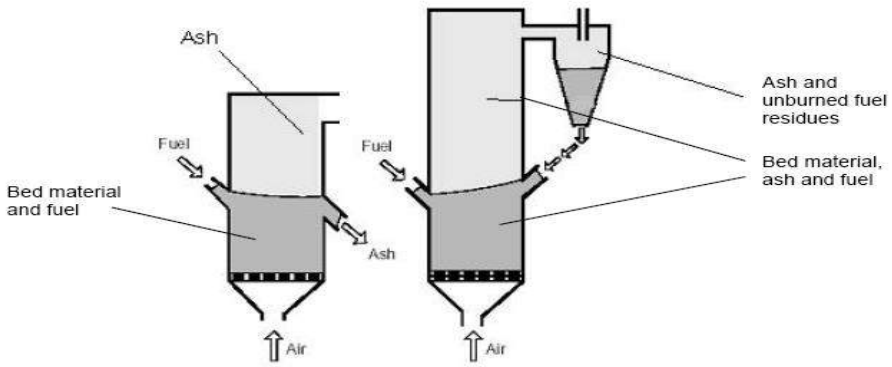

Figure 2.1 Bubbling fluidized bed (BFB) (left) and circulating fluidized bed (CFB) (right) [95]

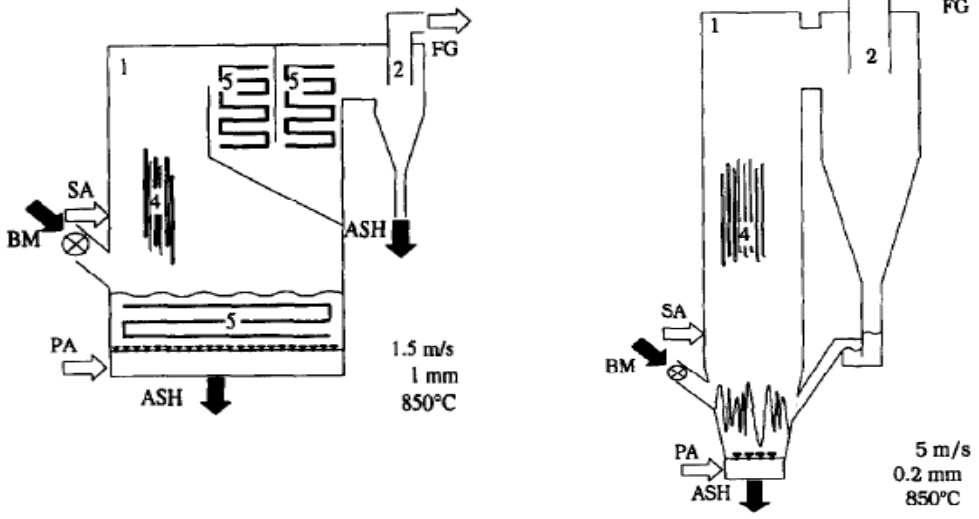

(a) Atmospheric bubbling FB (ABFB) (b)Atmospheric circulating FB (ACFB)

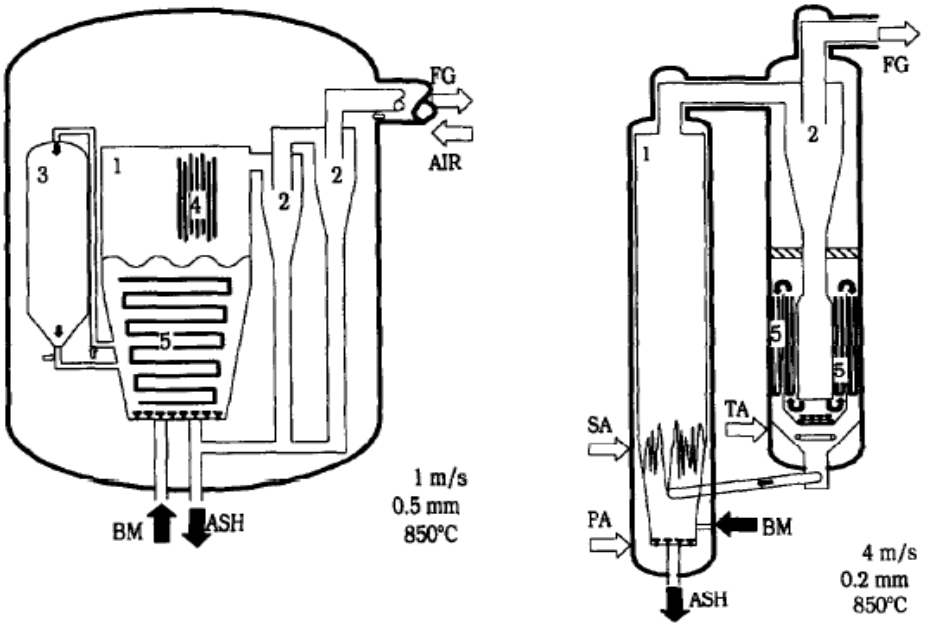

(c) Pressurized bubbling FB (PBFB) (d) Pressurized circulating FB (PCFB)

1. Combustion chamber; 2. Cyclone; 3. Bed ash vessels; 4. Membrane-tube walls; 5. Heat exchanger tube bundles; BM (Bed Material); PA (Primary Air); SA (Secondary Air); TA (Tertiary Air); FG (Flue Gas)

Figure 2.2 Principal designs of fluidized bed combustor [95]

There are many advantages of FBC boilers [32]. Some of them are as follows: high efficiency, reduction in boiler size, fuel flexibility, ability to burn low-grade fuel, ability to burn fines, etc.

2.1.1 The Mechanism of a ABFBC

ABFBC is a method of burning particulate fuel in which the fuel is fed continuously into a bed of reactive or inert particles suspended by an upward flow of flooding gas during the combustion process. In fact, the flooding gas is the air needed for combustion.

A fluidized bed consists of a cylindrical vessel with a hole in the bottom plate filled with the suspended hot material, inert and granular (usually silica sand or dolomite). The result is a turbulent mixing of gas and solids. Scrubbing action on the bed material particles bubbling liquid fuels improves the combustion process by removing carbon dioxide and char layers that originally come from around the fuel particles. This allows oxygen to reach the combustible material more easily, providing more effective chemical reactions hence increasing the rate and efficiency of the combustion process. Bed material provides high thermal inertia and stabilizes the combustion process.

Operation of FBC system begins by supplying air into the combustion chamber from the bottom to float the bed material. The required air is provided by either a blower or compressor. At the same time, the bed material is heated based on either direct heating method using flames or heating coils or indirect heating method using hot fluidizing air or flame tube.

As the heating progresses, the temperature of the combustion chamber increases continuously until reaching a value slightly above the operating temperature and a small amount of fuel is still continuously put into the combustion chamber. The magnitude of the temperature overshoot is based on the type of fuel

and combustion chamber used. Typically, this magnitude is obtained by experience rather than theoretical analysis. As fuel in the chamber, the temperature will drop due to the heat absorbed by the fuel. Meanwhile, the fuel temperature rises, combustion of the fuel will begin when the temperature reaches the ignition point, thereby releasing the heat into the combustion chamber. The combustion chamber temperature rises until it reaches the operating temperature.

Because the temperature is stable with only small fluctuations in the magnitude, the fuel feed rate can be increased. In addition, stable the temperature difference can be observed. This procedure is repeated until the temperature reaches its optimum value which is achieved when the fuel feed rates have been achieved. After that, pre-heating system can be turned off. Combustion chamber temperature must remain stable when the fuel feed rates have been achieved. This is because the bed material serves as a heat storage container, but rather continually absorbs heat from the burning fuel and also releases heat to fire the unburned fuel. Combustion processes not only occur in the combustion chamber, but also in the freeboard when travelling with the flue gas. In the bed, the particles in a fluid state is heated to the ignition point of fuel and fuel is injected continuously into the bed hence the fuel will burn rapidly and bed reaches a uniform temperature.

The combustion occurs at 800°C to 950°C. In this temperature, the ash fusion temperature, ash melting and associated problems can be avoided. The lower combustion temperature is reached due to the high heat transfer coefficient resulted from rapid mixing in a fluidized bed and effective extraction of heat from the bed through in-bed heat transfer tubes and walls of the bed. The gas velocity is the minimum fluidization velocity and particle velocity of entertainment. This is to ensure stable operation of the bed and to avoid entertainment particles in the gas stream.

Heat generated by the combustion process is extracted by a heat exchanger in the combustion chamber and in the freeboard or even both in the chamber and bed. Exhaust gas directed into the flue gas system is cleaned from hazardous particles and harmful gases before being released into the atmosphere. It is possible that some

unburned or semi-burned fuel still left in the flue gas. The waste of fuel is trapped by the mechanism in the gas cleaning system and then recycled into the combustion chamber hence significantly reducing the fuel waste. Finally, ash is stored in containers pending to be discharged.

2.1.2 Biomass Combustion in ABFBC

Conventional energy sources based on oil, coal, and natural gas proved very effective driver of economic progress, but at the same time damaging the environment and human health. In addition, they tend to cycle in nature, due to the effects of oligopoly in the production and distribution. Fossil fuels-based on energy sources faced increasing pressure in some areas of the environment, for example, the most serious challenges facing the future use of coal to the Kyoto Protocol greenhouse gas (GHG) emissions reduction target. Therefore, efforts to maintain the level of CO_2 in the atmosphere below 550ppm may not even be based on the fundamentals of oil and coal-powered global economy, or limiting the absorption of carbon radicals. The potential of renewable energy sources is very large as they can meet many times bigger than the world energy demand. Renewable energy sources like biomass, wind, solar, hydroelectric, and geothermal can provide sustainable energy services, based on the routine use of available original resources [12-1].

Renewable energy sources currently supply somewhere between 14% of world energy needs, shown in Figure 2.3 [93]. Supply is dominated by 9.6% traditional biomass, mostly wood fuel used for cooking and heating, especially in developing countries in Africa, Asia and Latin America. A major contribution was also obtained from the use of water power, with nearly 22% of global electricity supply provided by these sources. New renewable energy sources (solar energy, wind energy, modern bio-energy, geothermal energy and small hydro) currently contribute about 2.2%. A number of studies have investigated the potential scenario of the renewable contribution to global energy supply. They showed that in 10 the

second half of the 21st century, their contribution might range from the current figure which is almost 20% to more than 50% with the right policies in place [93].

Based on the incentives that offer biomass, governments in various countries also do more serious for the energy without significant environmental impact. In Malaysia, a report in 2005 of the Malaysia Energy Centre showed that 60 projects using various types of renewable energy has been approved. Among all renewable sources, especially biomass energy from empty fruit bunches seems to be the most promising, since Malaysia is the largest producer of palm oil in the world. Under the policy of India, biomass electricity access to reach 35GW in 2035 (9% power India) as compared to 10GW in 2010. And also the U.S. Energy Information Administration (EIA) estimates of biomass consumption for electricity generation will increase significantly from 60 billion kWh in 2008 to 188 billion kWh in 2020, while 165 billion kWh is derived from wood and other biomass [32].

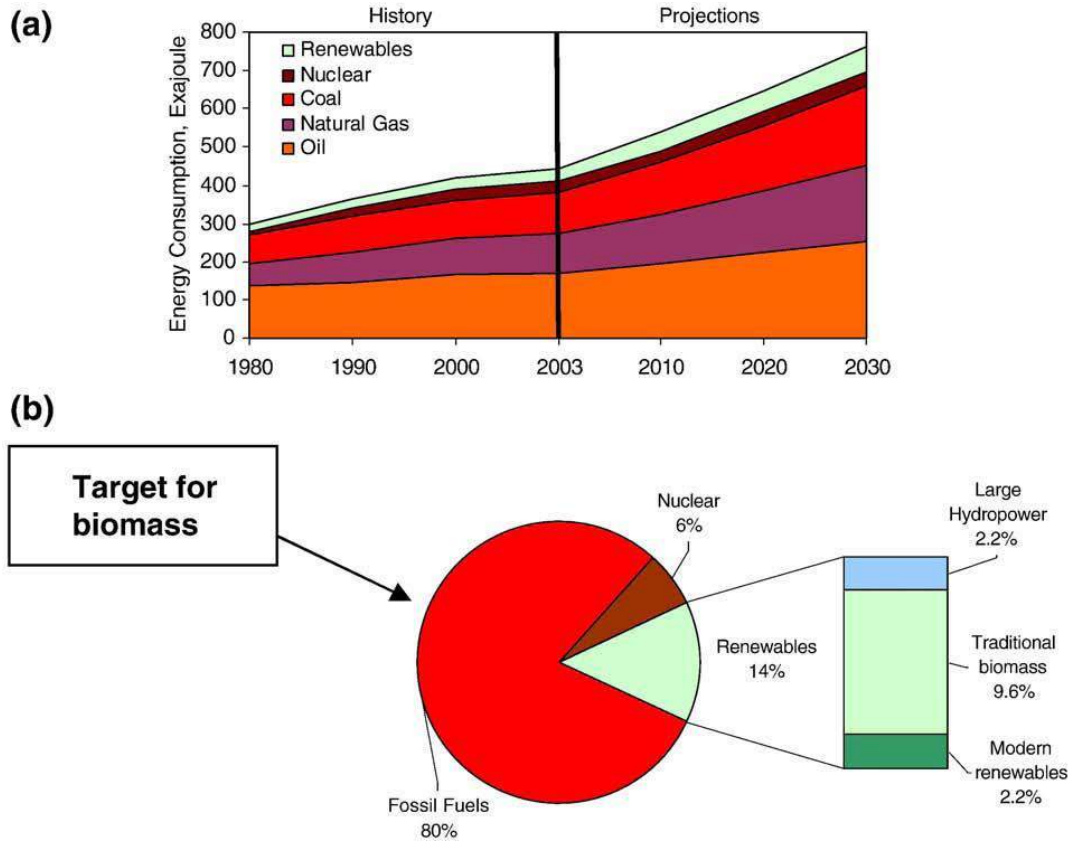

Figure 2.3 a. World marketed energy consumption, b. Different fuels contribution to total world energy consumption 1998 [93]

Biomass absorbs carbon dioxide during growth, and emits it during combustion. Utilization of biomass as fuel for power production offers the advantage of a renewable and CO_2-neutral fuel. Some estimates about contribution of biomass for future energy supply have been made, especially in the next 30-50 years. In 2010, annual energy use of biomass currently represents approximately 8-14% of world final energy consumption as listed in Table 2.1.

Table 2.1 : Annual Global Energy Consumption Gtoe, 2010 [96]

Fossil Fuels	10.45
Oil	4.03
Coal	3.56
Natural Gas	2.86
Nuclear	0.63
Renewables	0.94
Hydro	0.78
Wind, commercial biomass, solar	0.16
Estimated biomass (traditional)	1 - 2
Total global energy consumption	12.00 Gtoe commercial energy, or 13.0 – 14.0 Gtoe including all biomass

There are some advantages and disadvantages using biomass as fuel, as described in Table 2.2.

Table 2.2 : Major Advantages and Disadvantages of Biomass Fuel [97]

Advantages	Disadvantages
Renewable energy source for natural biomass	Incomplete renewable energy resource for biomass fuel with respect to the complete life cycle assessment
CO2 neutral conversion and climate change benefits	Miss of accepted terminology, classification systems and standards worldwide
Commonly low contents of ash, C, S, N, and trace elements	Insufficient knowledge and variability of composition, properties and quality
Normally high concentrations of volatile matter, Ca, H, Mg, O, and P	Commonly high contents of moisture, Cl, K, Na, Mn, and some trace elements
Great reactivity during conversion	Low energy density

Mitigation of hazardous emissions (CH_4, CO_2, NO_x, SO_x, trace elements) and wastes separated	Potential competition with food and feed production
Capture of some hazardous components by ash during combustion	Possible soil damage and loss of biodiversity
Huge availability and relatively cheap resource	Odor, potential emission and leaching of hazardous components during disposal
Diversification of fuel supply and energy security	Possible hazardous emissions during heat treatment
Rural revitalization with creation of new jobs	Potential technological problems during heat treatment
Potential use of oceans and low-quality soils, and restoration of degraded lands	Regional availability
Reduction of biomass-containing wastes	Great collection, transportation, storage and pre-treatment costs
Cheap resource for production of sorbents, fertilizers, liming and neutralizing agents, building materials, and for some synthesis or recovery of certain elements and compounds	Unclear utilization of waste products

2.1.2.1 Biomass Fuel Properties

Fuel properties for combustion analysis of biomass can be grouped according to physical, chemical, thermal, and mineral properties [98]. Physical properties such as density, porosity and internal surface area associated with biomass species as bulk density, particle size, shape and distribution of fuel associated with the preparation method.

Chemical properties for combustion are the proximate and ultimate analysis, calorific value and ash fusion point. Proximate analysis includes fixed carbon (char), moisture and ash content in the fuel while the ultimate analysis is the %age of the elements C, S, H, N, Cl, and O. Biomass values vary within wide ranges. The chemical composition of biomass is simpler than solid fossil fuels. However, semi-biomass system is quite complicated as a result of incorporation of various non-biomass materials for biomass treatment. Composition of biomass was significantly different from the coal. Biomass generally contains less carbon, more oxygen, more

potassium, less aluminum and iron, and has a lower caloric value and higher moisture content compared to coal. Variation among biomass composition is also found to be larger than coal [97]. The range of moisture content of biomass can vary from 10–70%. The content of water in fuel influences the combustion and the volume product of flue gas per energy unit. The calorific value of the fuel decreases with increasing moisture content [99].

Biomass materials can be classified into groups based on general assessment of their sources. The resulting main groups, shown in Table 2.3, namely (i) wood: pine chips, energy crops, and willow, (ii) herbaceous: two energy crops list: miscanthus and switch grass, (iii) agricultural residues: wheat straw, rice husks, palm kernel expeller, baggasse (sugarcane residue), olive residue or olive cake (waste from olive oil mill). Animal waste such as cow dung comes from another category even though it is not entirely biomass. Data for lignin and cellulose are given in Table 2.3 for comparison.

Ash is the inorganic un-combustible part of fuel left after complete combustion, which contains the bulk of the mineral fraction of the original biomass. Inorganic material in biomass categorized into two fractions, one of which is inherent in the fuel and the other is added to the fuel through some step of processing.

Figure 2.4 shows a wood combustion process. When the wood starts to be heated, constituents begin to hydrolyze, oxidize, dehydrate, and pyrolyse with increasing temperature forming combustible volatiles, tarry substances and highly reactive carbon char. At a temperature of ignition of volatile materials and tarry substances, an exothermic reaction known as combustion begins. Resin compounds and decomposition products of cellulose, hemicellulose, and lignin, together with water vapor are released, and then undergo either a partial to complete combustion in the fire zone. During the burning process, considerable heat is produced and the charring process to deploy an additional release of decomposition products of wood volatile.

Table 2.3 : Typical proximate (%) and ultimate analyses (%) and higher heating calorific values (HHV) for a range of biomass types [96]

Fuel	Proximate analysis				Ultimate analysis				S	Cl	HHV
(Oven dried)	Moisture	VM	FC	Ash	C	H	O	N			MJ/kg (dry)
Wood pine chips	4.00	81.3	14.6	0.10	52.0	6.2	41.59	0.12	0.08	0.01	20.23
Willow, SRC	6.96	75.7	16.31	1.03	51.62	5.54	42.42	0.38	0.03	0.01	18.68
Miscanthus giganteus	142.0	70.40	14.10	1.30	49.10	6.40	43.98	0.26	0.13	0.13	19.88
Switch Grass	7.17	73.05	15.16	4.62	49.40	5.70	44.25	0.45	0.10	0.10	17.82
Straw-wheat straw	7.78	68.83	17.09	6.30	49.23	5.78	43.99	0.64	0.10	0.26	17.42
Palm PKE	7.60	72.12	16.18	4.10	51.12	7.37	38.21	2.80	0.30	0.20	20.00
Sugar cane bagasse	10.4	76.70	14.70	2.20	49.90	6.00	43.15	0.40	0.04	0.51	19.47
Olive residue	6.40	65.13	19.27	9.20	54.42	6.82	37.29	1.40	0.05	0.04	19.67
Cow dung	13.90	60.50	11.90	13.7	54.00	6.40	36.70	0.83	0.03	1.00	17.36
Lignin	9.00	73.50	1.50	16.0	72.00	6.60	21.34	0.00	0.00	0.00	25.00
Cellulose	4.10	94.00	0.20	1.70	44.40	6.17	49.30	0.00	0.00	0.00	18.60

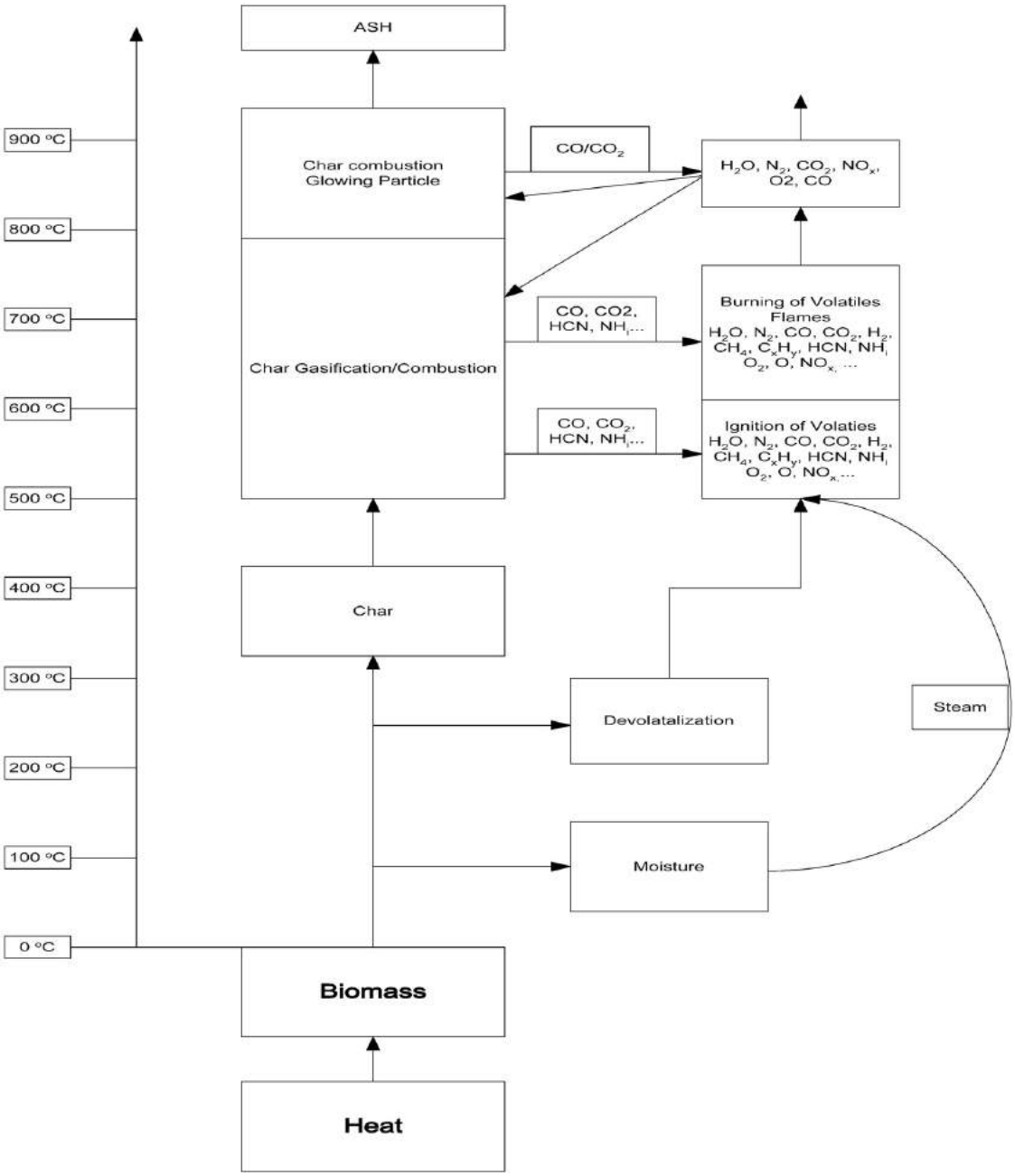

Figure 2.4 Schematic description of the combustion process of a wood chip [93]

2.1.2.2 Biomass Classification

Biomass fuels can be divided into three main segments: wood, waste, and alcohol fuels, as shown in Figure 2.5. The categorization of the fuel-related challenges in the design of the installation is shown in Figure 2.6. On the right, the

fuel used with standard boiler design, moved to the left of the characteristics of the fuel becomes more challenging for multi-fuel boiler design and operation. Experience with firing difficult fuels started early in the development of FBC.

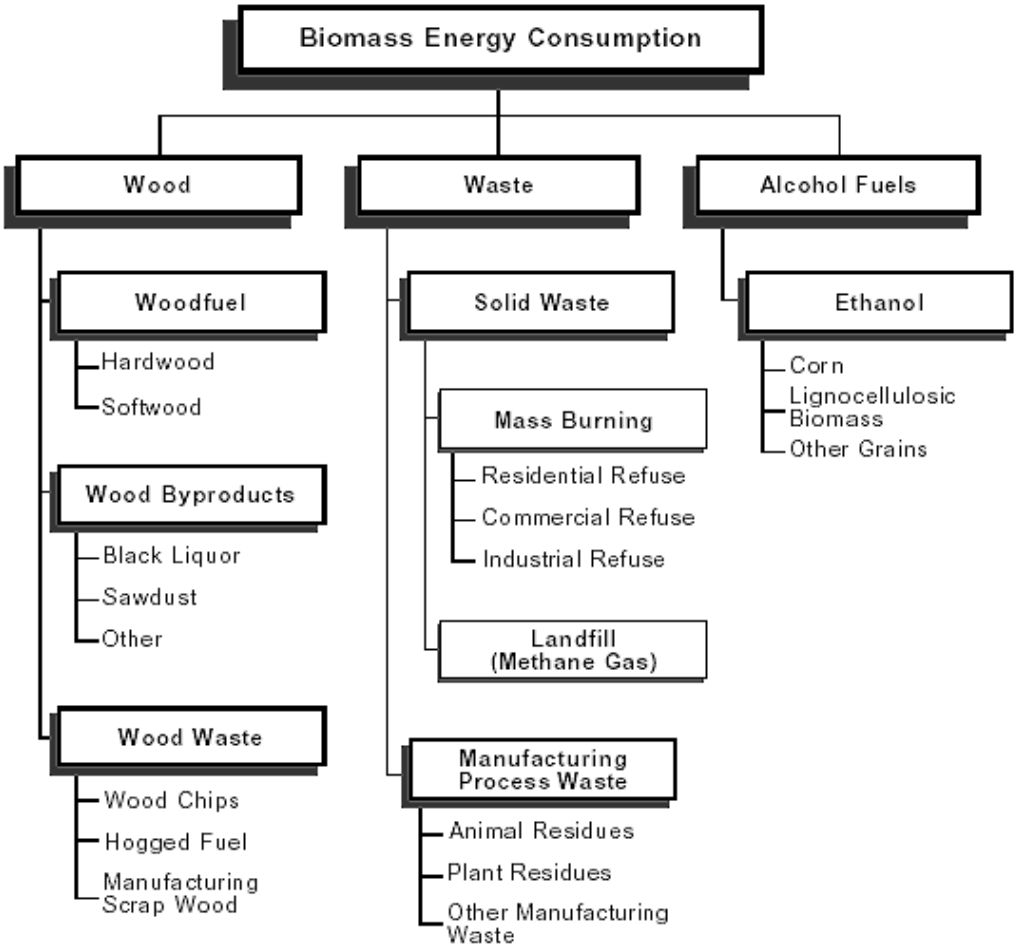

Figure 2.5 Biomass Energy Resource Hierarchy [100]

Therefore, before feeding fuel into the combustion chamber requires some preparation. Several methods are available to process the fuel between storage and combustion. The main function of this method is the size of the fuel, fuel drying and separation of non-combustible from the fuels. The two last-mentioned functions are generally required when firing waste as fuel and biomass [1]. Modifications in the preparation of fuel and feeding were necessary to maintain the combustion process, and further emission control and efficiency, at the desired operating conditions.

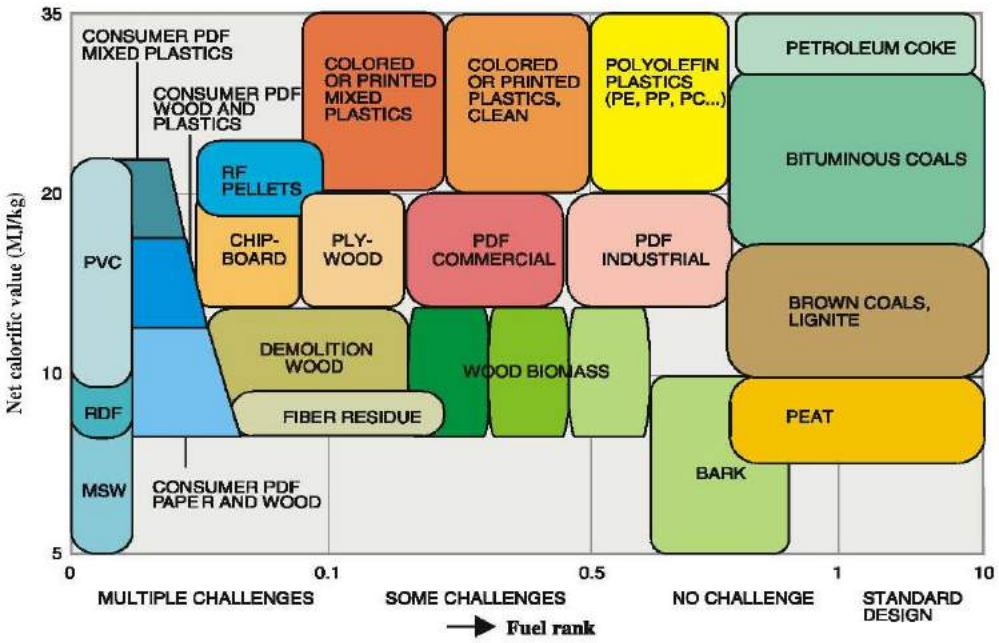

Figure 2.6 Range of Applied Fuel for FBC [90]

2.1.3 Staged Air Combustion

Air staging is one of the emission control techniques and it is quite familiar nowadays. Air staging is a method to be studied in an effort to reduce the combustion emissions; these are NO_X, CO, unburned hydrocarbon and smoke. Supplying additional air into the combustor will increase the air fuel ratio (AFR) in the combustor, which will reduce the emissions from the combustion process [101-104].

Air staging involves introducing a portion of the total combustion air above the level of the primary air distributor. In other words, secondary air or maybe tertiary air is supplied into the combustor in order to increase the amount of air for the combustion process. After the fuel is partially combusted, the staged air is added, where this remaining air will then slowly complete the combustion process. This technique variously referred as biased firing, delayed air admission and staged-air combustion.

To create air staging, the primary combustion zone starved of its air. This will create a pyrolisis reaction that will supply unburned gas. Pyrolisis involves heating the solid fuel in absence or lack of air, so that all volatile components are distilled off. These volatile products comprise of combustible gases. The unburned combustibles leaving the bed are then burnt while leaving the chamber, where the secondary air will burn off these unburned gases. This method also ensures complete combustion of fuel. The second stage of burning disposes of the combustible gases produced by the primary stage.

The concept of staged-air combustion consists of injecting secondary air downstream of a first staged combustion zone that will change its characteristics. With air staging, the fluidization velocity, bubbles sizes and combustion efficiency will be changed [101-103].

The excess air (EA) affects the number size distribution. In some cases indicated, the number maximum was found in larger particle sizes for low excess air than for high excess air. Low load and low density of the fuel also make to displacement of the number mode towards larger particle sizes compared to normal density fuel (briquettes) [68]. To certain of excess air, the rate of oxygen consumption along the combustor height is almost independent of both the nature of the biomass fuel or the fuel load. However, the bed height has little influence on the emission profile [59, 67].

2.1.4 Pollutant of Biomass Combustion in ABFBC

When biomass fuel combustion is complete, the presence of the products are carbon dioxide (CO_2) and water (H_2O), which is not harmful, contrary to incomplete combustion releases health-damaging pollution and greenhouse gas (GHG) emissions such as carbon monoxide (CO), nitrous oxide (N_2O), methane (CH_4), polycyclic aromatic hydrocarbons (PAH) and other organic compounds. And

products of incomplete combustion (PICs) have three undesirable effects such as loss of energy, impacts on human health and environment [18-19].

Pollutants itself can be classified into two categories such as unburnt pollutants and pollutants that are produced by combustion [93]. Unburnt pollutants include CO, HC, tar, PAH, CxHy, and char particles. Pollutants are usually caused by poor combustion is the result of burning low temperatures, inadequate mixing of combustible products (i.e. char and volatiles) with air and too short residence time in the combustion zone. They can be resulted from all categories of fuel depending on furnace design and firing system-operating conditions. By conducting in such conditions, lower emissions of pollutants and burnout higher efficiency can be achieved.

The second category includes ash, nitrogen, and sulfur related emissions are not the product of incomplete combustion. These pollutants are associated with the properties of biomass and produced during combustion. These are such particulate matter (PM), nitrogen oxides (NO_x, primarily NO and NO_2 and N_2O), and sulphur oxides (SO_x, especially as SO_2). Acid gases, such as HCl, and heavy metal (heavy on the fine ash fraction or in the gas phase) can also be emitted. The formation of these species can be influenced to some extent by the stoichiometric air-fuel and other combustion parameters or methods. Heavy metals may be present in high concentrations in certain fuel and RDF such as urban wood treated or painted wood.

2.1.4.1 Carbon Monoxide Emission

Carbon monoxide (CO) emission is essentially the result of incomplete combustion and include in the category of un-burnt pollutants. They may be considered as a benchmark of combustion efficiency, although some studies reported higher combustion efficiencies with higher CO emission [93].

The CO formation presented by lower excess air, restricted residence time, lower temperature, and diffusion controlled reactions due to fuel composition (high ash content). The CO concentrations emitted from biomass fuels in BFB combustion can be higher when combusted in the small scaling units designed for coal combustion and not modified for biomass or co-combustion. This is usually because of the high volatile content of biomass [63-67]. CO emissions are frequently a major concern for biomass (co) combustion.

Obviously, differences between coal and biomass are the basic fuel composition. Small scaling units can produce high CO emissions due to shorter freeboards characterized by smaller residence times. Another reason is related to fuel properties of the biomass. Biomass contains a comparatively higher volatile; therefore needs more residence time in the freeboard to completely burn the volatiles.

CO concentration in the flue gases is generally affected by both fuel calorific value and size of the fuel itself [105]. Operating conditions and fuel properties also affected the emission performance and combustion efficiency. Excess air also identified as one of the important factor for the burn out of the fuel. The system load and air staging used as operating variables to increase the fuel residence time in the hot zone. CO is well mitigated by injection of secondary air into the bed splash zone which results in low emission of CO and high (over 99%) combustion efficiency [106].

Beside that design improvements, longer freeboards are recommended for biomass combustion in FBs, taking the high volatile content of biomass into account and increasing the total time of residence. Also, an internal heat exchanger possibly presents in the freeboard and splashing zone in small scale FBs should be removed to keep these sections at higher temperature and therefore helping the conversion of CO to CO_2 [107].

CO_{max} for rice husk is much larger than the sawdust and the bagasse as coarse char particles and higher concentrations of ash leads to a higher char valid in the

region of the bed and the significant contribution of char-carbon to CO formation. The CO_{max} for distinct fuels were rapidly diminished with an increase in excess air of up to 50–60% demonstrating however a weak dependence on excess air in the region of 60–100%. The CO_{max} for different fuels rapidly decreased with an increase up to 50-60% excess air shows however a weak dependence on the excess air in the region of 60-100%. CO reduction rate for different biomass fuels found to be in correlation with the concentration of CO in the freeboard region. Therefore, the highest rate determined for the rice husk [59].

The CO_2 emission profiles along the combustor height were found to be almost independent of the combustor load and fuel quality. When the CO_2 concentration increases gradually along the combustion chamber is high, both CO and NO_x profiles have an extreme in the active combustion zone. Effect of FBC load, excess air and fuel moisture, the max CO has been found to be very strong in tests with low excess air from the critical EA (40-45% when firing regular sawdust; 65-70% when firing high moisture sawdust). CO emissions from the conical FBC fired with a high moisture sawdust are found much higher (about 1000ppm) compared to those, when firing regular sawdust (200-300ppm) [67].

2.1.4.2 Oxides of Nitrogen Emission

Nitrogen compounds include nitrogen monooxide (NO) and nitrogen dioxide (NO_2), which usually summarized as nitrogen oxide (NO_x) and nitrous oxide (N_2O). NO_x emissions play an important role in the atmospheric reactions that create harmful particulate matter, ground-level ozone (smog), and acid rain. These emissions along with HC (hydrocarbons) photo chemically lead to the formation of ozone, which are a lung and eye irritant and a major problem in urban environments. NO_x emissions are a part of a suite of year-round environmental problems such as acid rain in the mountain regions to eutrophication (the buildup of nutrients in coastal estuaries), leading to oxygen depletion that degrades water quality and harms fish. And it also contributes to haze air pollution in parks and wilderness areas [93].

NO_x formation in combustion systems involves four major parts such as [93] as shown in Figure 2.7:

i. Formation of thermal NO_x.

Thermal NO refers to NO formed through high temperature oxidation of the diatomic nitrogen found in combustion air. Thermal NO is the primary source of uncontrolled NO_x emissions in the combustion of clean fuels that do not contain organically bound nitrogen with air in which contains atmospheric N_2. At high temperature, both nitrogen (N_2) and oxygen (O_2) molecules in the combustion air are dissociated into their respective atomic states N and O, and participate in a series of reactions.

ii. Formation of fuel NO_x.

Fuel NO formation is the process where nitrogen compounds (primarily organic) contained in fuels evolved and reacts with the oxygen in the combustion air to form NO. It is the primary source of nitrogen oxide production formed in their combustion. During combustion, the nitrogen bound in the fuel is released as free nitrogen radical in the flame zone and ultimately forms free N_2 or NO. The extent of conversion of fuel nitrogen to NO is dependent on the local combustion characteristics (temperature and stoichiometry conditions) and the initial concentration of nitrogen-bound compounds in the fuel-air mixture. Gas fuels have a relatively low amount of bound nitrogen while solid and liquid fuels have more bound nitrogen. This is the reason for fuel NO formation of these fuels to be much bigger than of gaseous fuels.

iii. Formation of prompt NO_x.

It is observed that NO_2 have significant concentration in certain combustion conditions, especially near the flame zone. Kinetic calculations have indicated that the NO_2 formation and destruction in flames can occur according to the following sequence:

$$NO + HO2 \rightarrow NO2 + OH \quad (2.1)$$

$$NO2 + H \rightarrow NO + OH \quad (2.2)$$

$$NO2 + O \rightarrow NO + O2 \quad (2.3)$$

In the low-temperature regions of flames, significant HO_2 concentrations found that react with NO formed in the high-temperature regions and transported by diffusion to the low-temperature region. The NO_2 removal reactions are rapid, and in the presence of high radical concentrations, NO_2 will be converted rapidly back to the NO [93, 108].

iv. Nitrous oxide mechanism [108].

N_2O is an important nitrogen oxide under fuel-lean conditions. N_2O is a very short-lived component in hot combustion gases. The principal N_2O formation reactions involve NO and various nitrogen-containing radicals such as:

$$NH + NO \rightarrow N2O + H \quad (2.4)$$

$$NCO + NO \rightarrow N2O + CO \quad (2.5)$$

There are many potential methods of reducing N_2O emissions according to present knowledge of N_2O formation and destruction. The major pathways of N_2O destruction are homogeneous reactions with hydrogen radicals to form N_2.

$$N2O + H \rightarrow N2 + OH \quad (2.6)$$

$$N2O + OH \rightarrow N2 + HO2 \quad (2.7)$$

However, the concentrations of hydrogen radicals are extremely low in low temperature combustion. This is another important factor leading to the significant amount of N_2O from FBC. In this case, injection of a gas, which can decompose to hydrogen radicals, can be expected to be an effective method of removing nitrous oxide. Increasing the combustion temperature is a primary means of N_2O destruction in FBC, since thermal decomposition of N_2O depends essentially on temperature.

The NO_{max} is strongly influenced by nitrogen and low fuel depending on the operating conditions of the state of fuel-NO formation mechanism for all fuels. NO

reduction rate for rice husk is much larger than those for sawdust and bagasse for the significant role of heterogeneous reactions (on the char surface) in the freeboard region and ash collector device (cyclone). Of the studied fuels, sawdust is a biomass fuel which is the most environmentally friendly while rice husk firing accompanied by significant environmental impact. For a maximum load of the engine and the air more than 50-100%, the combustion efficiency of over 99% can be achieved when firing sawdust and bagasse. For the case of rice husk burning at maximum load, the combustion efficiency is lower because of higher losses due to unburned carbon. The maximum combustion efficiency of 86% for rice husk firing is obtained for about 60% excess air, excess air increased to 100% yield reduction in combustion efficiency (to 81%) [59].

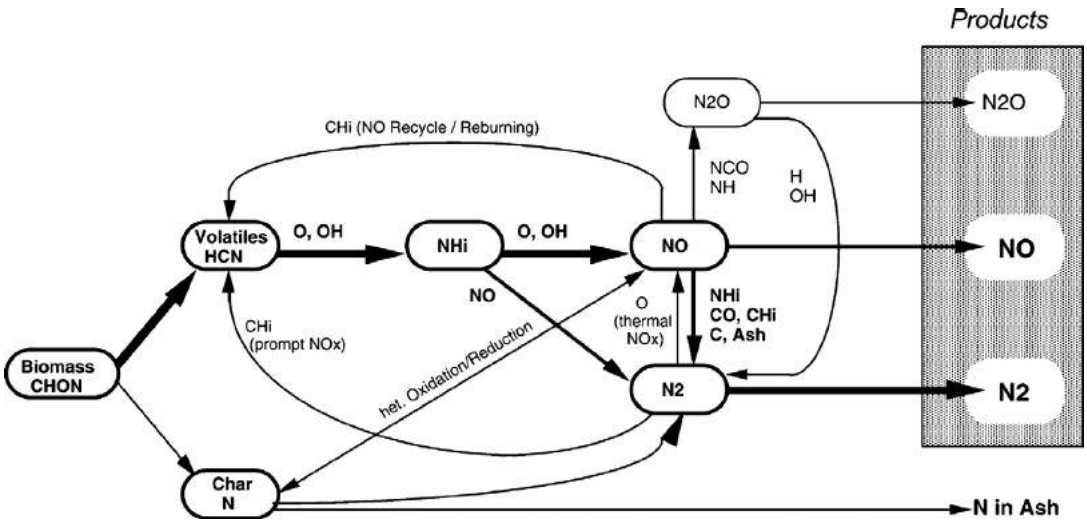

Figure 2.7 Conversion of fuel nitrogen in biomass combustion [93]

$NO_{x,max}$ value that is less influenced by combustion conditions, close to 1.5 to 3 times the concentration of NO_x in waste gases, showed that the NO_x reduction process occurs in the freeboard of the conical FBC. NO_x emissions from the conical FBC were found to be in the range of 110-120ppm for regular sawdust, and 80-90ppm for the high moisture sawdust fired at a maximum rate of fuel feed to the EA of 80-100% [67].

Generally, nitrous oxide emissions from FBC are strongly dependent upon fuel characteristics, operating bed temperature, excess air level, residence time, and many more factors [54-55, 58]. In order to reduce NO_x formation, primary measures (air and fuel staging) investigated for grate firing, BFB and CFB furnaces. Flue gas recirculation as a primary measure is of minor influence on NO_x emissions [50, 57, 61, 109]. Other research indicates that CaO, $CaSO_4$, Fe_2O_3 and char have an important influence on decomposition of N_2O; co-combustion of coal and biomass effectively measures to low N_2O and NO_x emission [10, 56].

2.1.4.3 Oxide of Sulphur Emission

It is an established fact that SO_x from combustion sources is one of the causes for acid rain. Sulfur together with chlorine may play an important role in corrosion of boiler components. Sulfur exists in plants in both organic (amino acids and sulfolipids) and inorganic (sulfates) forms. The concentration of organic sulfur is reported to be usually constant but inorganic sulfur can vary by a factor 100 [70].

For coal Turkish lignite in CFB combustors, the research results showed that an increase in excess air decreases SO_2 and NO_x emissions. Although NO_x emission increases with the operational bed velocity while SO_2 emission decreases. A bigger value of inlet bed pressure results in lower emissions of SO_2 and NO_x if other parameters are set unchanged [110].

Characteristics of pure cotton stalk combustion in a 10-100mm long have been studied in a CFBC. The fluidizing medium was alumina. Although as the fluidizing velocity is 4.5m/s (N=10.2), there will exist a little more segregation in the cold-state tests, but the dense bed can keep steady state combustion. A dense bed temperature between 830ºC and 880ºC obtained. Because of the high volatile content of fuel, a significant amount of combustion takes place in the dilute phase. The results show that as the fluidizing velocity increases, the temperature of the dense phase decreases. Meanwhile, the temperature of the dilute phase increases and

becomes uniform. To ensure a stable combustion, the secondary airflow and gas flow to the loop seal should be controlled enough. During the tests, the concentrations of major gaseous pollutants in flue gas measured. The results show that SO_2 emission varies from 32ppm to 55ppm and NO emission ranges from 110ppm to 153ppm at the basis of oxygen concentration of 6% in volume in flue gas. The highly efficient combustion, over 98.5%, is reached. The excess air ratio of 1.3 and air split ratio of 1:0.88 seems optimal to provide higher combustion efficiency of the fuel [111-112].

2.1.4.4 Suspended Particulate Matter

Mass and number concentrations of separator particles downstream, in boilers with multi-cyclones, are dominated by submicron particles. The mass concentration of particles increases under unsatisfactory combustion conditions yields from incomplete combustion. These include soot and condensable organic particles. High moisture content in the fuel, low excess air or imperfections in the boiler design caused the unsatisfactory combustion conditions.

2.1.5 Palm Shell Combustion

Biomass, one of the renewable energy sources defined as the biodegradable fraction of products, waste and residues from agriculture including vegetable and animal substances, forestry and related industries. Biomass residues from palm oil are potential usage because of many palm oils planting area in Asia countries, like in Thailand [44], Indonesia [61] and Malaysia [113].

In Thailand, rotation period of both crops is 25–30years, the time which yield drops and the trees are cut down for re-plantation [44]. In Indonesia, the Agriculture Ministry anticipates Indonesia’s oil palm plantation area to expand by 18.7%, from

the current 7.5Mhectares producing 18.7Mtonnes/y of crude palm oil (CPO) to 8.1Mhectares yielding 23.2Mtonnes of CPO in 2010, and 28.4Mtonnes of CPO by 2014 [61, 114].

Malaysia itself has very substantial potential for biomass energy utilization given its equatorial climate that is ideal for dense tropical forest growth and agricultural vegetation. Palm wastes are strategically feasible because they can contribute to the sustainability of energy supply and minimize the negative impact of energy generation on the environment [113, 114]. Biomass power potentials from wood processing and palm oil estimated at 280TJ and 250TJ, respectively. By the year 2010, the biomass energy potential is expected to increase to 820TJ [31]. Cultivation of oil palm under the existing practice does not pose a threat to the environment and energy crops. Press fiber and shells produced by palm oil mills used as solid fuel for steam boilers. The resulting steam used to run turbines for electricity production. Both solid fuels are capable of producing more than enough energy to meet the energy needs of palm oil mill [31].

The main by-product and wastes produced from the processing of palm oil are the empty fruit bunches (EFB), palm oil mill effluent (POME), sterilizer condensate, palm fiber and palm kernel shell. EFB and POME have been used extensively as mulch and organic fertilizer in oil palm areas while palm fiber and shell are used as fuel [48], making the palm oil mill self-sufficient in energy. The excess shells used to build road surfacing on estates. Table 2.4 and Table 2.5 in below show the various compositions and components of the oil palm.

Malaysia has the potential to be one of the major contributors of renewable energy in the world via oil palm biomass. Subsequently, Malaysia can then become a role model to other countries in the world that has huge biomass feedstock [113, 46, 47].

Utilization of oil palm waste as an energy source will bring other environmental benefits such as reducing CO_2 emissions. Greenhouse gases that are

present in the atmosphere including water vapor, CO_2, methane and ozone, and the increasing mainly CO_2 is the main cause of global warming. Waste such as oil palm fiber, shell and EFB used to generate steam for processing and to generate electricity. Currently, there are more than 300 palm oil mills operated with self-generated electricity from palm oil waste.

Table 2.4 : Dry matter production by oil palm [31]

Period	Part	Dry matter (t/ha)
Annual (mature palm)	Pruned fronds	10.4
	Empty fruit bunches	1.6
At replanting	Trunk	75.5
	Fronds and rachis	14.4

Table 2.5 : Availability of fresh and dry weight of EFB, shell, fiber and effluent in tons per hectare per year after milling from 1 ha of mature palms [31]

	1 ha of mature palms	
	Fresh wt. (t/ha/year)	Dry wt. (t/ha/year)
FFB	20.08	10.60
EFB at 22% of FFB	4.42	1.55
Fibre 13.5% of FFB	2.71	1.63
Shell 5.5% of FFB	1.10	1.10
(i) Sterilizer condensate 12% FFB	2.41	0.12
(ii) Clarification sludge 50% of FFB	10.04	0.50
(iii) Hydrocyclone washing 5% FFB	1.00	0.05
Total POME	13.45	0.67

The electricity generated is for their internal consumption and also enough for some remote areas. A cement company in Malaysia has been using palm shell as fuel in boilers and they found that CO_2 emissions can be reduced by 366.260metric tons in 2006 alone. Therefore, the CO_2 emissions in Malaysia can be significantly reduced if all the industries in Malaysia can replace or partially replace fossil fuels with oil palm waste to produce energy without lowering environmental [113].

FBC of solid fuel combustion is an attractive alternative as result of price increase and the depletion of fossil fuels, the presence of high amounts of waste to be disposed off and the issue of global warming. ABFBC is a general model that can provide many advantages such as compact boiler design, fuel flexibility, higher combustion efficiency and reduce emissions of pollutants such as SO_x and NO_x gases harmless. Air staging as one of the emission control techniques, can reduce emissions of combustion, it is the NO_x, CO, unburned hydrocarbons and smoke. Utilization of oil palm waste as an energy source will bring other environmental benefits such as reducing CO_2 emissions. As we know, a greenhouse gas that is present in the atmosphere including water vapor, CO_2, methane and ozone, and especially the increase in CO_2 is the main cause of global warming. The renewable energy is abundant in Malaysia, such as palm oil waste, used to generate steam for processing and to generate electricity. Therefore, our study focused on using palm oil waste oil, palm shell, as fuel in a laboratory scale ABFBC. For controlling and reducing emissions of combustion, we used staged air method.

2.2 Fluidization

Fluidization is a technique or a substantial reduction in the phenomenon of internal friction in the bed of solid particles with a counter force that the bed can flow like a fluid. Internal friction is caused by compression of the bed by gravity in many cases, but sometimes even by the buoyancy force when the particle density is lighter than the fluid density, by the magnetic force or by the centrifugal force. The counter forces, is a drag force of fluid flowing through the bed in the direction opposite the bed compression force. Direction of fluid flow is generally vertically upwards, but downwards to the floating particles. For centrifugal fluidization, it into the drum rotates. Sometimes counter-action is mechanical vibrations or sonic vibration [115].

The fluidization technology continuously developed such as the evaluation and validation of CFD models by measurements in industrial fluidized beds, the

investigation of 3D effects in large-scale fluidized beds and the development of measurement techniques for better process control [115-116]. Because, the general application of the gas/particle flow systems and fluidization in the industry calls for an increase in efficiency and the development of fundamentally based on realistic simulations, accurate and detailed experimental data and design tools for such systems.

The measurement and numerical predictions of gas vortices formed by single eruptions in the freeboard of a BFB)investigated by S. Vun et al. [117]. Also B. Peng investigated the theoretical and numerical on the flow multiplicity phenomenon for gas–solids two-phase flows in CFB risers [118].

Meanwhile, Van Wachem et al. [119] investigated about the dynamic characteristics of the gas-solids behavior at different superficial gas velocities, at different column diameters, and at different pressures. He also evaluated, namely the velocity of pressure and void age waves through the bed, the power of the low and high frequencies of the pressure and void age fluctuations, the reorientation of the gas-solids flow just above minimum fluidization and the effect of elevated pressure upon this reorientation, and the Kolmogorov entropy.

CFD simulations carried out for the predictions of flow pattern in bubble column reactors using 1D, 2D and 3D with k–ε models. All the models showed good agreement with the experimental data for axial liquid velocity and the fractional gas hold-up profiles. However, for eddy diffusivity, only the 3D model predictions agree closely with the experimental data [120].

Therefore, in this study, the measurement and numerical predictions of solid velocity were investigated in the freeboard of an ABFB. The experiments used a PIV measurement technique to visualize and measure the solid flow within the freeboard after a single bubble eruption. A computational study was carried out using Eulerian–Eulerian, kinetic theory of granular flow approach with k-ε model used to account for solid turbulence. Results from a three dimensional (3D)

simulation of the experimental fluidized bed were compared with experimental velocity profiles of gas flow in the freeboard of the gas–solid fluidized bed after a bubble eruption.

2.2.1 Laser Based Measurement Techniques

During the last two decades, significant advances have been made studying both in the multiphase approach to gas/solid flow systems and in detailed experimental using nonlinear laser spectroscopic techniques [121-125].

There are many kinds of laser based measurement techniques, e.g.: Laser/Phase Doppler Anemometry (LDA/PDA) and Particle Image Velocimetry, PIV. Nowadays, LDA technique [126-128] and PIV [82-84, 117, 127, 129-131] were used to measure extensively for flow parameter. The laser based measurement techniques have the advantage that they are non-intrusive and therefore do not disturb the flow. The fact that the measuring device is not in contact with the flow has the further advantage that it is possible to measure in hazardous environments, e.g. obtaining velocity components in a flame.

Some numerical [118, 132-142] and experimental studies [137, 143-146] have been conducted to obtain hydrodynamic properties such as investigation of bubble fluidizing flow and pattern structure [147], particle size diameter, bulk density, fluidizing velocity, etc. The solid material can use some kind of granular material Geldart B like sand [148-149], polypropylene particles [87] and various biomass like rice husk, sawdust, peanut shell, coconut shell, palm fiber [148, 150-153].

2.3 ABFBC CFD Simulation

ABFBC are becoming important in many industry; however, their hydrodynamic characteristics, and hence their scale-up, is still poorly understood. Models describing the characteristics of fluidized beds in many cases are semi-empirical and have been mostly determined under laboratory conditions. Therefore, numerical modeling through CFD simulation is a very useful tool for a better understanding of these characteristics, especially the combustion process and emissions of pollutants [154]. On the one hand, there are still many uncertainties of the ABFBC hydrodynamics, combustion and pollutant formation mechanisms. On the other, in most models of combustion for fluidized bed, an empirical correlation to describe the fluid dynamics in the reactor is used to avoid solving the momentum equations.

CFD modeling has reached a high level of success when the numerical modeling of reactive multiphase flow started. Therefore, the literatures on numerical modeling of flow process and combustion mechanism in the FBC are still very limited. Many of the study reported were about the 2D simulation of coal combustion in BFBC [155-156] and of coal and biomass, such as olive cake, peat, rice husk and wood combustion in CFB [154, 157-159].

CFD is the science of predicting fluid flow, heat transfer, mass transfer, chemical reactions, and related phenomena by solving the mathematical equations that govern these processes by means of computer based simulation. The availability of affordable high-performance computing hardware and the introduction of user-friendly interfaces have led to a recent upsurge of interest, and CFD has entered into the wider industrial community since the 1990s [160]. The result of CFD analyses are relevant engineering data used in conceptual studies of new designs, detailed product development, troubleshooting, and redesign.

CFD is a suitable modeling tool to study the combustion processes in a fluidized bed. It offers an economical and effective solution. CFD simulation models

can optimize the fluidized bed unit's design, can predict inert material concentration in the bed and fuel mixing efficiency. Temperature profiles of solid and gaseous phases present in the dense bed, temperature profile of the furnace and heat flux can also be simulated. Therefore, simulation with aid of CFD is one of the most appropriate approaches for the prediction of critical parameters required for the control of fluidized bed operation efficiently.

For a successful CFD simulation, a good understanding of the numerical solution algorithm is also crucial. Three mathematical concepts are useful in determining the success or otherwise of such algorithms: convergence, consistency and stability. Convergence is the property of a numerical method to produce a solution which approaches the exact solution as the grid spacing, control volume size or element size is reduced to zero. Consistency of numerical schemes produce systems of algebraic equations which can be demonstrated to be equivalent to the original governing equation as the grid spacing tends to zero. Stability is associated with damping of errors as the numerical calculation progress. If a solution technique is not stable, even round off errors in the initial data can cause wild oscillations or divergence [160].

The process of CFD simulation is split into three analysis process sequences, i.e. pre-processor, solver and post-processor [161]. The first process, it begins with geometry, which has to be either created or imported from an external package, such as CAD, GAMBIT, SOLIDWORKS, etc. GAMBIT is a software package designed to help analysts and designers build and mesh models for CFD and other scientific applications. GAMBIT receives user input by means of its graphical user interface (GUI). The GAMBIT GUI makes the basic steps of building, meshing, and assigning zone types to a model in a simple and intuitive way, yet it is versatile enough to accommodate a wide range of modeling applications [162-163].

The geometry of interest is first divided or discretized into a number of computational cells. Discretization is the method of approximating the differential equations by a system of algebraic equations for the variables at some set of discrete locations in space and time. The common discretization techniques are finite

difference, finite volume and finite element. The discrete locations are referred to as the grid or the mesh. In other words, basically, discretization is a transformation of human's complexity to computer's simplicity, and a process by which a closed-form mathematical expression (function, differential or integral equation involving functions) is approximated by analogous expressions which prescribe values at only a finite number of discrete points (*grid points*) or volumes in the domain.

Next, secondly, a CFD code applies the governing equations of fluid flow, the Navier Stokes equations, to each cell within the mesh. The computer process communicates information across all the cells and proceeds in an iterative manner towards solving the problem. After much computation a solution is reached where forces and mass flows balance in every cell, and across the whole flow domain.

Finally, when the calculation is finished, the CFD solution contains all the pressures and velocities both on and off the surfaces of the object being studied, this is usually millions of numbers. Computer visualization is the key to fully interpret the solution from a CFD solver.

ANSYS FLUENT is a computer programming for modeling fluid flow, heat transfer, and chemical reactions in complex geometries. It is written in the C computer programming language and makes full use of the flexibility and power offered by the language. Consequently, true dynamic memory allocation, efficient data structures, and flexible solver control are all possible. In addition, it uses a client/server architecture, which allows it to run as separate simultaneous processes on client desktop workstations and powerful computer servers. This architecture allows for efficient execution, interactive control, and complete flexibility between different types of machines or operating systems.

ANSYS FLUENT provides complete mesh flexibility, including the ability to solve problems using unstructured meshes that can be generated about complex geometries with relative ease. Supported mesh types include 2D triangular/quadrilateral, 3D tetrahedral/hexahedral/pyramid/wedge/polyhedral, and mixed (hybrid) meshes. It also allows refining or coarsening the mesh based on the

flow solution. After a mesh has been read into ANSYS FLUENT, all remaining operations are performed within ANSYS FLUENT.

These include setting boundary conditions, defining fluid properties, executing the solution, refining the mesh, and post processing and viewing the results. Schematic diagram of ANSYS FLUENT processing is shown in Figure 2.8.

ABFBC is a multiphase reactive flow phenomenon. It is a multiphase problem between gases and fuel particles and also a reactive flow problem, which involves homogeneous reactions among gases and heterogeneous reactions between fuel particles and gases. ABFBC consists of solid (fuel), gas (medium) and inert particles. The fuel exists in the solid form in the inert sand particles. The involvement of multiphase flow combustion in fluidized bed devices makes modeling of these phenomena an extremely complicated and continues to be a challenge to the scientific community and practicing engineers. Researcher use CFD as a tool to study fuel, char, ash, physical and chemical behavior in the fluidized bed reactor.

There are some aspects to model the combustion [164] in a fluidized bed as shown in Figure 2.9 and can be summarized as:

(a) Governing reacting Navier-Stokes equations are accurately formulated.

i. Turbulence

- Large range of time and length scales, model by time (Reynolds) averaging that imagine a long exposure photograph of the visualized flow and introduces terms (the Reynolds stresses) which must be modeled.
- Turbulence models: k-ε, RNG k-ε, RSM, Realizable k-ε and LES

ii. Chemistry

- Realistic chemical mechanisms have tens of species, hundreds of reactions, and stiff kinetics (widely disparate time scales) that are determined for a limited number of fuels.

(b) Gas Phase Combustion: generalized finite rate formulation (Magnussen model), conserved scalar PDF model (one and two mixture fractions),

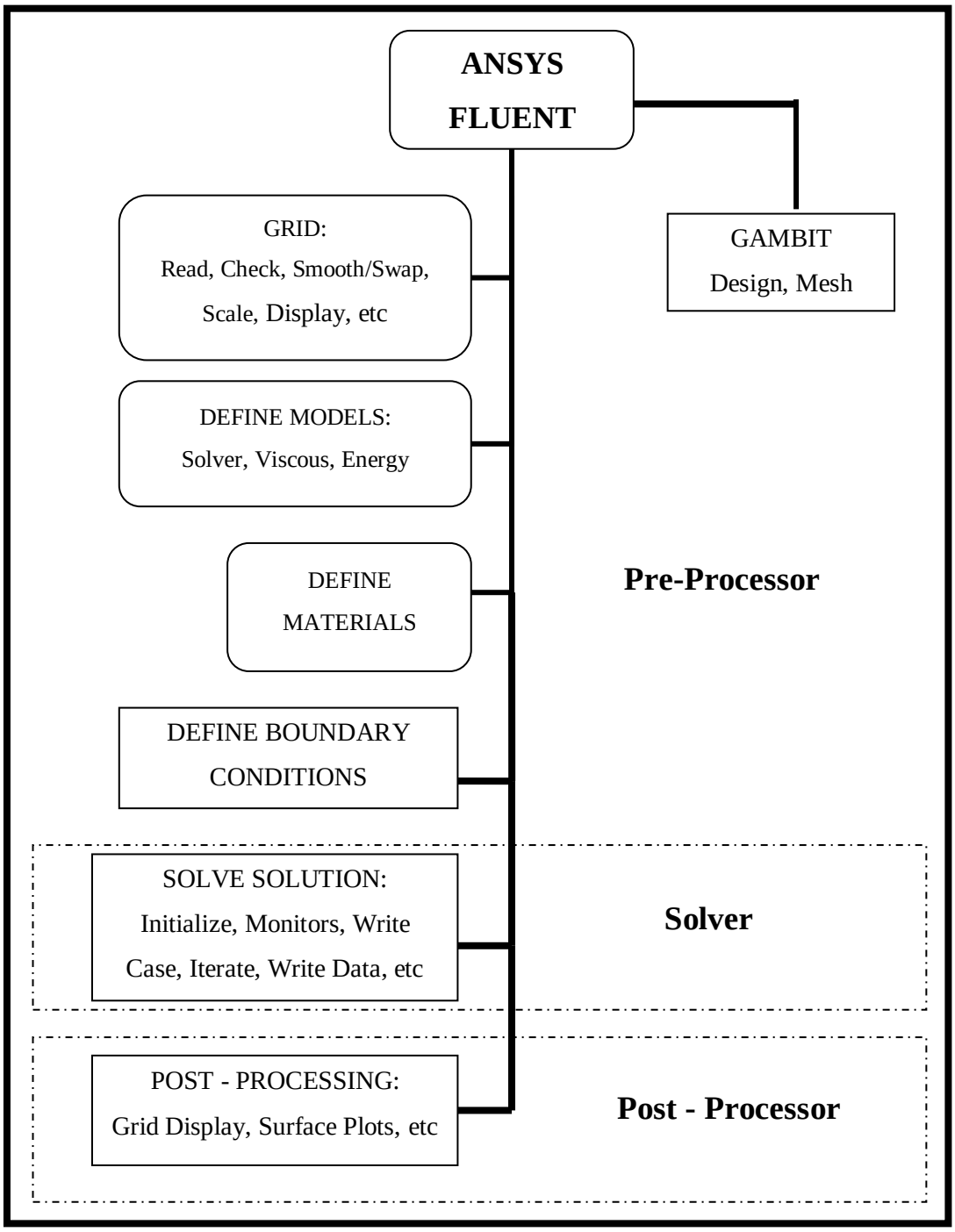

Figure 2.8 Schematic Diagram of FLUENT Processing

(c) laminar flamelet model and Zimont model. Gas phase combustion is classified by:

i. Non-Premixed combustion (diffusion flames):

- Fuel and oxidizer convect/diffuse from either side into a flame sheet
- Can be simplified to a mixing problem

- Turbulent eddies distort the laminar flame shape and enhance mixing

ii. Premixed combustion

- Cold reactants propagate into hot products
- Rate of propagation (laminar flame speed) depends on the internal flame structure, hence much more difficult to model than non-premixed combustion
- Turbulence wrinkles the laminar flame and accelerates flame propagation

iii. Partially premixed combustion

- Combustion system with both non-premixed and premixed fuels.

(d) Discrete phase model:

i. Turbulent particle dispersion: stochastic tracking, particle cloud model,

ii. Pulverized coal and oil spray combustion sub-models

(e) Radiation models: DTRM, P-1, Rosseland and Discrete Ordinates.

(f) Pollutant models: *NOx* with reburn chemistry and soot.

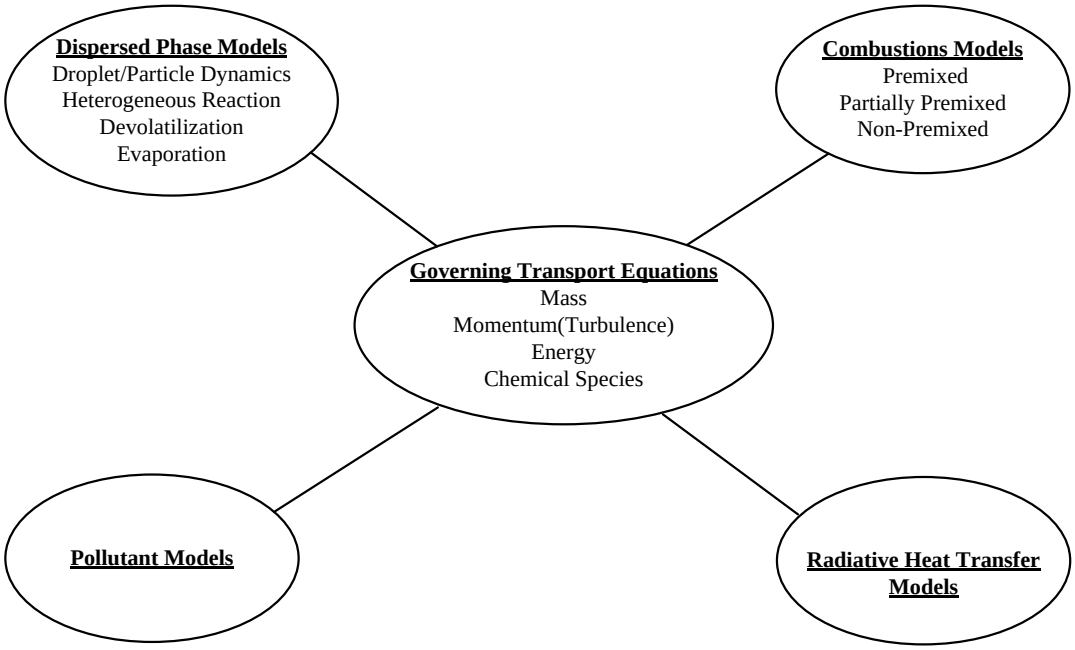

Figure 2. 9 Aspects of Combustion Modeling

Prior to the simulation of the full 3D model of the ABFBC experiment using ANSYS FLUENT it was first started in 2D. The 2D model was validated for the physics of the model such as: the mesh resolution requirements (resolve shear

layers), the solution parameters and the convergence settings.

Apart from that, before the simulation was carried out in ANSYS FLUENT, boundary conditions, initial conditions, under relaxation factors, discretization method, radiation model, turbulence model and convergence criteria were also determined. If the simulation results good condition, the 2D model was developed into a 3D model. Same aspects in the 2D model also were conducted for the 3D model. Finally, the 3D model was also simulated by ANSYS FLUENT. These modeling developments are shown in Figure 3.

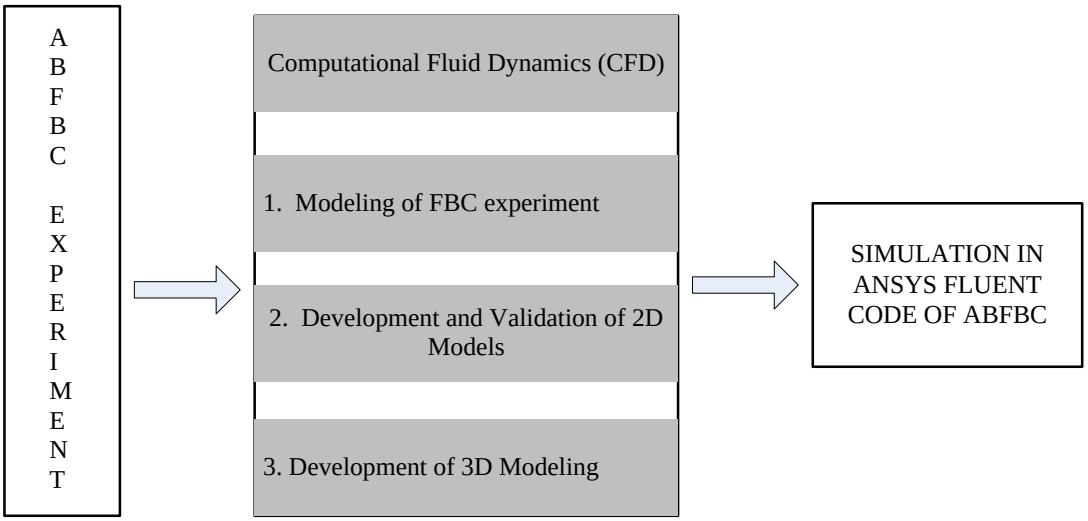

Figure 2. 10 Development of the modeling of a FBC in ANSYS FLUENT

In this study, initially a user-define function (UDF) was used to define a few simulation parameters. In the ANSYS FLUENT solver a UDF can be dynamically loaded to enhance the standard features of the code. UDF can be written to define boundary conditions, material properties, and source terms for its flow regime, as well as specify customized model parameters (e.g., DPM, multiphase models), initialize a solution, or enhance post-processing.

One source file can contain a single UDF or multiple UDFs written in the C programming language using any text editor and are saved with a .c extension (e.g., myudf.c). A UDF on C programming (example of FBC case) can be seen in

Appendix E. At the beginning of the source code file, every UDF must contain the udf.h file inclusion directive (#include "udf.h"). Code for UDFs using DEFINE macros and functions also supplied by ANSYS FLUENT to access ANSYS FLUENT solver data and perform other tasks during the compilation process [164].

The source files can be either interpreted or compiled when it is first built and then it is loaded into ANSYS FLUENT. After being interpreted or compiled, UDFs will become visible and selectable in ANSYS FLUENT solver using a graphical user interface dialog box and it use and return values specified in SI units.

Multiphase flow is simultaneous flow of materials with different states or phases (i.e. gas, liquid or solid) or materials with different chemical properties but in the same state or phase (i.e. liquid-liquid, such as, oil-water). Multiphase flow regimes can be grouped into four categories: gas-liquid or liquid-liquid flows; gas-solid flows; liquid-solid flows; and three-phase flows. In case of fluidized bed, the category is gas-solid flows.

Currently, there are three numerical techniques used for the studying of multiphase combustion in fluidized beds, e.g. Eulerian-Lagrangian (EL) model, Eulerian-Eulerian (EE) model and Discrete Element Method (DEM-CFD) within Eulerian Lagrangian concept [165]. The EE method is one of the affordable CFD modeling approaches for performing simulations of an industrial scale gas-solid flow system.

Most of FBC studies adopted EE model because tracking each particle with the Lagrangian method is not practical with current computational capacity. Furthermore, in the Lagrangian model, the interactions between particles and gases are all limited to a single particle or diluted particle concentration conditions so it cannot be used for dense condition as found in a fluidized bed [166]. Therefore, the EE model was widely used to describe the gas–solids two-phase flows or granular flows, such as flows in risers, fluidized beds and other suspension systems.

A multiphase flow containing dispersed particles may be modeled using either the particle transport (Lagrangian Particle Tracking) model or the Eulerian-Eulerian multiphase model. Some facts comparison between Eulerian-Eulerian Multiphase and Lagrangian Particle Tracking model are given in Table 1[164].

Table 2. 6 : Comparison between Eulerian-Eulerian Multiphase and Lagrangian Particle Tracking

Eulerian-Eulerian Multiphase	Lagrangian Particle Tracking
Complete global information for the particle phase is available. But, expensive if many sets of equations are used; that is, if there are many particle sizes. However, the homogeneous MUSIG model is an Eulerian-Eulerian model that uses a single velocity field for multiple size groups	Complete information on behavior and residence time of individual particles is available. But, expensive if a large number of particles have to be tracked
The different phases are treated mathematically as interpenetrating continua. Since the volume of a phase cannot be occupied by the other phases, the concept of phase volume fraction is introduced. These volume fractions are assumed to be continuous functions of space and time and their sum is equal to one.	The fluid phase is treated as a continuum by solving the time averaged Navier–Stokes equations, while the dispersed phase is solved by tracking a large number of particles (or bubbles, droplets) through the calculated flow field. The dispersed phase can exchange momentum, mass, and energy with the fluid phase. A fundamental assumption made in this approach is that the dispersed second phase occupies a low volume fraction.
Applicable for wide range of volume fractions. But, knowledge of the diffusion coefficients is incomplete	Better detail for mass and heat transfer. But, essentially only possible as a post-process for a large number of particles.
Relatively cheap for one additional set of equations. But, difficult to get accuracy over a range of particle sizes for combustive flows	Relatively cheaper for wide range of particle sizes. But, very expensive to include turbulence.
Turbulence is included automatically. But, when there is phase change, the particle diameter must be user-specified rather than calculated automatically by the model. This can decrease accuracy. And a momentum equation needs to be solved for each representative size which becomes very expensive (The droplet condensation model is an exception).	More flexible when there is a significant size distribution leading to different particle velocities. But, restricted to low particle volume fractions.

CHAPTER 3

RESEARCH METHODOLOGY

This chapter describes the methodology for conducting the cold flow and hot flow both studies were carried out experimentally and numerically, as shown in Figure 3.1. The cold or isothermal flow study shows the fluidizing multiphase phenomenon of mixing bed material (silica sand) with air; meanwhile, the hot flow study shows the combustion phenomenon in the Atmospheric Bubbling Fluidized Bed Combustor (ABFBC).

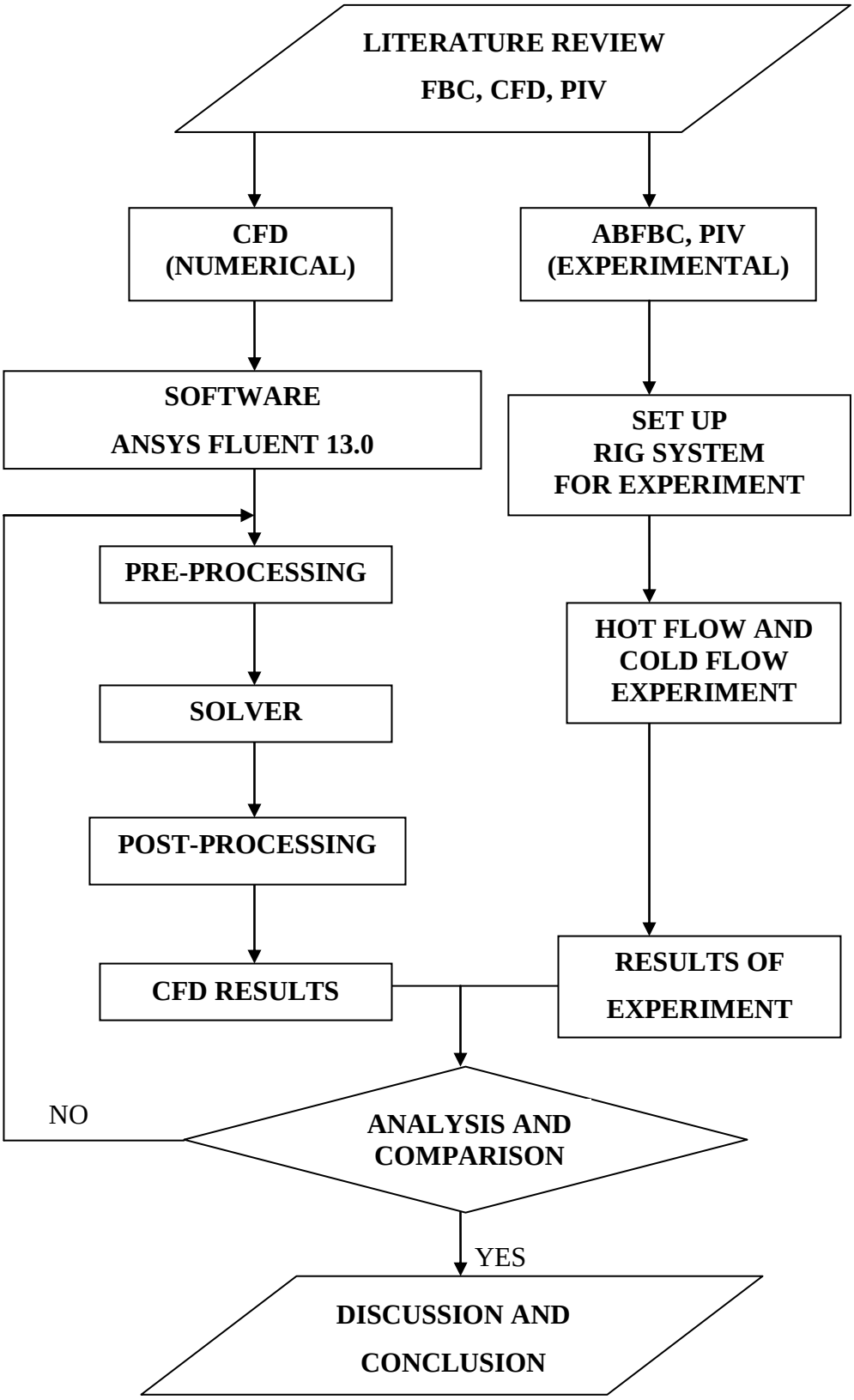

Figure 3.1 Schematic of Research Methodology

3.1 Cold Flow Experiment using Particle Image Velocimetry

Particle Image Velocimetry (PIV) experiments were conducted to obtain the two-phase, solid-gas flow phenomena. Then the results obtained will be used to validate the simulation results.

3.1.1 Experimental Rig

The main components of the experimental set up as were discussed below:

i. ABFBC (Bubbling Fluidized Bed Combustion)

The ABFBC as fabricated earlier was set as the core of the air distributor ($Ø_{airdist}$=49mm) and the cylindrical Perspex ($Ø_{cyl}$=144mm). Perspex provides space for the movement of bed material to move freely when the airflow was provided. The ABFBC was also joined to the piping system.

ii. Air Distributor

A major component of the experiment, the air distributor ($Ø_{air\text{-}dist}$=49mm), allowed air to flow through the holes in it in order to move the sand particles upwards. This contributed to the formation of a fluidized bed. The selected type of air distributor was 'tuyere' type whereas the air was distributed horizontally. There were six layers in the selected air distributor with six holes in each layer to give 36 channels of airflow. The diameter of the hole was 5 mm respectively. The model of the air distributor was shown in Figure 3.2.

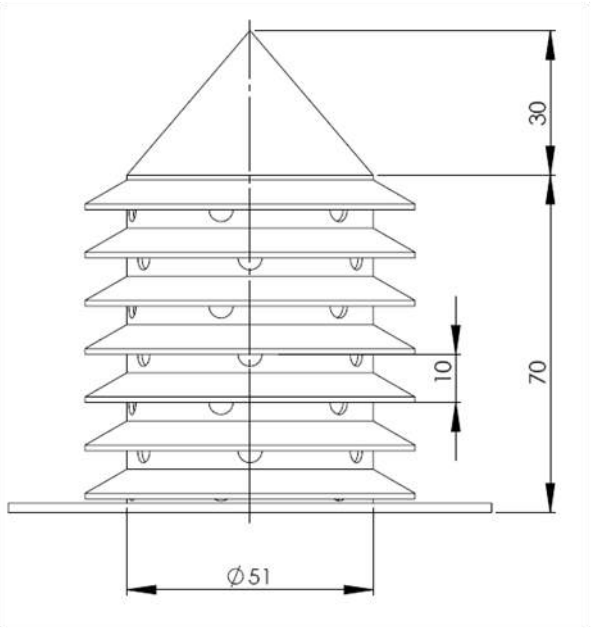

Figure 3. 2: Air Distributor

iii. Bed Material

Bed material was selected according to the Geldart's classification of solid particles. The particles selected for both experimental and simulation methods were included in category B which was silica sand, as shown in Figure 3.3. The selected material was sand particles that falls in the range 300-425μm with a density 2500kg/m^3. This sand was sieved using a sieving machine to obtain the desired particle size. This density was obtained through a small experiment.

iv. Air Flow meter

Air flow meter was a device for measuring the flow rate of air entering the air distributor in the experiment. Type of velocity meter used was a system unit CFM (Cubic Feet per Minute), with a range between 8-30CFM, as shown in Figure 3.4.

v. Blower

The blower was a Tornado Centrifugal Fan. The flow rate could be adjusted by using a controller on the blower.

vi. Piping System

Piping system served as a joining system to channel the airflow from the blower to the air distributor. Various diameter PVC pipe, elbows and joints were used to change the diameter to join the two ends fit. The designed piping system was adjusted with the blower diameter of 76.34mm to match the air distributor diameter of 51mm.

Figure 3. 3: 300-425μm Sand Particles

Figure 3. 4: Airflow Meter

3.1.2 Experimental Set-Up and Procedure

The experiments were conducted in a three-dimensional (3D) column cylinder Perspex fluidized bed of a 2m height and $Ø_{cyl}$ = 144mm. The cylindrical bubble column was used because of their widespread applications in the industry. A PIV system was specially constructed to measure the gas solid flow characteristics in the ABFBC, shown in Figure 3.5 and 3.6. The bed particles consisted of silica sand with nominal diameters 300-425µm. The density of the particles was 2500kg/m^3. The minimum fluidization velocities were respectively 5.01m/s, 5.76m/s and 6.26m/s. The heights of laser view were respectively 100-200mm; 270-370mm; 350-450mm; 500-600mm; 650-750mm from the bed's base.

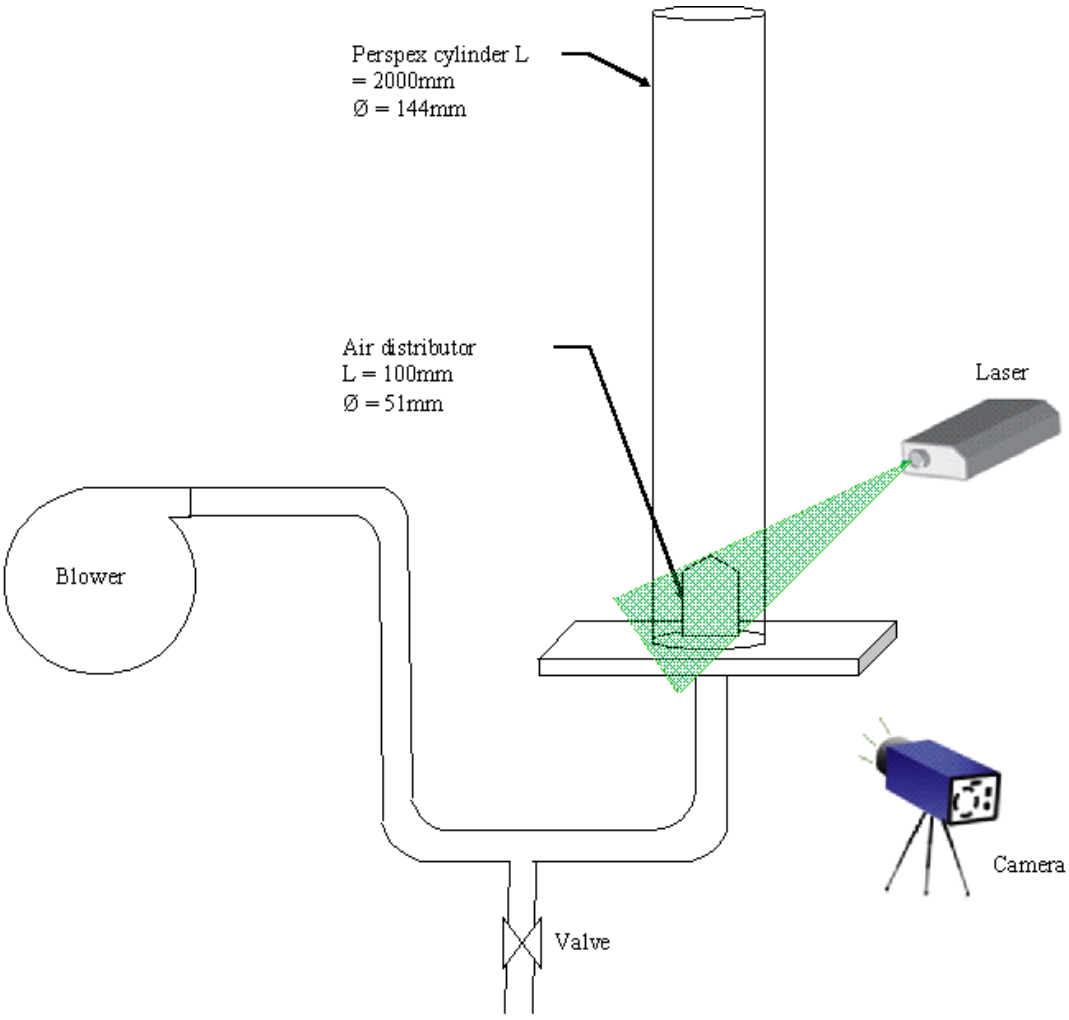

Figure 3. 5: Schematic Experimental Set Up

A Q-switched, double cavity pulsed Nd: YAG laser was used as the illumination source, which had a repetition rate of 10Hz and provides two thin (0.3-1mm) green laser sheets (nm=532). An 80C42 Double Image 700 camera with a Nikon AF Micro-Nikon lens 60/2.8 was used to capture two consecutive images. The images were analyzed using a cross-correlation algorithm yielding the local displacements vector for each interrogation area.

3.2 Hot Flow Experimental Method

Combustion (Hot Flow) experiments were conducted to obtain the combustion performance i.e. temperature distributions and performance of gaseous emission. Then the results obtained were used to validate the simulation results.

3.2.1 Experimental Test Rig

The Atmospheric Bubble Fluidized Bed Combustor (ABFBC) had five main systems as shown in Figure 3.12. The systems were:

1. Pre-heating System
2. Air Distribution System (tuyere)
3. Fuel Feeding System (hopper)
4. Combustion System (combustion chamber and freeboard)
5. Gas Separation and Dust Collecting System.

i. Pre-Heating System

Both pre-heating and stabilizing temperature were the steps before solid fuel was fed into the combustor. Getting these conditions was not easy in FBC, it used

Liquefied Petroleum Gas (LPG) and adjust primary air flowing. Solid fuel was fed into the bed after the bed temperature was stable around 450°C. All process to increase the bed temperature to its stable operating temperature used to needed one hour. After the bed temperature achieved 800°C-950°C, the data was taken. Eleven K-type thermocouples (see Appendix B) were installed into the combustor in depth of 10mm for measuring the bed temperature of the combustor.

ii. Air Distributor System (Tuyere)

Air distributor and blower were the two main devices in an air distribution system. Actually, the blower was used to supply air to the bed and pass through air distributor (tuyere) at a certain flow rate. Meanwhile, air distributor was used to distribute the air to the bed uniformly, as shown in Figure 3.7. Airflow rate hasdto be high enough to fluidize the bed particles. The right mixing between airflow and fuel feeding ensured the achievement of better combustion performance.

Tuyere is used as the designated air distributor for this combustion unit. Single tuyere which was installed consists of three main parts circular tubes, cone and flange. This tuyere had 36 air outlets. The diameter of each outlet was 5mm. All air outlets pointed horizontally and arrayed around the circular tube in six rows. That means each row consisted of six air outlets. Meanwhile, rings were used to avoid the air outlets being blocked by bed particles. These rings were welded just above the air outlets. Finally, the cone was added to the top of the tuyere to promote good fluidization and to minimize the formation of dead zone.

iii. Fuel Feeding System (Hopper)

The purpose of feeding system was as a medium of continuous transportation for solid fuel into the combustion unit during operation. Feeder and hopper were the two main devices in the feeding system, as shown in Figure 3.8. Hopper was a storage that was used to store solid fuel before the fuel being introduced to the combustion chamber by the feeder. The feeder controlled feed rate of the fuel to the bed.

Figure 3. 6 Cross Section of Air Distribution System

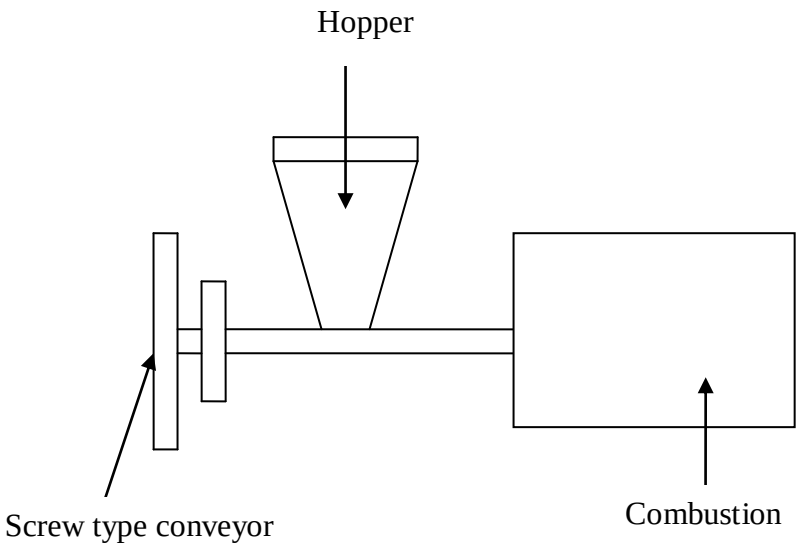

Figure 3. 7: Fuel feeder unit

Power transmission of the feeding system consisted of a motor with 1hp output, gearbox, a set of Miki pulley and a type of A V-belt. The rotation of the motor was fixed at 1420rpm pulling the set of Miki pulley, as shown in Figure 3.9.

Function of the Miki pulley was to reduce the rotational speed to the ratio of 1:4 (see Appendix C). In other word, the rotational speed could be altered from

1420rpm to 335rpm depending on the requirements of the experiment. The Miki pulley was also connected to the gearbox at its output. The constant speed change ratio of the gearbox was 1:10 to that the output. Speed rotation of the gearbox was between 33.5rpm to 142rpm. Miki Pulley had eight rotations, which were mean different rotational speeds.

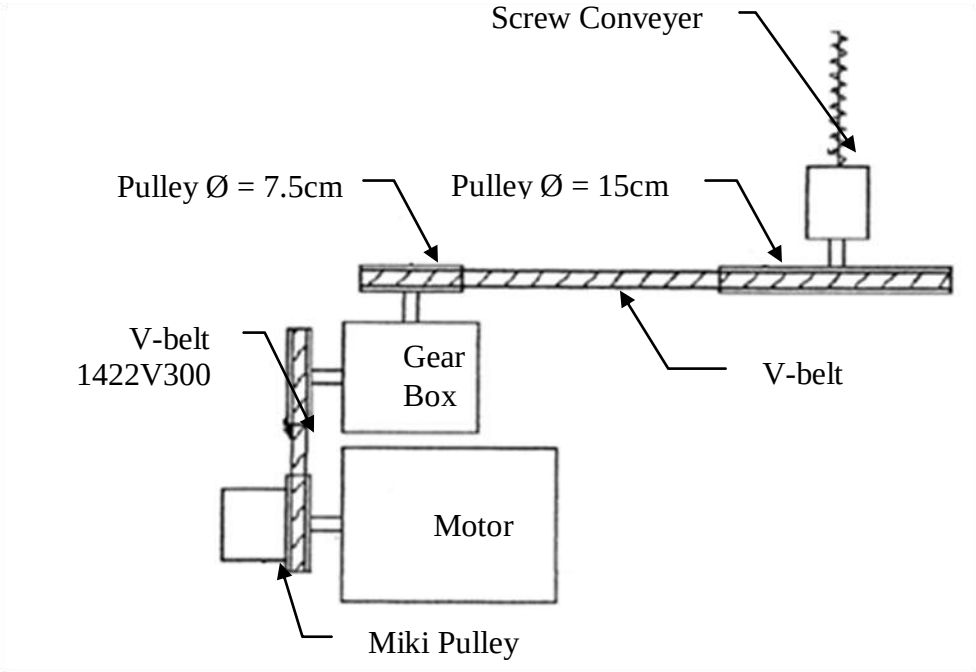

Figure 3. 8: Fuel feeding system

iv. Combustion System

The cylindrical combustion system (Ø = 164mm) was the part where the combustion happens. The system consisted combustion chamber and freeboard as shown in Figure 3.10. Inert bed material (silica sand), air distributor and fed fuel would mix in this system.

The operating temperature of the combustion unit was approximately 850°C. However, it was possible that the temperature in the combustion chamber achieved to 1000°C higher. Refractory materials were used to reduce the heat loss from the bed.

The purpose of freeboard was to reduce the entertainment of particles and to allow the fuels to burn completely by increasing the residence time of solid fuel. As the fuel particle burnt, it's meant size reduces and the weight of these particles decreases. When the terminal velocity was reached, these particles would be entrained but not burnt completely yet. As these particles travel along the freeboard, the combustion of smaller fuel particles could still take place. Thus, the residual fuel in the exhaust was reduced and the combustion efficiency was improved.

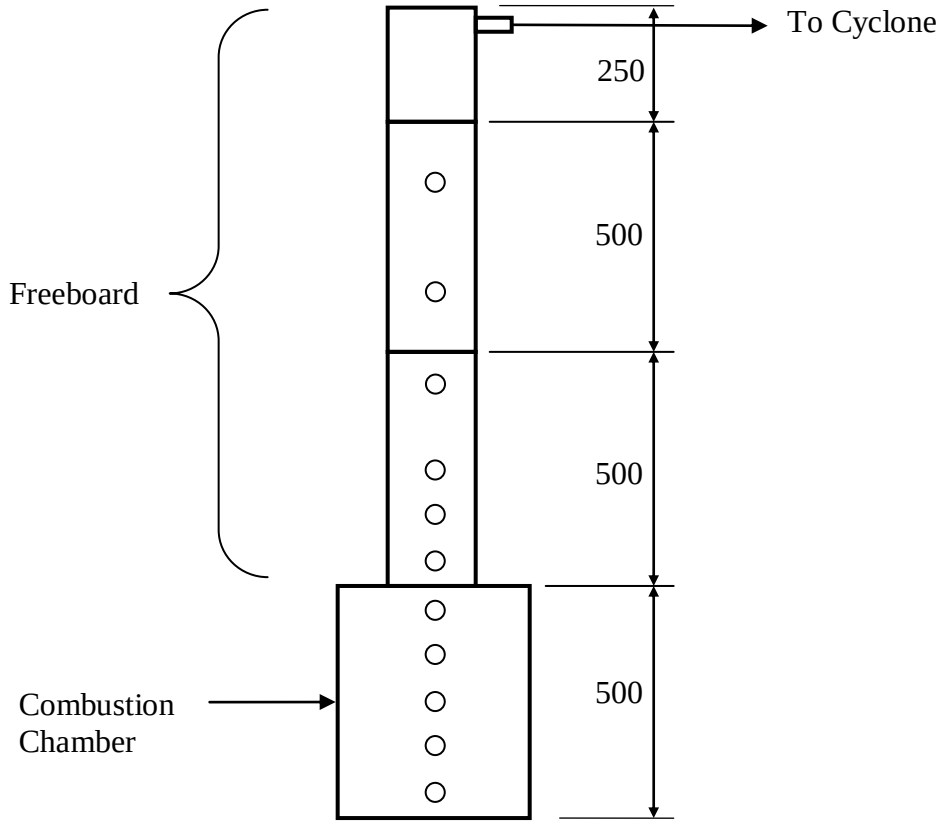

Figure 3.9 Combustion system

v. Gas Separating and Dust Collecting System

Generally, combustion of solid fuel would release gas and dust. Thus, the gas had to be separated with ash before being released to the environment. Cyclone was used to separate the clean gas and dust, as shown in Figure 3.11 . When the dirty gases went into the cyclone, the dust or small particles would separate from the dirty

gas. Then, dust and small particles were collected at the dust collector, which was at the bottom of the cyclone.

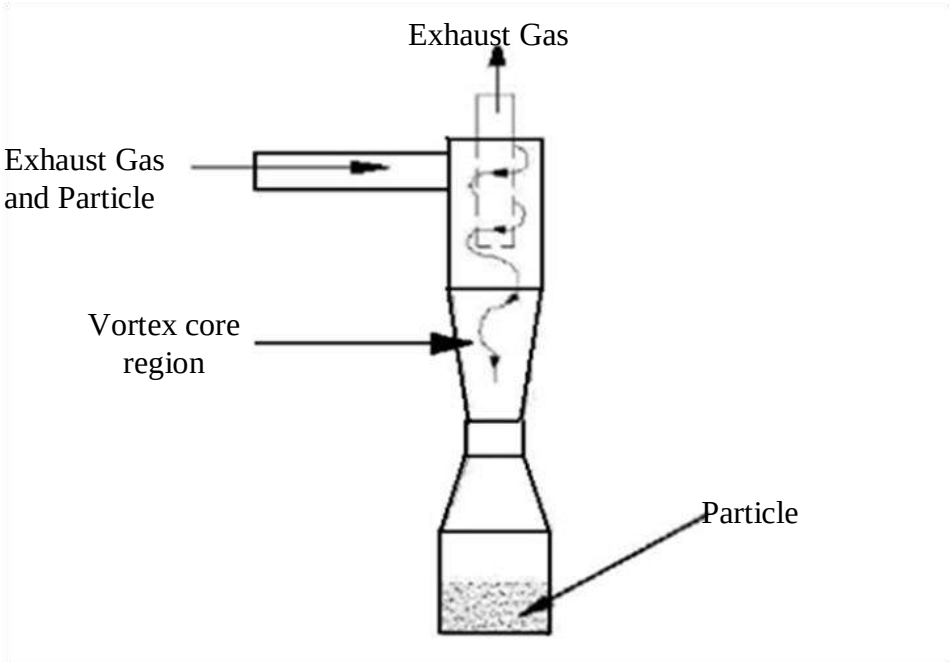

Figure 3.10 Cyclone unit

Figure 3.11 Experimental Rig

3.2.2 Fuel Preparation

There are several criteria were considered in selecting the fuel, such as:

1. Fluidization of the fuel
2. The calorific value of the fuel
3. Moisture contained in the fuel
4. Availability of the fuel
5. The size of the fuel
6. Economical value of the fuel

Oil palm wastes had high calorific values, so it was sufficient to meet the desired thermal output at a low combustion rate (the quantity of fuel to burn for a certain time). Besides that, the size of the fuel was one of the factors affecting feeding efficiency and the combustion efficiency. The actual size of oil palm wastes was quite large for the operation of the fluidized bed combustor used in this experiment. Nevertheless, after grinding into 3mm average diameter, the size reduced to a suitable size to obtain proper fluidization of the solid fuel. Grinding of oil palm wastes would surely increase the operating cost, but this was compensated by the low price of the fuels.

An oil palm waste such as palm shells was selected as the source of fuel for the experiment. The quantity of oil palm wastes in Malaysia was abundant since Malaysia was the largest producer of palm oil product in the world [25, 31, 34, 36, 46-47]. Thus, palm wastes were obtained freely and easily from Kulai Palm Oil Mill of the Federal Land Development Authority (FELDA), Johor, Malaysia. From the sample, the fuel size was grinded for average diameter 3mm. Figure 3.13 shows the fuels (before and after grinding). Meanwhile, detail of fuel preparations was explained in Figure 3.14.

Figure 3.12 Palm shell fuel (before and after grinding)

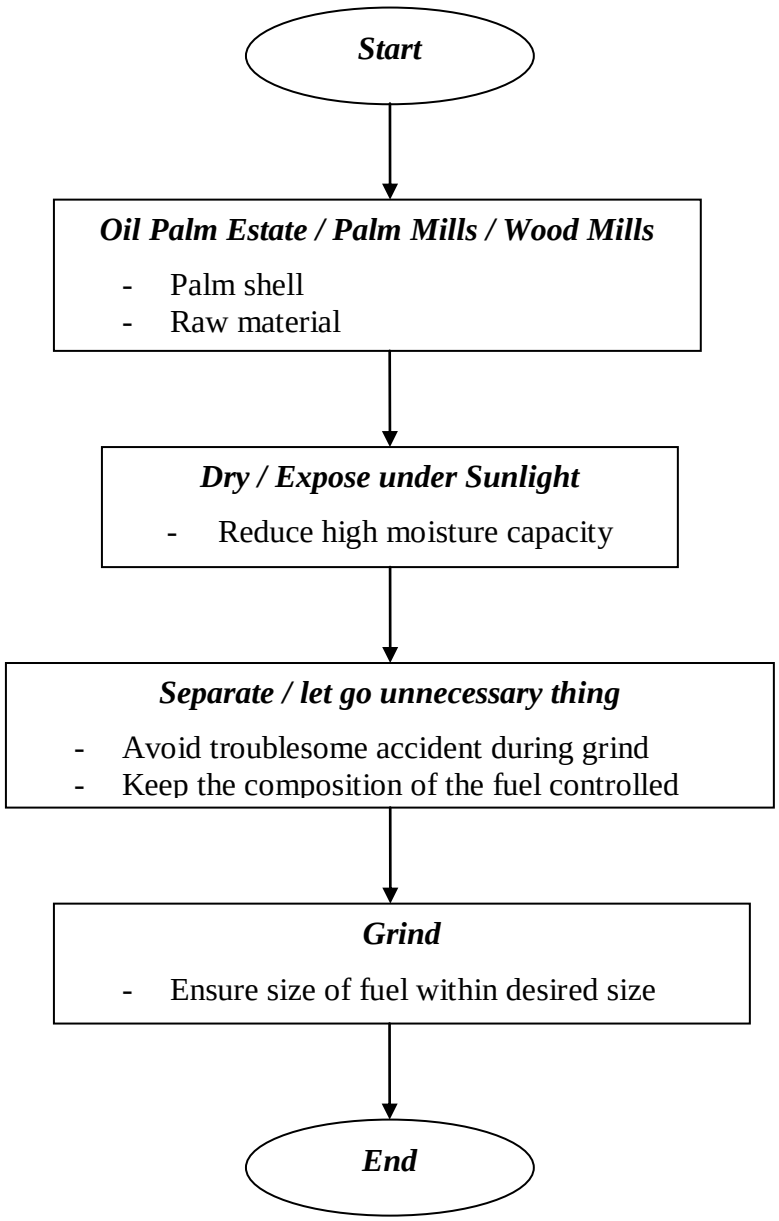

Figure 3.13 Flow chart of fuel preparation [171]

3.2.3 Bed Material Preparation

Generally, sand was classified as Geldart A, Geldart B or even Geldart D particle depending on its size and the fluidizing air. The bed material used in this experiment was silica sand with diameter Ø=300-425µm. This means, the sand type was Geldart B which had a density ρ_s=2500kg/m^3 and with its sphericity Φ_s=0.67 and a high specific heat capacity C=840J/kgK. However, high specific heat meant more time to heat up the bed to the operating temperature, which was one of the factors that enable the substance of fuel combustion. The total amount of sand was approximately 1.5kg and the static height was 3.2cm from the bottom of the combustion chamber.

3.2.4 Proximate Analysis and Ultimate Analysis of Fuel

Biomass, as a fuel had high moisture and volatile content, low bulk density, low specific energy and normally low ash content. The proximate and ultimate analysis of palm shell was shown in Table 3.2. The property tests were analyzed by Tenaga National Berhard (TNB) Research using ASTM Standard.

Table 3. 1 Proximate Analysis and Ultimate Analysis of Palm Shell

Fuel	Proximate Analysis (%)				Ultimate Analysis (%)					GCV (MJ/kg)
	Moisture	Volatile	Fixed Carbon	Ash	C	H	O	N	S	
Palm Shell	7.14	78.05	17.64	4.32	57.94	5.65	31.38	0.65	0.06	20.43

3.2.5 Stoichiometric Air Fuel Ratio Calculation

A balanced chemical equation for complete combustion of the reactants with no excess air in the products was known as a stoichiometric equation. A premixed gas mixture was stated to be stoichiometric if the fuel and oxidizer consumed each other completely. The minimum amount of air required for the complete combustion of a fuel was known as theoretical air. If the fuel composition was known, the requirement of oxygen or air could be calculated either by mass balance or by the mole method. The calculation of oxygen required of 1kg of each fuel as shown in Table 3.3.

Table 3.2 : Calculation of oxygen required of 1kg palm shell

PALM SHELL			
Constituent	Weight per kg	Oxygen required per kg of constituent	Oxygen required per kg of palm shell
C	0.5794	$C + O_2 \rightarrow CO_2$ 12 kg + 32 kg → 44 kg	$0.5794x\frac{32}{12} = 1.5451$
O	0.3138	-	- 0.3138
H	0.0565	$4H + O_2 \rightarrow 2H_2O$ 4 kg + 32 kg → 36 kg	$0..0565x\frac{32}{4} = 0.4520$
N	0.0065	$2N + O_2 \rightarrow 2NO$ 28 kg + 32 kg → 60 kg	$0.0065x\frac{32}{28} = 0.007428571$
S	0.0006	$S + O_2 \rightarrow SO_2$ 32 kg + 32 kg → 64 kg	$0.0006x\frac{32}{32} = 0$
Total oxygen required = 1.5451 - 0.3138 + 0.4520 + 0.007429 + 0 = **1.6913kg**			

In fact, air is contained of approximately 23.3% oxygen by mass. Therefore, the calculation of stoichiometric of air/fuel ratio (AFR) as below:

Minimum air required for complete combustion of 1kg of palm shell

$$= \frac{1.6913kg}{0.233} = 7.2588$$

Therefore, the stoichiometric air/fuel ratio = 7.2588kg air/ kg palm shell.

3.2.6 Fuel Feeding Rate Calculation

Fuel feeding rate was one of the important thing to be calculated before running the experiment. This data was essential in determination of air ratio for the fluidized bed combustion. The solid fuels were inserted into feeder with a particular mass. Then, the time was taken just after the fuels were fed into combustion chamber. Time had to be stopped when the fuel obviously finish in the feeder. This method was iterated for different rotation of Miki Pulley such as rotation 1, 2, 4, 6 and 8. The fuel feeding rate for palm shell for the experiment as shown in Table 3.4 as below:

Table 3.3 : Fuel feeding rate for palm shell

Rotation of Miki Pulley	Mass of fuel (g)	Time (min)	Fuel feeding rate (g/min)
1	50	6	87.9
2	50	7.5	98.5
3	50	9	109.1
4	50	10.5	139.7
5	50	12	170.2
6	50	15.33	197.7
7	50	18.67	225.1
8	50	22	252.6

The calculation for airflow rate for different Excess Air (EA) was shown in Appendix D. Excess air level was varied from 0%, 20%, 40% and 60%. Excess air (EA) level was calculated taking into account both are primary and secondary air. The ratios of primary air (PA): secondary air (SA) used were 100:0, 90:10, 80:20, 70:30 and 60:40 for all excess air levels while the total air rate was maintained constant. The thermocouples were placed at 11-different locations.

3.2.7 Combustion Efficiency Calculation

Actually, the combustion efficiency of a fluidized bed combustor was influenced by the following factors as below

(i) Excess air level

(ii) Bed temperature

(iii) Residence time of the particle (bed depth, freeboard height & recycling fly ash)

Three sources of losses that associated with fuel burning, as below:

a) **Losses due to flue gas:** Moisture & hydrogen, dry flue gas loss, unburned gas, sensible heat of water vapour.

b) **Losses due to refuse:** Combustible in ash, combustible in riddling, combustible in dust.

c) **Other losses:** Radiation, conduction, convection, other unmeasured losses.

There were three types of data to determine the efficiency of the fluidized bed combustion, such as,

a) Known fuel data: Gross calorific value, Q_{gr} (kJ/kg); Net calorific value, Q_{net}(kJ/kg); Net calorific fuel constant, $K1_{net}$; Gross calorific fuel constant, $K1_{gr}$; % Maximum theoretical CO_2 (dry basic), K2%; Wet loss, K3%.

b) Measured data: Flue temperature, T_f ; Inlet temperature, T_i ; % Oxygen in flue gas, O_{2m}.

c) Calculated data:

i. Net temperature, $T_{net} = (T_f - T_i)$

ii. % Dry flue gas loss $= \dfrac{20.9 x K1 net x Tnet}{K2x(20.9 - \%O_2 m)}$

iii. % Wet loss $= \dfrac{9x\%H + \%H_2O}{Q_{gr}x[2488 + 2.1T_f - 4.2T_i]}$

$= \dfrac{9x\%H + \%H_2O}{Q_{gr}x[2488 + 2.1T_f - 4.2T_i]} x2425x(1 + 0.001T_{net})$

Wet loss $= K3x(1 + 0.00\mathcal{Q}T_{net})$

iv. Net efficiency, η_{net} = 100% - [% dry flue gas loss]

$= 100\% - \dfrac{20.9 x K1_{net} x T_{net}}{K2x(20.9 - \%O_2 m)}$

v. Combustion efficiency, η_{gr} =100% - [% dry flue gas loss + % wet loss]

$$= 100\% - \left[\frac{20.9 x K1_{net} x T_{net}}{K2x(20.9 - \%O_2 m)} + K3(1 + 0.001 T_{net}) \right]$$

3.2.8 Experimental Set-Up and Procedure

The experimental combustor was fabricated from mild steel and the height was 0.5m. The reactor was made from stainless steel cylindrical tube of 164mm internal diameter and 2.0m height. The overall rig was divided in five flanged sections. Silica sand with a mean size (diameter) of 300µm was used as the bed material. The height of the sand bed was 32mm.

Combustion air from a blower was introduced into the bed through an air distributor with 36 air outlets that was 6 outlets in each row of 5mm diameter each. Reactor preheating was achieved using Liquefied Petroleum Gas (LPG). Secondary air was introduced at 1000mm above the air distributor with 4 holes in 5mm diameter each, and it was made by stainless steel tube. Flue gas exits the top of the freeboard and enters the cyclone.

Temperature variations along the height of the bed and freeboard were monitored using thermocouples. Gas samples were taken continuously at 1.9m above air distributor by using a portable gas analyser, Tempest 100. The fuel particle size of oil palm shell used is with a mean size (diameter) of 3mm.

The task of heating the material was fulfilled by the pre-heating system. The simplest was to introduce a flame directly into the combustion chamber by using LPG. When the bed temperature reached 450ºC and stabilizes, the fuel was fed through the screw feeder. The fuel was fed into the combustor through the screw feeder at two feed rates, respectively 87.9g/min and 98.5g/min, with mean size particle diameter of a 3mm. When the temperature reached approximately 950ºC

and stabilizes, the emission readings from this combustion unit were taken. Gas samples were taken continuously at 1.9m above the air distributor using a gas analyser. The temperature variations along the height of the bed and freeboard were monitored using thermocouples. The thermocouples were placed at 11-different locations 10mm from the wall into the chamber, and at heights of 60mm (location1), 160mm (location2), 260mm (location3), 360mm (location4), 460mm (location5), 570mm (location6), 670mm (location7), 770mm (location8), 950mm (location9), 1150mm (location10) and 1380mm (location11) above the bed of primary air distributor. Four experimental (0, 20, 40 and 60% excess air) were carried out. For each experiment, air staging combustion tests were performed with the secondary air to total air ratio varied from 0 to 0.4 at 0.1 increments.

3.3 Cold Flow Simulation Method

CFD simulation has become an essential tool of enormous benefit to the engineering field. These have been possible due to the significant advanced in computer technology as well as the advancement in mathematical formulation of many physical processes. With the reduction in the cost of more powerful computer technology and the increase in predictive capability of numerical procedure, CFD simulation of complicated flow has become feasible. Today, CFD simulations can be used successfully to simulate various kinds of flow phenomena to various degree of complexity. However the degree of success will very much depend on the knowledge and understanding of the user of the CFD code regarding the nature of the flow problem in question, the non-linearity of the fluid flow descriptive equations in general and the application of computer simulation in the prediction of such physics.

The phenomena associated with flow inside ABFBC was known to be extremely complex, involving aspects of complicated geometries coupled with a growing complexity in terms of multiphase flow hydrodynamics. Proper design and scale-up of the combustor depend a great deal on the understanding of its hydrodynamics characteristics. To better understand the ABFBC flow behavior,

detailed information was needed especially the dynamic mixing of gas and solid. To this end, experimental study has been one of the approaches for a long time. However, the huge size of current ABFBC design, lab-scale model has not been able to provide enough information for better design. Due to this, numerical simulation of FBC has been receiving growing interest with the rapid development of computational technologies, especially CFD.

For the present study of, silica sand was used as the solid phase, which experience fluidization. For a multiphase flow simulation, the areas of concerns are mainly around the air distributor and the lower end of the freeboard where relatively dense gas-solid flows interactions occur. There are two basic approaches in computational techniques on how to model the solid particles in dense gas-solid flow simulation i.e. the Eulerian-Eulerian approach and the Eulerian-Lagrangian approach. In the Eulerian-Eulerian approach, the solid particles are considered to form a pseudo-fluid and they are modeled with equations similar to the classical Navier-Stokes flow equations. This approach is currently commonly used in FBC simulations and it is a relatively fast and practical approach. It has been implemented in ANSYS FLUENT codes and it is the method of used in this study.

3.3.1 Three Dimensional Model

The simulation case used geometrical model with the same geometry as the lab-scaled ABFBC for cold flow study. A picture of the simulated device is shown in Figure 3.7 and Figure 3.8 shows the computational domain. A 3D full solid model of the ABFBC was drawn using the GAMBIT software version 2.4.6.as shown in Figure 3.6. The whole model was divided into two parts: the combustor and the air distributor. Both parts were drawn as solids.

With the completed full simulation from GAMBIT software, the first step before meshing was to make sure that solid air distributor was subtracted from the whole model. Subsequent to that, the whole model was split into two volumes; the

volume of air inside the air distributor as ‘fluid 2’ and the volume of air outside the air distributor as ‘fluid 1’. This step would be a great help in defining the patch area of the solid phase later on during the ANSYS FLUENT analysis.

The first step in the meshing was to ensure that all faces were meshed. The spacing for the face mesh was set to 1mm. Following the face meshing, the volume was meshed, as this was a 3D simulation case. A size function of 1.5mm to 8mm with a growth rate of 1.05mm was set for the volume mesh as to refine the mesh at the critical area only. This step ensured that the optimum number of meshed elements was obtained as a higher number of elements would produce a higher computing time. The total number of elements for the completely meshed model was 2,161,199. In addition, the skewness of the worst element was 0.78. This value was reasonable and falls in the acceptable range, as it did not exceed 0.85. The number of mesh was able to produce independent solution.

(a) (b)

Figure 3.14 (a) Fabricated Model and (b) 3D Simulated Model

3.3.2 Basic Governing Equation of Solid-Gas Phase

The Eulerian granular model in ANSYS FLUENT was used to study the flow behavior in the model lab-scale ABFBC, in which the stress of the solid phase was described with the kinetic theory of granular flow; the drag coefficient correlation was corrected with consideration of particle clusters. The continuity and momentum equations for multiphase flow are obtained by time averaging process for each phase. These equations are analogous to the single phase Navier-Stoke equations but with some additional terms related to the interactions between the phases and there is also a pressure term for the solid phase. The basic governing equations of mass and momentum conservation of fluidizing theory for both phases are summarized as follows [118]:

.

Finite volume method was used to solve the set of governing equations. The steady state equations of continuity for phase gas and solid with temporal and spatial gradients are given as:

$$\frac{\partial}{\partial t}\left(\alpha_g + \rho_g\right) + \nabla.\left(\alpha_g\, \rho_g\, \vec{v}_g\right) = 0 \tag{3. 1}$$

$$\frac{\partial}{\partial \mathrm{t}}(\alpha_\mathrm{s} + \rho_\mathrm{s}) + \nabla \cdot (\alpha_\mathrm{s}\, \rho_\mathrm{s}\, \vec{v}_\mathrm{s}) = 0 \tag{3. 2}$$

The phase volume fractions satisfy the following condition: $\alpha_\mathrm{s} + \alpha_\mathrm{g} = 1$

The momentum balance for each phase given by the Navier–Stokes equation is modified to include an interphase momentum transfer term and a solid phase source term:

$$\frac{\partial}{\partial t}\left(\alpha_g\, \rho_g \vec{v}_g\right) + \nabla.\left(\alpha_g\, \rho_g\, \vec{v}_g \vec{v}_g\right) = -\alpha_g\, \nabla \mathrm{p} + \nabla \cdot \left(\alpha_g \left(\overline{\overline{\tau_g^m}} + \overline{\overline{\tau_g^{Re}}}\right)\right) + \alpha_g\, \rho_g\, \vec{g} + K_{sg}\left(\vec{v}_s - \vec{v}_g\right) \tag{3. 3}$$

$$\frac{\partial}{\partial t}(\alpha_s\, \rho_s \vec{v}_s) + \nabla \cdot (\alpha_s\, \rho_s\, \vec{v}_s \vec{v}_s) = -\alpha_s\, \nabla \mathrm{p} + \nabla p_s\, \nabla \cdot \left(\alpha_s \left(\overline{\overline{\tau_s^m}} + \overline{\overline{\tau_s^{Re}}}\right)\right)$$

$$+ \alpha_s \rho_s \vec{g} + K_{gs}(\vec{v}_g - \vec{v}_s) \quad (3.4)$$

where the left side represents the temporal and spatial transport terms and the right side represents the various interacting forces. The interactions of each phase involve various momentum exchange mechanisms such as the drag, the lift and added mass force, etc. However, its effect of the other forces was ignored while its contribution of drag force was considered.

Analogous to the thermodynamic temperature for gases, the granular temperature Θ_s can be introduced as a measure of the particle velocity fluctuation, i.e.

$$\Theta_s = \frac{1}{3}\vec{v}_s'^2 \quad (3.5)$$

where: $\vec{v}_s'$ the solids fluctuating velocity.

The granular temperature is obtained by solving its transport equation that is:

$$\frac{3}{2}\left[\frac{\partial}{\partial t}(\rho_s \alpha_s \Theta_s) + \nabla \cdot (\rho_s \alpha_s \Theta_s)\right] = (-p_s \bar{\bar{I}} + \bar{\bar{\tau}}_s) : \nabla \vec{v}_s + \nabla \cdot (k_{\Theta_s} \nabla \Theta_s) - \gamma_{\Theta_s} + \Phi_{gs} \quad (3.6)$$

where:

$(-p_s \bar{\bar{I}} + \bar{\bar{\tau}}_s) : \nabla \vec{v}_s$ the generation of energy by the solid stress tensor because of the interaction between the normal and shear stress matrix with the mean velocity field,

$k_{\Theta_s} \nabla \Theta_s$ acounts for the transport of energy due to diffusion

k_{Θ_s} the diffusion coefficient

γ_{Θ_s} the dissipation of energy due to collision and is given as,

$$\gamma_{\Theta_s} = \frac{12(1-e_{ss}^2) g_{0,ss}}{d_s \sqrt{\pi}} \rho_s \alpha_s^2 \Theta_s^{3/2} \quad (3.7)$$

Φ_{gs} the exchange of kinetic energy between the solid and the gas phases, given as,

$$\Phi_{gs} = -3k_{gs}\Theta_s \tag{3. 8}$$

The granular temperature at the wall is

$$q_s = \frac{\pi}{6}\sqrt{3}\Phi\ \frac{\alpha_s}{\alpha_{s,max}}\ \rho_s g_0 \sqrt{\Theta_s}\ v_{t,w}^2 - \frac{\pi}{4}\sqrt{3}\ \frac{\alpha_s}{\alpha_{s,max}}\ (1 - e_{sw}^2)\rho_s g_0 \Theta_s^{3/2} \tag{3. 9}$$

The stress–strain tensor for each phase is given as,

$$\overline{\overline{\tau_s^m}} = \left(\lambda_s - \frac{2}{3}\mu_s\right)\nabla \cdot \vec{v}_s\ \bar{\bar{I}} + \mu_s(\nabla \vec{v}_s + \nabla \vec{v}_s^T) \tag{3. 10}$$

$$\overline{\overline{\tau_g^m}} = \left(\lambda_g - \frac{2}{3}\mu_g\right)\nabla \cdot \vec{v}_g\ \bar{\bar{I}} + \mu_g\left(\nabla \vec{v}_g + \nabla \vec{v}_g^T\right) \tag{3. 11}$$

The Reynold stress tensor for each phase is given as,

$$\overline{\overline{\tau_s^{Re}}} = -\frac{2}{3}\left(\rho k_s + \mu_{s,t}\nabla \cdot \vec{v}_s\right)\bar{\bar{I}} + \mu_{s,t}(\nabla \vec{v}_s + \nabla \vec{v}_s^T) \tag{3. 12}$$

$$\overline{\overline{\tau_g^{Re}}} = \frac{2}{3}\left(\rho k_g + \mu_{g,t}\nabla \cdot \vec{v}_g\right)\bar{\bar{I}} + \mu_{g,t}\left(\nabla \vec{v}_g + \nabla \vec{v}_g^T\right) \tag{3. 13}$$

The turbulent viscosities $\mu_{g,t}$ and $\mu_{s,t}$ are obtained by a modified standard *k*–ε turbulence model include the interaction between the two phases. Its turbulent viscosity for each phase is given as:

$$\mu_{g,t} = \rho_g C_\mu \frac{k_g^2}{\varepsilon_g} \tag{3. 14}$$

$$\mu_{s,t} = \rho_s C_\mu \frac{k_s^2}{\varepsilon_s} \tag{3. 15}$$

For the *k*-ε model, the *k* equation for each phase is given as:

$$\frac{\partial}{\partial t}\left(\alpha_g \rho_g k_g\right) + \nabla \cdot \left(\alpha_g \rho_g \vec{v}_g k_g\right) = \nabla \cdot \left(\alpha_g \frac{\mu_{g,t}}{\sigma_k} \nabla k_g\right) + \left(\alpha_g G_{g,k} - \alpha_g \rho_g \varepsilon_g\right) + K_{sg}\left(C_{sg} k_s - C_{gs} k_g\right) - K_{sg}\left(\vec{v}_s - \vec{v}_g\right) \cdot \frac{\mu_{s,t}}{\alpha_s \sigma_s} \nabla \alpha_s + K_{sg}\left(\vec{v}_s - \vec{v}_g\right) \cdot \frac{\mu_{g,t}}{\alpha_g \sigma_g} \nabla \alpha_g \quad (3.16)$$

$$\frac{\partial}{\partial t}\left(\alpha_s \rho_s k_s\right) + \nabla \cdot \left(\alpha_s \rho_s \vec{v}_s k_s\right) = \nabla \cdot \left(\alpha_s \frac{\mu_{s,t}}{\sigma_k} \nabla k_s\right) + \left(\alpha_s G_{s,k} - \alpha_s \rho_s \varepsilon_s\right) + K_{gs}\left(C_{gs} k_g - C_{sg} k_s\right) - K_{gs}\left(\vec{v}_g - \vec{v}_s\right) \cdot \frac{\mu_{g,t}}{\alpha_g \sigma_g} \nabla \alpha_g + K_{gs}\left(\vec{v}_g - \vec{v}_s\right) \cdot \frac{\mu_{s,t}}{\alpha_s \sigma_s} \nabla \alpha_s \quad (3.17)$$

The ε equation for each phase is given as:

$$\frac{\partial}{\partial t}\left(\alpha_g \rho_g \varepsilon_g\right) + \nabla \cdot \left(\alpha_g \rho_g \vec{v}_g \varepsilon_g\right) = \nabla \cdot \left(\alpha_g \frac{\mu_{g,t}}{\sigma_k} \nabla \varepsilon_g\right) + \frac{\varepsilon_g}{k_g}\left(C_{1\varepsilon} \alpha_g G_{g,k} - C_{2\varepsilon} \alpha_g \rho_g \varepsilon_g + C_{3\varepsilon}\left(K_{sg}\left(C_{sg} k_s - C_{gs} k_g\right) - K_{sg}\left(\vec{v}_s - \vec{v}_g\right) \cdot \frac{\mu_{s,t}}{\alpha_s \sigma_s} \nabla \alpha_s + K_{sg}\left(\vec{v}_s - \vec{v}_g\right) \cdot \frac{\mu_{g,t}}{\alpha_g \sigma_g} \nabla \alpha_g\right)\right) \quad (3.18)$$

$$\frac{\partial}{\partial t}\left(\alpha_s \rho_s \varepsilon_s\right) + \nabla \cdot \left(\alpha_s \rho_s \vec{v}_s \varepsilon_s\right) = \nabla \cdot \left(\alpha_s \frac{\mu_{s,t}}{\sigma_k} \nabla \varepsilon_s\right) + \frac{\varepsilon_s}{k_s}\left(C_{1\varepsilon} \alpha_s G_{s,k} - C_{2\varepsilon} \alpha_s \rho_s \varepsilon_s + C_{3\varepsilon}\left(K_{gs}\left(C_{gs} k_g - C_{sg} k_s\right) - K_{gs}\left(\vec{v}_g - \vec{v}_s\right) \cdot \frac{\mu_{g,t}}{\alpha_g \sigma_g} \nabla \alpha_g + K_{gs}\left(\vec{v}_g - \vec{v}_s\right) \cdot \frac{\mu_{s,t}}{\alpha_s \sigma_s} \nabla \alpha_s\right)\right) \quad (3.19)$$

The last two terms on the right-hand side of k–ε equations are used to account for the effect of the solids phase on the gas phase turbulence or the gas phase on solids phase turbulence.

The interaction between gas and solids was expressed in the form of drag force, which is used to model the momentum exchange between gas phase and solids phase. Drag is caused by relative motion between phases. The drag coefficient is related to the flow regime and the properties of the two phases. The drag coefficient, Syamlal and O'Brien correlation, is commonly used to estimate for fluidized beds.

$$K_{sg} = \frac{3\alpha_s \alpha_g \rho_g}{4 v_{r,s}^2 d_s}\left(0.63 + \frac{4.8}{\sqrt{\mathrm{Re_s}}/v_{r,s}}\right)^2 \left(\frac{\mathrm{Re_s}}{v_{r,s}}\right)\left|\vec{v}_s - \vec{v}_g\right| \quad (3.\ 20)$$

3.3.3 ANSYS FLUENT Analysis

The ANSYS Fluent analysis was conducted by adhering closely to the following steps.

i. Model simulation : 3D

ii. Turbulence model : standard *k*-ε

iii. Properties of material:

Gas phase

Air density : ideal gas

Inlet air velocity : 5.76m/s

Silica Sand as solid phase

Diameter : 0.365mm

Density : 2500kg/m^3

iv. Drag correlation : Syamlal-O'Brien (see Appendix E)

v. Operating temperature: 300K

vi. Volume fraction of sand: 0.5

vii. Boundary Conditions

- Boundary condition specifies the flow and thermal variables on the boundary of its physical model. Therefore, it was a critical component of ANSYS FLUENT simulations and it is important that they are specified appropriately. In ANSYS FLUENT, boundary conditions are associated with zones, not with individual faces or cells. To combine two or more zones that will have the same boundary conditions, it has to merge zones.
- To carry out the simulation in the present ABFBC study, the boundary conditions at the inlet, wall and outlet were specified respectively as follows:
  - Inlet: the inlet gas phase passes through a distributor plate, which produces a relatively uniform inlet gas velocity profile. The gas phase was presented in the inlet stream and enters with a uniform velocity profile with homogeneous temperature and pressure.

- Wall: No-slip boundary condition for the gas phase interaction. And partial slip condition for the solids interactions. The velocity normal to the wall was specified as zero, i.e. no solids mass flow across the wall, while the solids phase is allowed to slip along the wall. Wall heat transfer was also set.
- Outlet: The outlet boundary condition was specified as a pressure outlet. The gas phase pressure at the outlet of the reactor was set equal to the atmospheric condition.

viii. Initial Conditions

➢ Initial conditions typically are not of interest because solutions are dependent on boundary conditions. However, initial conditions must be specified as realistic values to promote convergence. The initial conditions that were specified in the bed region and the freeboard were the gas velocities, and the volume fractions of each phase.

To validate developed model, results from a three dimensional (3D) simulation were compared with experimental velocity vector profiles.

3.4 Hot Flow Simulation Method

Mathematical modeling of turbulent multiphase reacting flow is of primary importance for design, optimization, and scale-up of many relevant processes, such as those occurring in the ABFBC. There are many aspects that need to be given special attention in order to properly model such flows. The fluid-dynamic interaction between the gas and solid phases is a crucial factor, in fact, it determines turbulence intensity, mixing rates, and mass and heat transfer. In the case of reacting multiphase flows, this interaction has a strong effect on reaction rates that, in turn, can greatly affect the reaction flow field.

To study multiphase turbulent reacting flow in a fluidized bed combustor, experimental tests are usually employed on small-scale fluidized beds. It is

impractical and cost prohibitive to employ such experimental techniques on huge-scale fluidized beds. An alternative method of study is computational fluid dynamics (CFD) modeling of fluidized beds. CFD models can be validated using small-scale experimental reactors or industrial full-scale reactors. Validated CFD models can be used to scale-up ABFBC design without large pilot-scale facilities. CFD modeling of reacting flow in fluidized bed reactors is a challenging area of study due to the complexities of gas-solid interactions, solid-solid interactions, and chemical kinetics.

In the present study, numerical modeling of multiphase turbulent reacting flow was carried out on the ABFBC which has the same geometry as the lab-scale experimental facility. The simulation was done using commercial CFD codes, the ANSYS Fluent 13.0 using Eulerian multiphase model kinetic theory of granular flow approach with species transport. Standard k-ε turbulence model was used to account for gas and solid phase turbulence.

3.4.1 Three Dimensional Model

All simulations have been done in three-dimensions (3D). The domain of ABFBC for the simulation is shown in Figure 3.17. The basic governing equations of mass and momentum conservation of fluidizing theory for both phases are given in Equation (3.1) to (3.20).

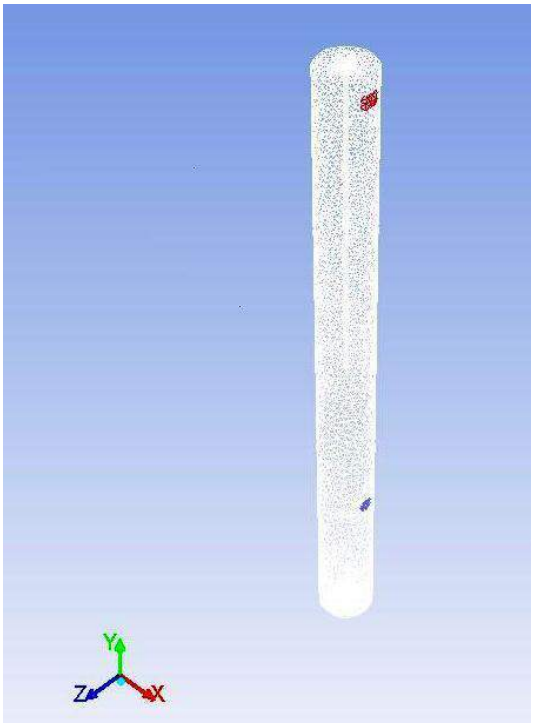

Figure 3. 15: Grid Meshing of ABFBC

3.4.2 ANSYS FLUENT Analysis

The ANSYS Fluent analysis was conducted by adhering closely to the following steps.

i. Model simulation: three-dimensions (3D)

ii. Reactions: single step reaction

$$C_{1.29}H_{2.15}O_{0.75}N_{0.0178} + 1.45O_2 \Rightarrow 1.29CO_2 + 1.07H_2O + 0.0089N_2$$

iii. Turbulence model: standard *k*-ε

iv. Turbulence Chemistry Interaction: Eddy Dissipation

v. Properties of material:

Mixture material (air + volatile) as gas phase

Density	:	incompressible ideal gas
Air density	:	ideal gas
Air velocity	:	5.76m/s
Fuel velocity	:	10m/s

Silica Sand as solid phase:

Average diameter : 0.365mm

Density : 2500kg/m^3

Viscosity :

vi. Drag correlation : Syamlal-O'Brien (see Appendix E)

vii. Operating temperature : 300K

viii. Volume fraction of sand : 0.5

viii. Boundary Conditions

➢ Boundary condition specifies the flow and thermal variables on the boundary of its physical model. Therefore, it was a critical component of ANSYS FLUENT simulations and it is important that they are specified appropriately. In ANSYS FLUENT, boundary conditions are associated with zones, not with individual faces or cells. To combine two or more zones that will have the same boundary conditions, it has to merge zones.

➢ To carry out the simulation in the present ABFBC study, the boundary conditions at the inlet, wall and outlet were specified respectively as follows:

- Inlet gas phase: the inlet gas phase passes through a distributor plate, which produces a relatively uniform inlet gas velocity profile. The gas phase was presented in the inlet stream and enters with a uniform velocity profile with homogeneous temperature and pressure.
- Inlet fuel: the inlet fuel passes through a hole of fuel feeder, which produces a relatively uniform inlet fuel velocity profile.
- Wall: No-slip boundary condition for the gas phase interaction. And partial slip condition for the solids interactions. The velocity normal to the wall was specified as zero, i.e. no solids mass flow across the wall, while the solids phase is allowed to slip along the wall. Wall heat transfer was also set.
- Outlet: The outlet boundary condition was specified as a pressure outlet. The gas phase pressure at the outlet of the reactor was set equal to the atmospheric condition.

ix. Initial Conditions

➢ Initial conditions typically are not of interest because solutions are dependent on boundary conditions. However, initial conditions must be specified as realistic values to promote convergence. The two

initial conditions that were specified in the bed region and the freeboard were the gas and (fuel) solid phase's velocities, and the volume fractions of each phase.

Then, the simulation results were validated with experimental temperature profiles in the combustor.

CHAPTER 4

COLD FLOW RESULTS AND DISCUSSION

4.1 Introduction

Practical FBC flows occur in large enclosures which make their internal hydrodynamics and flow patterns difficult to be studied and substantially characterized. To better understand the FBC flow behavior, detailed of information especially the dynamic mixing of gas-solid and solid-wall interaction was needed. One of the successful methods to study the hydrodynamics in real FBC is through isothermal or cold flow modeling, either physically through flow visualization experiments or numerically through CFD simulation. A cold flow is one in which no reaction take place and no heat is added by an energy source. This makes cold flow models to become of particular interest since the flow inside the combustor can be studied without the additional complexities of combustion models. Furthermore, the flow in a FBC is a multiphase flow and multiphase combustion condition is a complex phenomenon and quite a daunting for CFD simulation especially in an unsteady state condition. In order to validate some of the physics of FBC hydrodynamics such as the behavior of gas-solid interaction and the turbulent models, cold flow modeling could be carried out. Cold flow performance can be used for preliminary evaluation of physical models for further CFD simulation. The understanding of cold flow non-reacting FBC hydrodynamics is also very important in the design phase, especially for the determination of an improved configuration for better design and scale-up of the combustor.

The present cold flow studies were carried out to study the flow patterns and the internal hydrodynamics of an ABFBC. These helped to improve the

understanding of the nature and description of the hydrodynamics and gas-solid mixing processes in a non-reacting environment. Experimental and CFD modeling were carried out on the cylindrical acrylic glass combustor employing 'tuyere' air distributor as shown in Figures 3.7 and 3.8 respectively. The region of interest for cold flow modeling was the area around the air distributor and the lower part of the freeboard. For experimental study, flow visualization was effected by the techniques of PIV. Since silica sand was used, no seeding was required for the PIV measurement. CFD simulation was achieved using ANSYS FLUENT commercial codes.

4.2 PIV Based Experimental Results

The PIV experiment was carried out at 5.76m/s inlet air velocity. The PIV measurement in term of high resolution images were taken at five different heights from the base of the chamber i.e. at 150mm (Height1), 350mm (Height2); 400mm (Height3), 500mm (Height4) and 700mm (Height5) using CCD camera. Height of the silica sand was initially 270mm, before introduction of the air.

The experiment resulted in 150 images of PIV running data. Each height produced 30 captured images, in which the lapsed time between two events of image captured was 0.5seconds. The best image, which was selected from the set of the 30 captured images during the experiment, was then, analyzed using PIV Flow Map software. Cross correlation procedure was carried out as described in the method of Flow Map Software, as shown in Figure 4.1, step 1 to step 8. For example, for the images taken at Height3, the images were cross correlated, validated and filtered resulting in the best velocity vectors as shown in Figure 4.2.

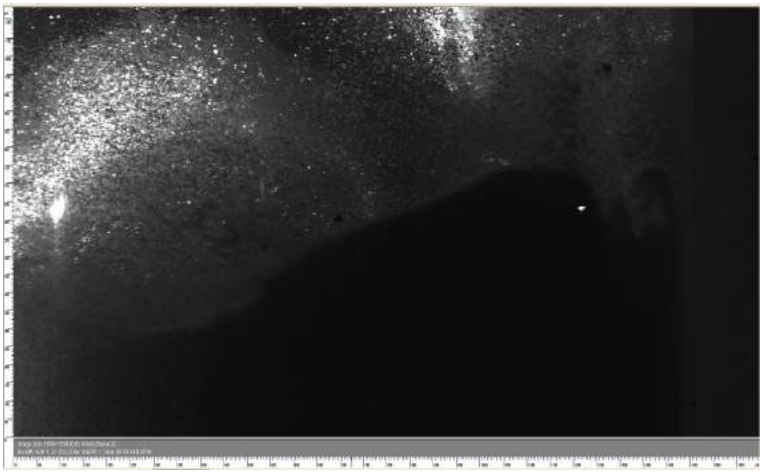

Step 1: Image captured by CCD camera

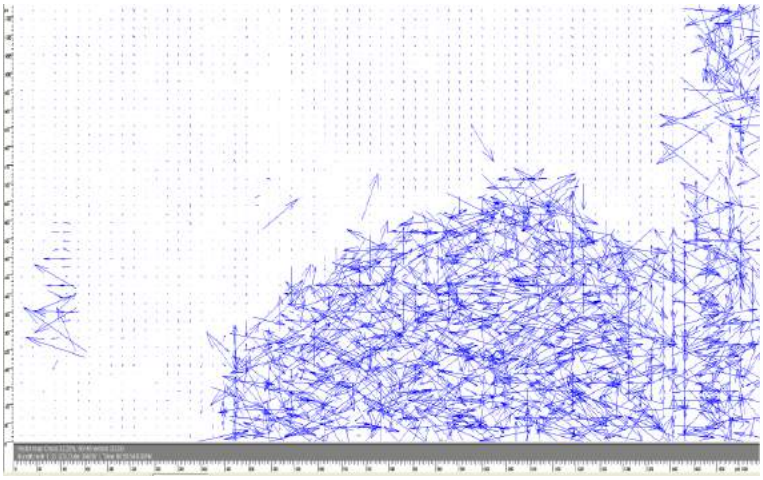

Step 2: Cross - Correlation Method 25%

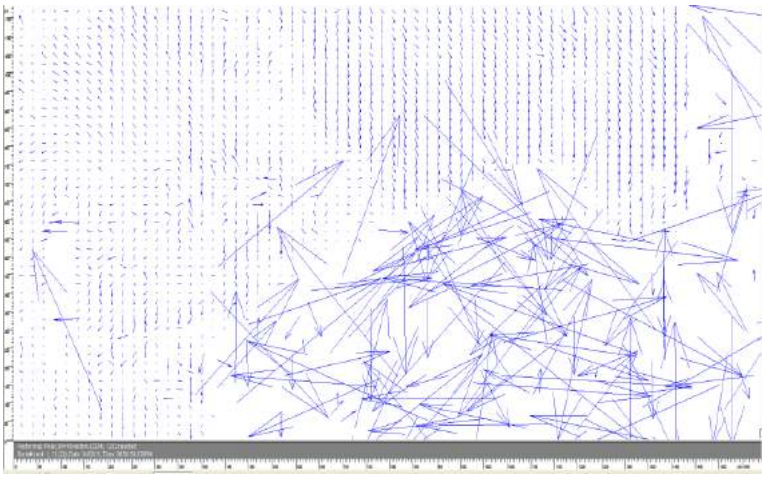

Step 3: Peak Height Validation

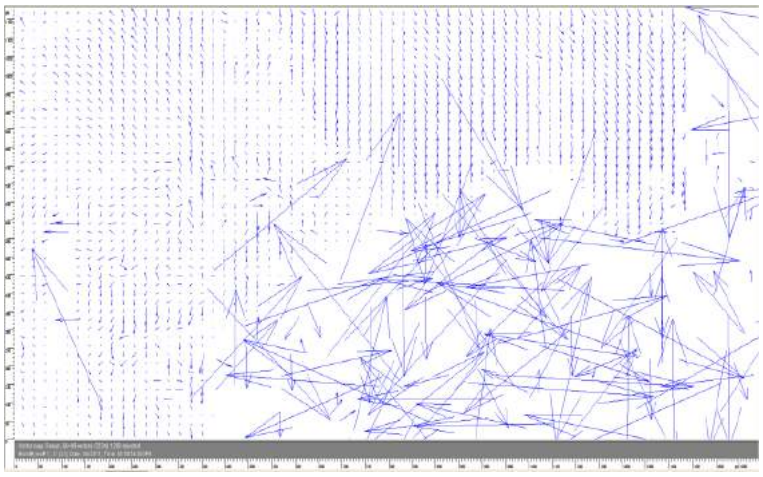

Step 4: Velocity Range Validation

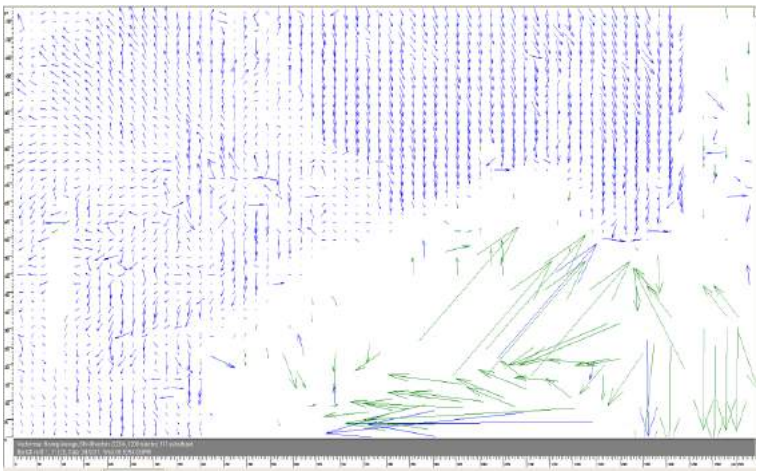

Step 5: Moving Average Validation

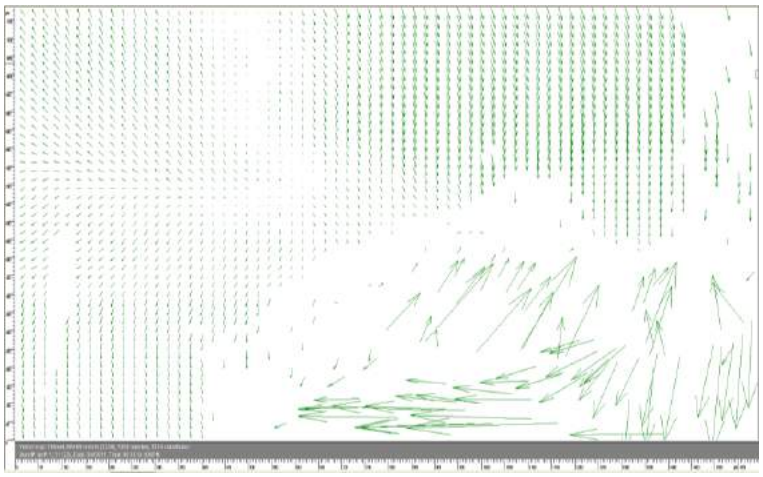

Step 6: Filtered Velocity Vector

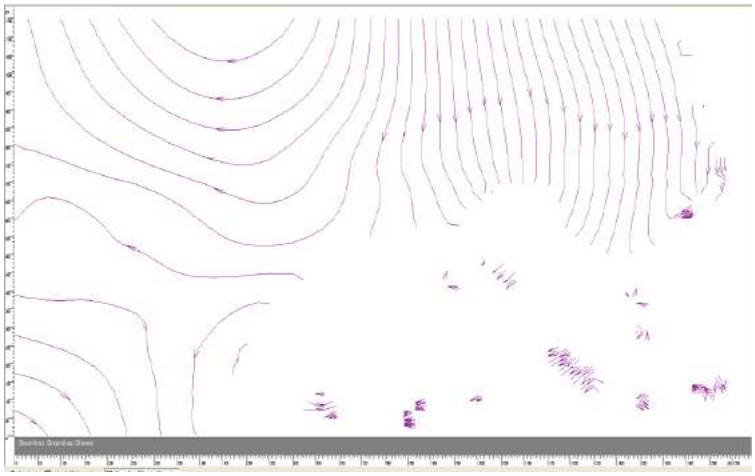

Step 7: Streamline

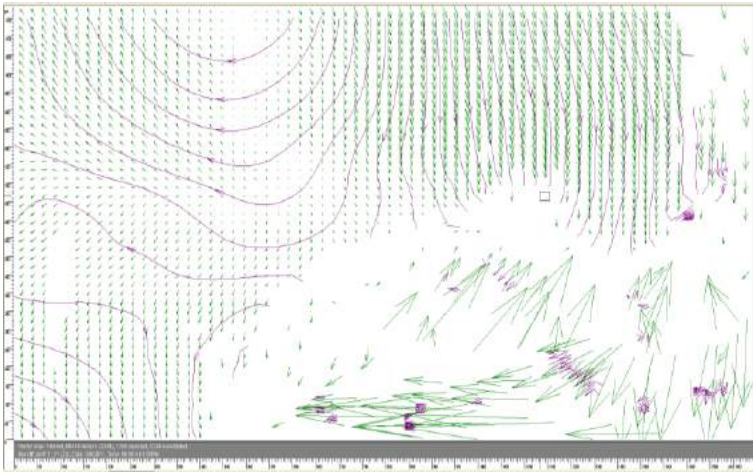

Step 8: Combination of Filtered Vector and Streamline

Figure 4.1 Processing steps for the PIV Measurement at Height3

Figure 4.1 also shows the velocity vectors at the bottom right side of the chamber could not be processed. The area where the velocities could not be processed were in the ranged between 30mm to 70mm radial distance from the center. This is due to the inability of the laser light of the PIV to penetrate dense gas-solid flow since the solid phase is opaque silica sand. For a better image, translucent solid material such as micro glass bead had to be used. The used of silica sand is only useful if the captured images are converted into movie.

Figure 4.2 shows, the velocities in the chamber at Height1 were between 1.5 to 3.5m/s and for Height2, Height3, Height4 and Height5 the velocities were 0.1 to 0.6m/s. The quality of the results was also affected by the cylindrical Perspex wall, which reduced the laser light to the camera. Again, the sand granules were also too dense, thus not allowing enough lasers light to pass through. The condition was worst at Height1, thus the camera could not capture the results at this height properly.

At other heights, the sand was thin enough to allow enough light for the solid particle to be captured by the camera, thus giving better results.

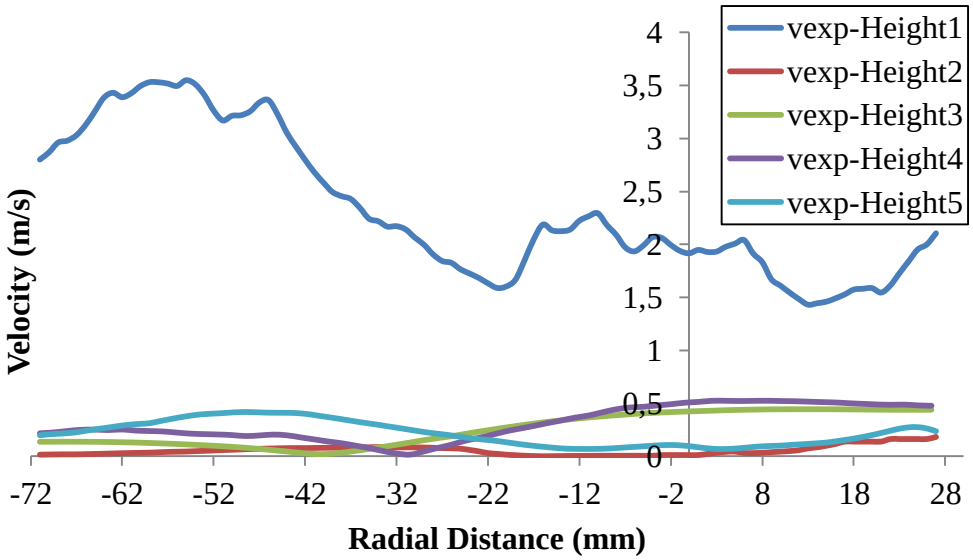

Figure 4.2 Velocity distribution of silica sand for 5.76m/s air intake velocity at Height1, Height2, Height3, Height4 and Height5 that obtained by PIV measurement

4.3 Results for numerical analysis for 5.76m/s air intake velocity

This numerical simulation was carried out using ANSYS Fluent 13.0 to simulate the flow hydrodynamics inside the same geometry as the experimental model ABFBC. The inlet boundary condition was set as velocity inlet 5.76m/s and the outlet was set as pressure outlet at atmospheric pressure. The configuration with

simulation condition as discussed in section 3.2.3 and Table 3.2 was performed using steady state model. Figure 4.3 shows the volume fraction of the sand during the simulation after 100, 200, 300, 800, 1300 and 1500 iterations. The results show that the calculations started to converge after 1300 iterations, with the sand filling the chamber to 2000mm height from the chamber base.

Figure 4.4 shows the velocity distribution in the chamber at different heights. The velocities at the central axis were 0.1m/s for Height1 and between 0.75m/s to 1.2m/s for the other heights.

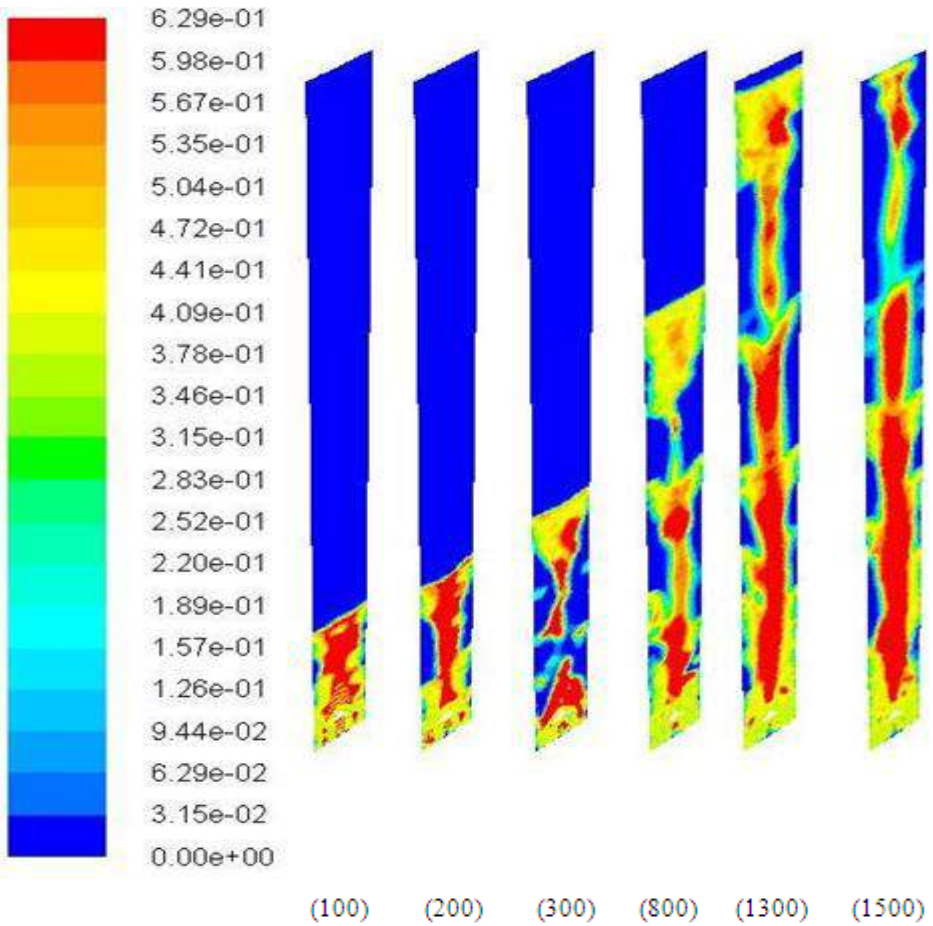

Figure 4.3 Central plane contours of volume fraction of silica sand (Phase 2) after different iterations

The horizontal velocity distribution shows that the velocity was highest at the central axis and decreased slowly along the radius until r=60mm (r/R=0.83). It then

increased to a peak at r=67mm (r/R=0.93), and then dropping sharply to near zero at the wall. These profiles were similar with the results by Nan Zhang, et al. [167].

The simulated results from the developed model were validated using the experimental measurement, in terms of the velocity vector of the sand at 5 chosen heights, as shown in Figure 4.4 to Figure 4.9. In these comparisons, both measured experimental results and the simulated results were based on similar input variables.

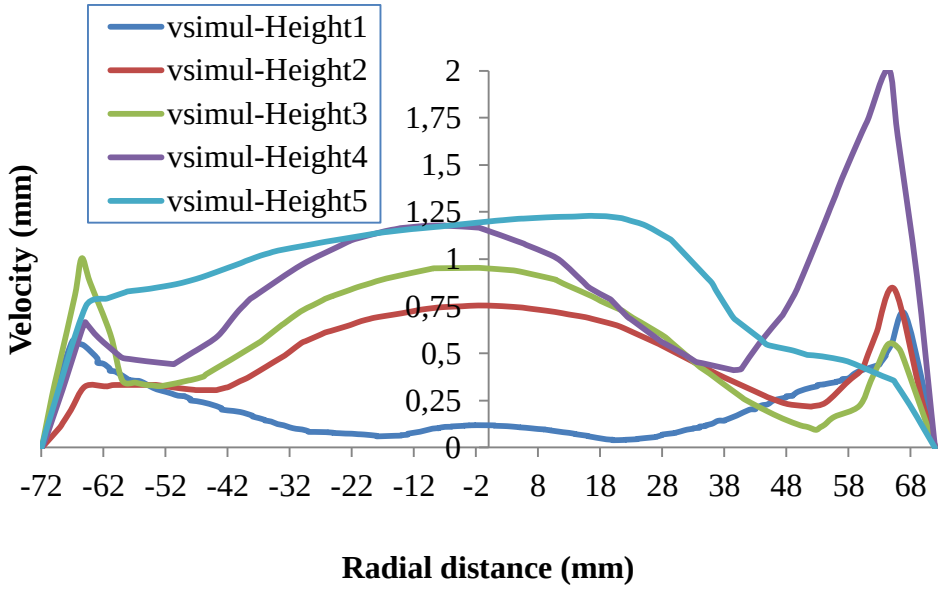

Figure 4.4 Numerical Velocity Vectors of Silica Sand at 5.76m/s Air Velocity at Height1, Height2, Height3, Height4 and Height5

At Height1, Figure 4.5 shows that there were some agreement in the trend between measured and simulated results as they produce similar trend that decreased in the centre and near the wall. In term of quantative value, the result is still not acceptable .the velocity of the experiment were much bigger than the simulation results.

At Height2, both results have no similar velocity trends. The simulation results show velocity vectors increase in the centre and then decrease near the wall. Meanwhile, from experimental results, the velocity vectors at the central region decrease to almost stationary. This does not agree with the simulation results, which

can be clearly seen in Figure 4.6. There is no result from experiment for the region r=28mm to 72mm

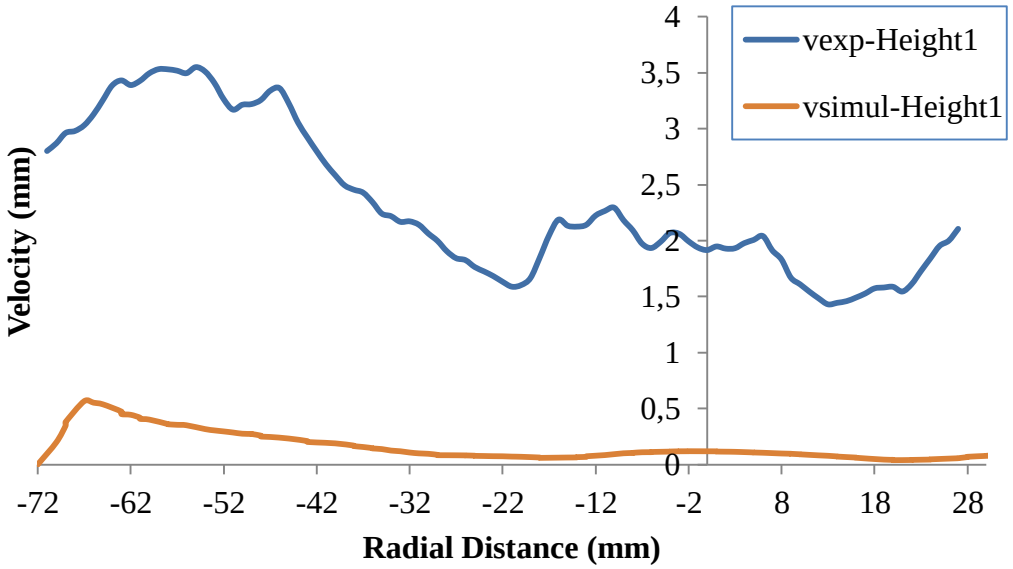

Figure 4.5 Velocity of Silica Sand at Height1 for 5.76m/s air intake velocity by experiment and Numerical analysis

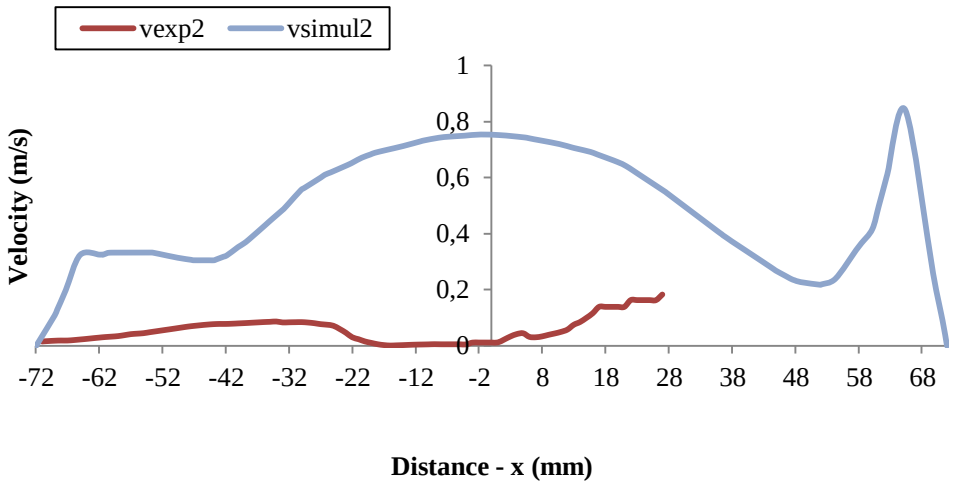

Figure 4.6 Experimental and Simulation Velocity of Silica Sand at 5.76m/s Air Velocity at Height2

At Height3 and Height4, the velocities are higher than Height 1, as shown in Figure 4.7 and Figure 4.8. The radial distributions show similar trends between experimental and simulation results. The velocity from simulation is highest at the

centre of the chamber but decreases towards the wall until about r=48mm. Then it increased sharply to a maximum at r=64mm. Then it falls again to almost zero at the wall. The profile is similar to the experimental results, although the velocities are much lower.

Figures 4.7 and Figure 4.8 show good agreement between experiment and simulation results for height; Height1, Height3, and Height4. Thus, it can be said that Height3 and Height4 are the ideal location to investigate velocity distribution using PIV measurements. This was so because of the sand concentration was much lower at these two heights, thus giving better image capture by the CCD camera. Furthermore, the thinner concentration allowed the sand to move more freely. The profiles are similar to those reported by Fan et al. [147].

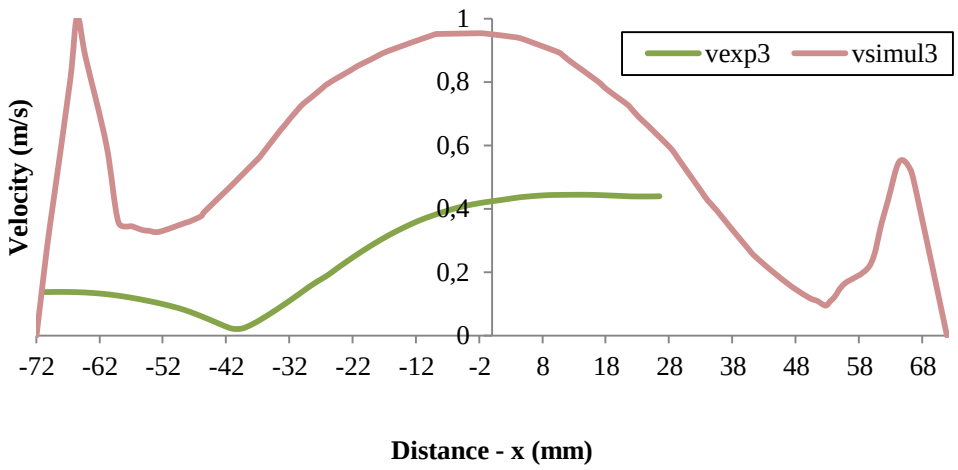

Figure 4.7 Experimental and Simulation Velocity of Silica Sand at 5.76m/s Air Velocity at Height3

Figure 4.9 shows the velocity distribution at Height5. The trend of velocity distribution from both experiment and simulation does not follow the same trend. The velocity vectors from simulation results are highest in the centre and decrease toward the wall. Meanwhile, the experimental results show low velocities of 0.1m/s in the centre which then increase to a maximum of 0.4m/s at r=50mm. Then it decreased to 0.2m/s at the wall.

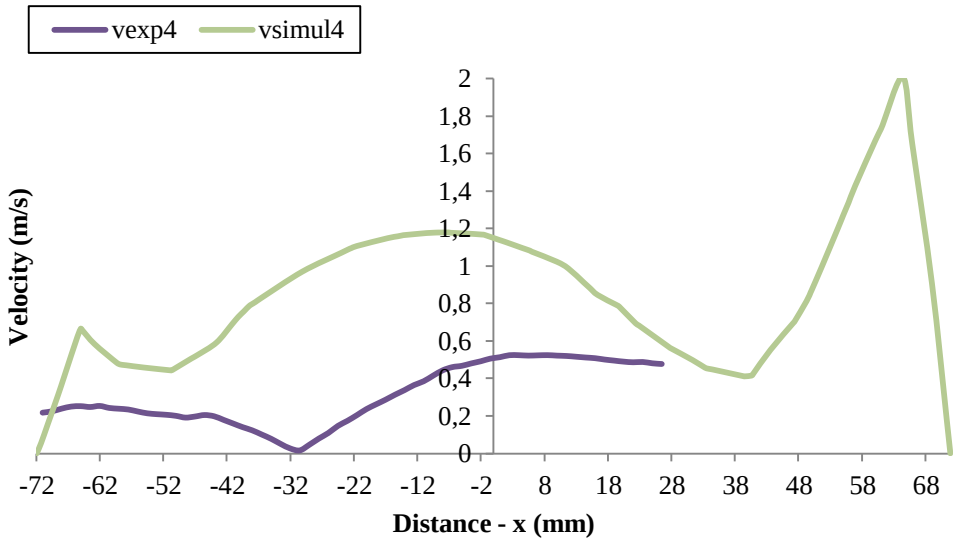

Figure 4.8 Experimental and Simulation Velocity of Silica Sand at 5.76m/s Air Velocity at Height4

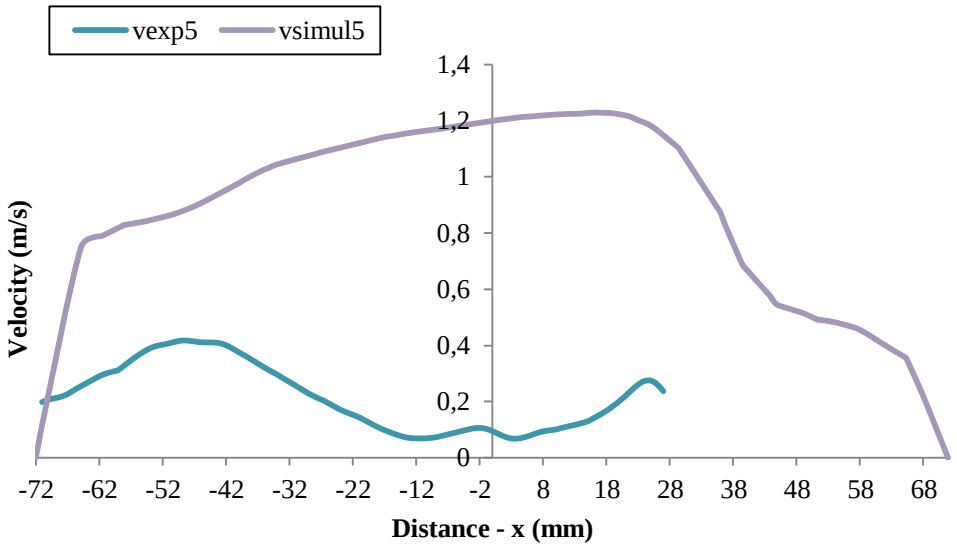

Figure 4.9 Experimental and Simulation Velocity of Silica Sand at 5.76m/s Air Velocity at Height5

Whenever there were similar trends in velocity distribution, their values still differ markedly. This can be explained by the fact that the sand granules were not spherical as was assumed in the simulation. Furthermore the sand granule sizes were actually very varied, with size variation from 300µm to 425µm. Smaller size

particles move up higher in the freeboard whilst bigger one tended to be at the bottom.

CHAPTER 5

COMBUSTION (HOT FLOW) RESULTS AND DISCUSSION

A series of steady state experimental tests has been performed to investigate air-staging effects on the combustion characteristics of palm wastes in ABFBC. The bed material (sand) weight is 1.5 kg and excess air (EA) level was varied from 0%, 20%, 40% and 60%. EA level was calculated taking into account of both primary air (PA) and secondary air (SA). The ratios of PA to SA are100:0, 90:10, 80:20, 70:30 and 60:40 for all EA levels were tested, for constant total air. The thermocouples were placed at 11-different locations 10mm from the wall into the chamber, and at heights of 60mm (location1), 160mm (location2), 260mm (location3), 360mm (location4), 460mm (location5), 570mm (location6), 670mm (location7), 770mm (location8), 950mm (location9), 1150mm (location10) and 1380mm (location11) above the bed . The locations of the thermocouples are shown in Figure 3.6.

The SA was introduced into the combustor on the central axis of the chamber 1000mm above the bed. The gas analyzer probe put at 1600mm above the bed in the flue gas flow. Two fuel feed rates were tested which were 87.9g/min and 98.5g/min.

5.1 Experimental Test Results and Discussion at Fuel Feed Rate 87.9g/min

5.1.1 Effect on Chamber Temperature Profile

The temperature profile of the bed has a significant role in determining the formation of emissions such as carbon monoxide (CO) and nitrogen oxide (NO_x). High combustion temperatures are required to reduce the formation of CO but it will increase the formation of NO_x.

The experimental results of temperature distributions measured by the thermocouples placed in the test rig for various SA ratios when the EA was kept constant. The EA were then changed to a new value. Overall 4 sets of experiments were conducted at EA values of 0%, 20%, 40% and 60% of which the results are shown in Figures 5.1 to 5.4 respectively.

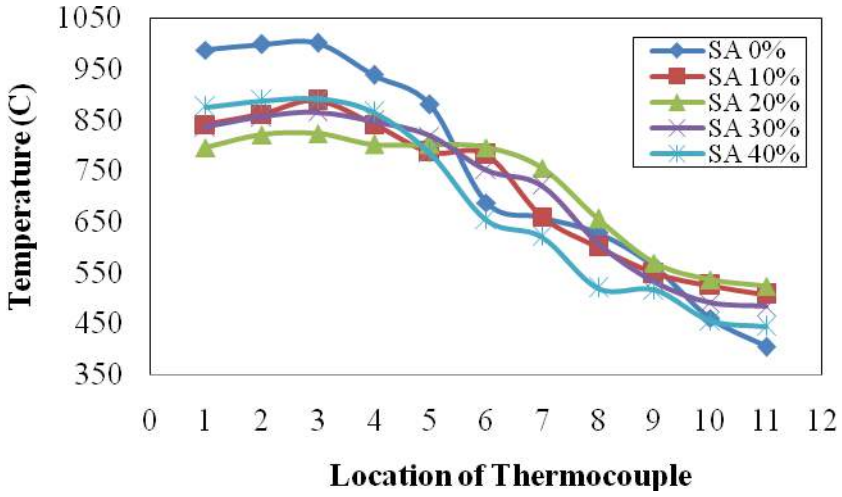

Figure 5.1 Effect of SA on temperature profile for EA0%

Generally, for EA0% the results showed that temperatures were affected by all SA ratios, but they have similar trends as shown in Figure 5.1. The temperatures were found to initially increase from 980˚C at bed height (location1) to 1000˚C at location3 then gradually decreased to 400˚C at location11. Regardless of EA conditions, the increases in the level of SA caused the decrease in the temperature distributions along the ABFBC.

The results for all other EA values showed the temperature distribution were similar, but decreased with the increment of EA. For example, the temperature at bed height (location1) was 980˚C for EA0% then decreased to 900˚C. For EA20% and continued to decrease to 800˚C for EA60%. This trend is also applicable to other SA values.

For all EA conditions, except at EA0%, it was found that for SA40%, the highest temperature were recorded at bed location, but at location11 the temperature recorded was the lowest at 420˚C. On the other hand for all EA conditions, it was found that SA20% gave the lowest temperatures of 770˚C at the bed location. Overall it could be seen that temperature distribution decreased from location5 continuously to location11, for all EA.

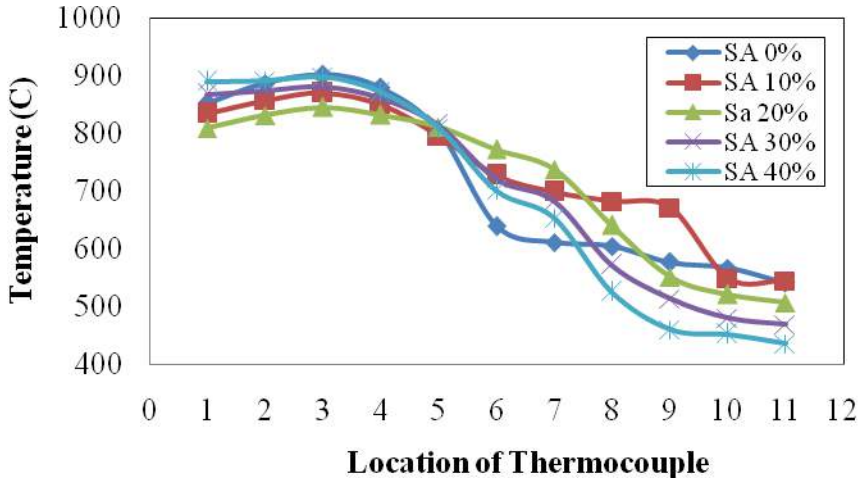

Figure 5.2 Effect of SA on temperature profile for EA20%

When SA was introduced in the vicinity of the location9 (introduction point was 1000mm, location9 at 950mm) the temperature in the chamber decreased drastically of 18% from location 5(combustion chamber) into location 6 (freeboard). After location 6, the temperatures tend to stabilize until location 8 then decrease again until the exhaust point. This can be seen in the Figures 5.1 to 5.4.

The variation of the proportion of SA also affected the temperature distributions in the chamber. At points before SA introduction, the temperatures

reduced with increasing proportion of SA until SA20%. Then the temperatures increased with increasing proportion of SA. This phenomenon can be seen on the left portion of the Figures 5.1 to 5.4. At points after the introduction of SA, the temperatures increased until SA10% then it decreased as the SA increases, all the way to SA40%.

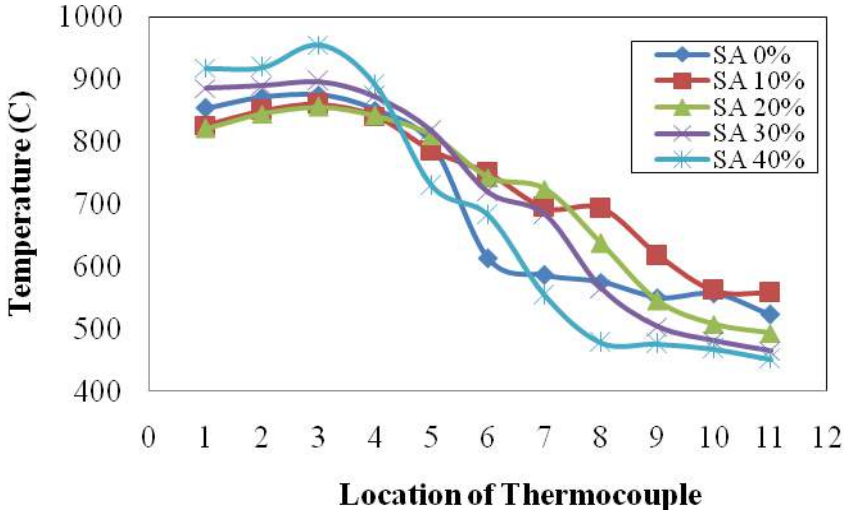

Figure 5.3 Effect of SA on temperature profile for EA40%

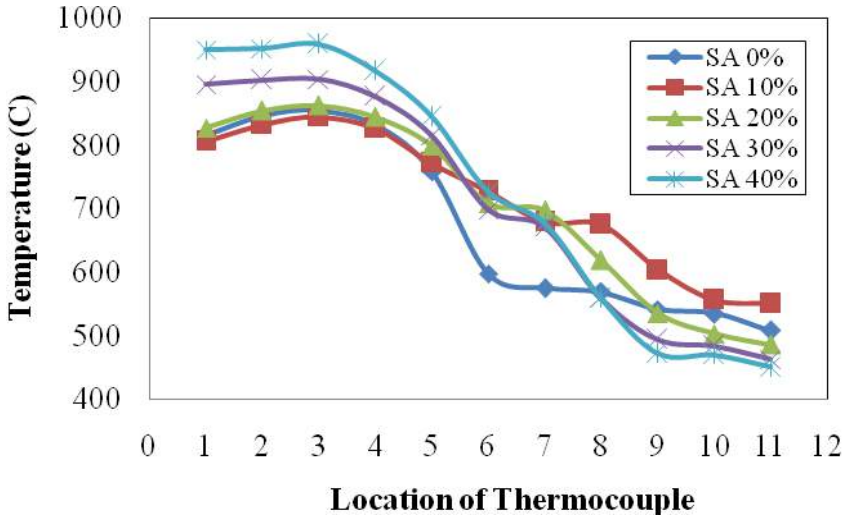

Figure 5.4 Effect of SA on temperature profile for EA60%

Introducing SA into the chamber initially caused temperature reduction because of the cold air and it made the fuel air ratio leaner. Then the combustion became more active due to extra oxygen. It also caused increased combustion

residence time promoting more complete combustion. The increased combustion residence time also means that the remaining volatiles and unburned carbon would be re-combusted to complete the combustion. Thus reducing temperatures past certain point along the chamber axis, as the SA increased. That point where the temperature start to reduce, is due to depletion of fuel materials.

5.1.2 Effects of EA and SA at Location 11

Finally it is imperative that the final output of the ABFBC be studied further. The last instrumented point of the ABFBC is at location11, thus the results at this point is presented in Figure 5.5. Figure 5.5 shows the effect of secondary air ratio on temperature for all EAs at location11. Without SA and EA the temperature recorded was 444ºC. With the introduction of EA the temperature initially increased to a maximum of 566.9ºC for EA20%, then it continue to reduce with the increase of EA to record a temperature of 540 ºC for EA60%.

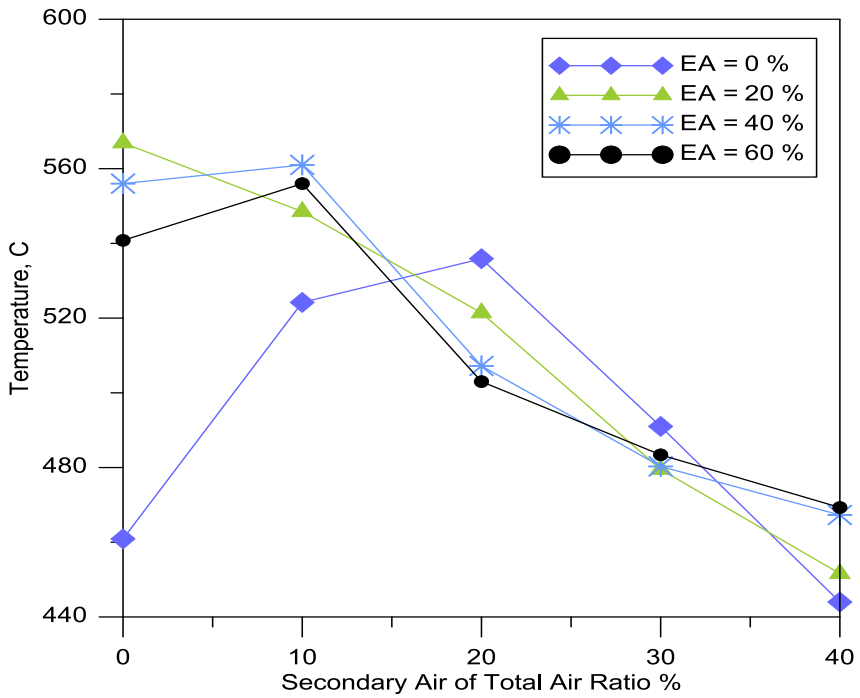

Figure 5.5 Effect of SA on temperature profile for different EA at location11

When SA was introduced the temperature initially increased (except EA20%) to a maximum then started to decrease with increasing SA. Without EA the temperature increased to a maximum of 535 ºC then reduces with increasing SA. For EA20%, the temperature decreased from the maximum 535 ºC with increasing SA. For the other EA setting, the temperature increased to maximum at SA20%, then reduced with increasing SA. From Figure 5.5 it can be seen that 4 combinations of (SA0%, EA20%), (SA0%, EA40%), (SA10%, EA40%) and (SA10%, EA60%) gave the highest temperatures. The combination of (SA10%, EA20%) recorded the 5th highest temperature. The five combinations show the most influential parameters on the temperature of the gas.

5.1.3 Effect on O_2 Concentration

The experimental results of O_2 concentration with respect to the increase of the EA from 0% to 60% for various SA (SA) ratios of 0%, 10%, 20%, 30% and 40% are shown in Figure 5.6. From the results, it could be seen that with the increase of EA, O_2 tends to increase for SA0% and SA40% and to decrease with a small gradient for SA10%, SA20% and SA30%. With 0% SA ratio (SA0%), O_2 was linearly increasing with a slope of about 0.6%, while for SA40%, O_2 was almost linearly increasing when the EA was between 20% to 60%. Thus, increasing the EA value affected to increase O_2 value. EA provided additional air beyond the stoichiometric air requirement.

The experimental results of O_2 with respect to the increase of the SA (SA) from 0% to 40% for various EA ratios of 0%, 20%, 40% and 60% are shown in Figure 5.7. Compared with others, under the EA of 60%, O_2 started with the highest value of about 12% at SA10% and ended also with the highest value of about 20% at SA40%, although in between SA0% and SA40%, the value of O_2 decreased momentarily at SA10% and SA20%. It is worthy to note that the EA60% had the largest increase of O_2 and the EA 20% had the smallest increase of O_2 concentration compared to other EA conditions. The EA20% yielded a slightly fluctuating increase in O_2 of about

2%. The O_2 concentration increases about 4% at SA10% dropped 2.5% below its initial value at SA20% and almost regained to its initial value at SA30%. The EA0% has caused a large increase of O_2 from about 1% at SA0% to about 15% at SA30% and significantly dropped to about 7% at SA40%. The EA40% produced a small increase in O_2 of about 3% from SA0% to SA40%, although O_2 concentration dropped momentarily to about 4% at SA10%.

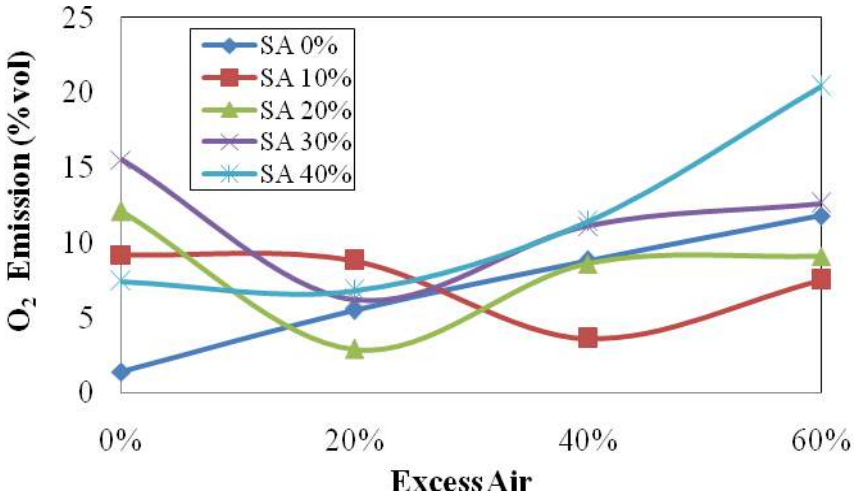

Figure 5.6 Effect of EA on O_2 concentration at different SA

From Figure 5.7, it could be seen that O_2 of all EA and for all SA increased, except for EA0% and SA60%. In addition, from the Figure 5.6, the smallest value of O_2 occurred at EA20%. The conditions of SA0% EA60% and SA40% EA60% gave higher values than the other conditions. Thus, increasing the SA value affected to increase the O_2 value.

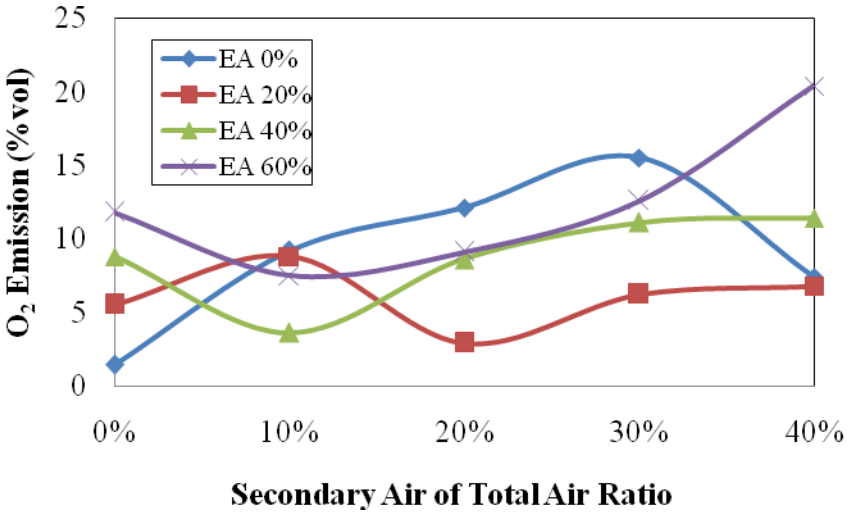

Figure 5.7 Effect of SA on O_2 concentration at different EA

5.1.4 Effect on CO Emission Concentration

Carbon monoxide (CO) emission is essentially the result of incomplete combustion and includes in the category of un-burnt pollutants.

The experimental results of CO emission with respect to the increase of the EA (EA) from 0% to 60% for various SA (SA) ratios of 0%, 10%, 20%, 30% and 40% are shown in Figure 5.8. The results showed that at EA0%, the SA0% had the highest CO emission of about 10000ppm, while the SA40% had the lowest one of about 800ppm. It seemed that at EA0% the higher the value of SA, the larger the CO emission would be, although this relationship was not necessary linearly proportional. Similarly, at EA60% the SA0% also had the lowest value of about 190ppm. The end values of CO emission for SA ratios, which were other than SA40%, were approximately between 1000 and 2000ppm.

The experimental results of CO emission with respect to the increase of the SA (SA) from 0% to 40% for various EA (EA) ratios of 0%, 20%, 40% and 60% are shown in Figure 5.9. From the figure, it could be seen that there was a big drop in CO emission for EA0% from SA0% to SA10%, then slowly decreasing from SA10%

to SA40%. The CO emission formation is presented by lower EA, restricted residence time, and lower temperature and diffusion controlled reactions due to fuel composition (high ash contended). By injection of SA into the bed, that results in low emission of CO. Other EAs tend to gradually slow increase the CO emission in which the EA60% was little bit faster than EA40%. The EA60% tends to have a constant CO emission, although there was a little bit increasing at SA40%.

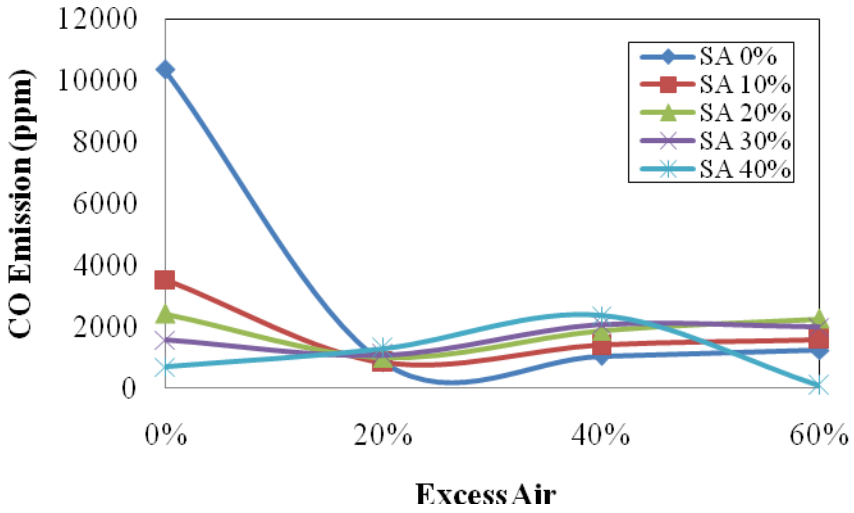

Figure 5.8 Effect of EA on CO emission concentration at different SA

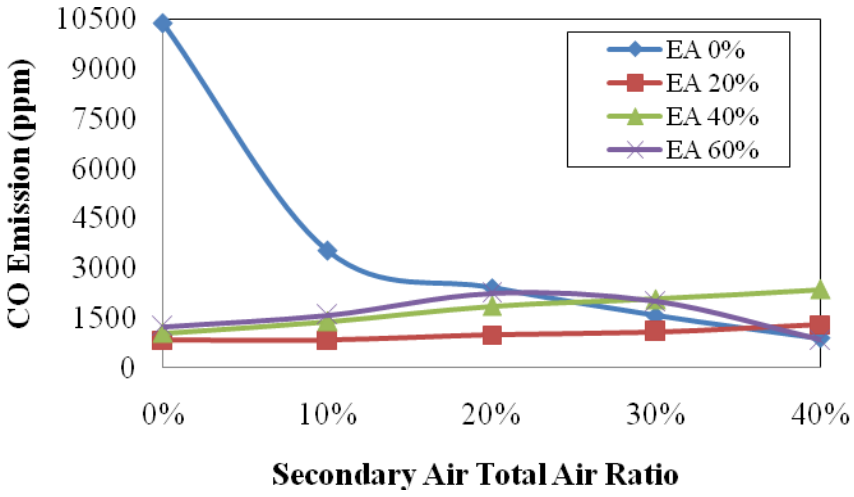

Figure 5.9 Effect of SA on CO emission concentration at different EA

Therefore based on the experiment, we could see in these figures, the highest EA and SA (EA60% and SA40%) gave the lowest CO emission of 1139ppm.

Kouprianov and Permchart [67] reported the lowest CO emission of 1800ppm for EA57.7% for sawdust. It explained that palm shell was better than sawdust, in term of CO emission. In other word, the air staging reduces the CO emission, as the results of some studies [63, 67, 69].

5.1.5 Effect on CO_2 Emission Concentration

The experimental results of CO_2 emission with respect to the increase of the EA (EA) from 0% to 60% for various SA (SA) ratios of 0%, 10%, 20%, 30% and 40% are shown in Figure 5.10. SA0% and SA40% both showed decreasing trends of CO_2 emission. For the SA0% the CO_2 emission decreases at a constant rate from about 14% at EA0% to 6.5% at EA60%. The SA40% was the only SA ratio which displays its final value decreasing from about 10% at EA20% to about 5% at EA60%. Both SA20% and SA30% had similar trends, but the SA20% show higher value than the SA0%. Also, the similar trends happened on their O_2 concentration and CO emission. Their CO_2 emission peaks took place at EA20%. The smallest increase of CO_2 emission for about 2% was experienced by SA10% which tops out at about 13%.

The experimental results of CO_2 emission with respect to the increase of the SA (SA) from 0% to 40% for various EA (EA) ratios of 0%, 20%, 40% and 60% are shown in Figure 5.11. It could be seen that there was a significant drop in CO_2 emission for EA0% from about 14.4% at SA0% to about 4% at SA30%, then increasing again to 10% at SA40%. The EA40% shows initial CO_2 emission of 9%. It had a CO_2 emission peak of about 13% at SA10%, and then slowly decreased to 7% at SA40%. Similarly, the EA60% shows initial CO_2 emission of 7%. It displays a CO_2 emission peak of about 10% at SA10%, and then slowly decreased to 5% at SA40%. The EA20% tends to produce a fluctuating CO_2 emission around 10.5%. Its lowest value was about 9% at SA10% and highest value was about 13.3% at SA20%.

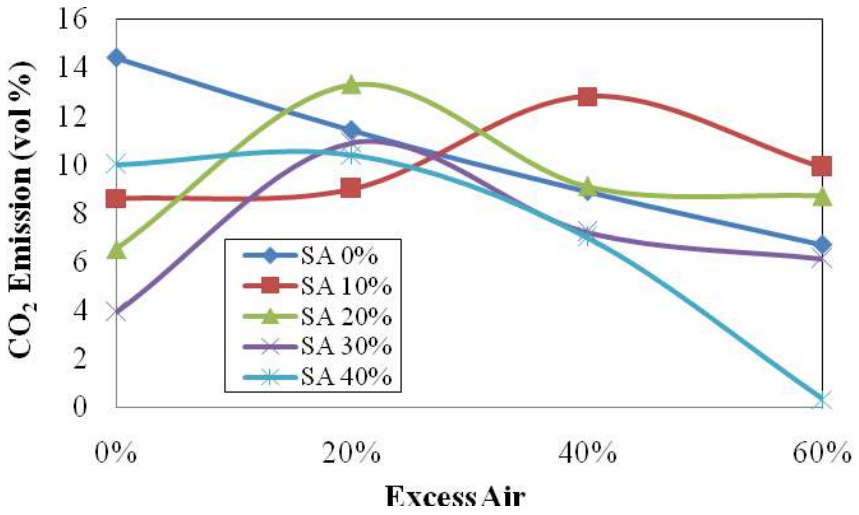

Figure 5.10 Effect of EA on CO_2 emission concentration at different SA

It could be seen in Figure 5.11, the highest EA and SA (EA60% and SA40%) produced the lowest CO_2 emission of 5%vol, due to the lowest CO emission in the same condition. Kouprianov and Permchart [67] reported the lowest CO_2 emission of 11%vol for EA57.7% for sawdust Decreasing CO emission was accompanied with increasing O_2 level. The presence of air staging can help in completing the oxidation of carbon monoxide (CO) to carbon dioxide (CO_2). However, the increase in O_2 concentration caused CO to be converted to CO_2. As the principal reactions for the combustion of the fuel: $2CO + O_2 \rightarrow 2CO_2$.

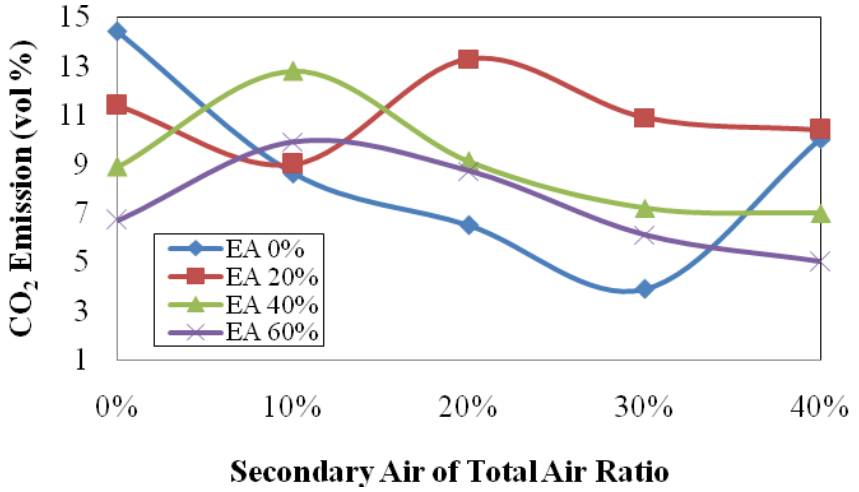

Figure 5.11 Effect of SA on CO_2 emission concentration at different EA

5.1.6 Effect on NO_x Emission Concentration

The experimental results of NO_x emission with respect to the increase of the EA (EA) from 0% to 60% for various SA (SA) ratios of 0%, 10%, 20%, 30% and 40% are shown in Figure 5.12. At SA0% NO_x emission gradually decrease from about 280ppm at EA0% to about 190ppm at EA60%. Conversely, the SA10% shows a slowly increasing quantity of NO_x emission from about 190ppm at EA0% to about 230ppm at EA60%. Both SA20% and SA30% show similar trends, but the SA20% produced a slightly higher value than the SA30% from EA0% to EA20%. Their NO_x emission peaks at 310ppm and 300ppm, respectively, which occured at EA20%, and their NO_x emission final values were the same of 200ppm.

From Figure 5.6 and Figure 5.12, we could see that the value of O_2 concentration decreases, the value of NO_x emission tend to increase. Conversely, we could see that when the value of O_2 increases, so the value of NO_x emission tend to decrease. Therefore, the present trend shows that the change of O_2 concentration, due to the effect of air staging, affected to the values of NO_x emission.

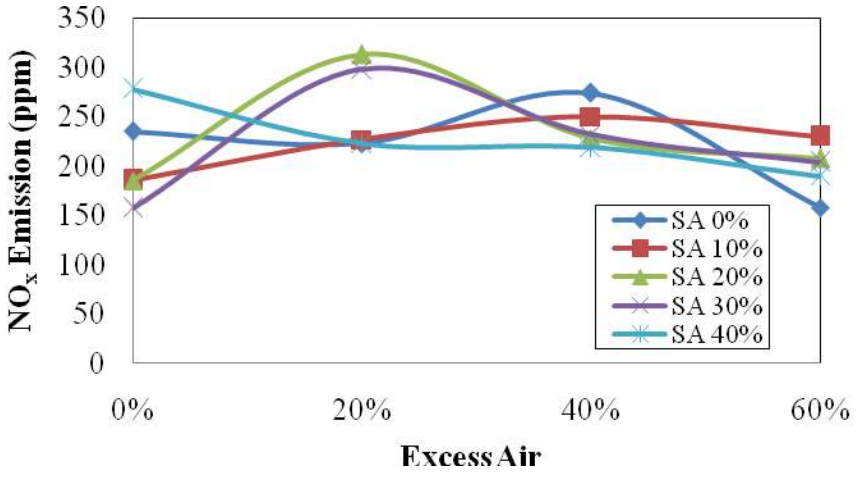

Figure 5.12 Effect of EA on NO_x emission concentration at different SA

The experimental results of NO_x emission with respect to the increase of the SA (SA) from 0% to 40% for various EA (EA) ratios of 0%, 20%, 40% and 60% are shown in Figure 5.13. From the figure, it could be seen that the EA40% showed

decreasing trends of NO_x emission from 270ppm at SA0% to about 220ppm at SA60%. Conversely, the EA20% shows an increasing NO_x emission from about 160ppm at SA0% to 190ppm at SA60%, with a peak value of about 225ppm at SA10%. Another increase of NO_x emission was given by EA0%. The EA 0% displays an increasing NO_x emission from about 240ppm at SA0% to about 280ppm at SA60%, with a tumbling value of about 150ppm at SA30%. The EA20% tends to produce a fluctuating value of NO_x emission of about 225ppm with a peak value of 310ppm at SA20%.

The same trend as previously discussed for Figure 5.6 and Figure 5.12 can be seen in Figure 5.7 and Figure 5.13, where it could be concluded that air staging affected the trend values of NO_x emission.

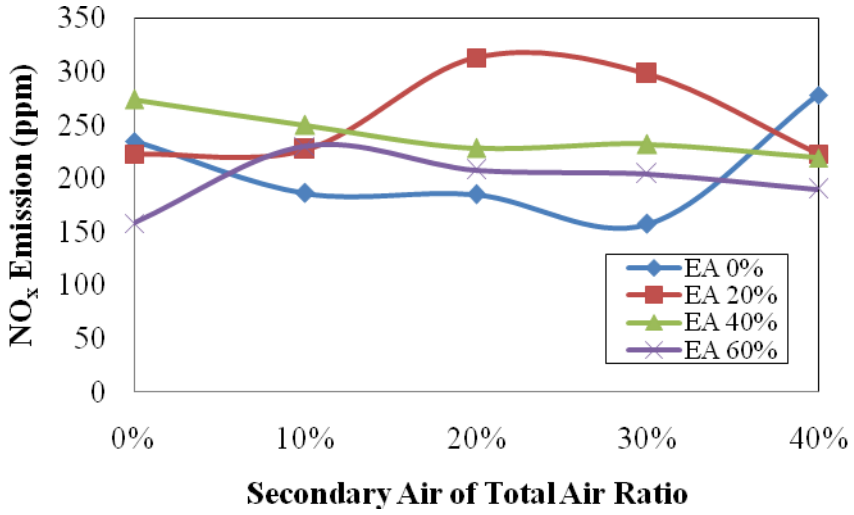

Figure 5.13 Effect of SA on NO_x emission concentration at different EA

Besides that, the bed temperature also had effect to the NO_x emission. For the EA40% and EA60% (Figure 5.3 and Figure 5.4), trend of that temperatures were lower than the other temperature conditions, it made for the same conditions, the NO_x emission also tend to decreases.

From Figure 5.12 and 5.13, the lowest NO_x emission happened at EA60% and SA20% of 153ppm. Permchart and Kouprianov have reported the NO_x emission

for some biomass for EA60% namely, sawdust of 112ppm, rice husk of 157ppm and bagasse 96ppm [59].

In addition, the average values of NO_x emission were still within acceptable level, except for SA20% and SA30%, at EA20%, where the Environmental Protection agency (EPA) requires it to be less than 250ppm.

5.1.7 Effect on Combustion Efficiency

The experimental results of combustion efficiency with respect to the increase of the EA from 0% to 60% for various SA (SA) ratios of 0%, 10%, 20%, 30% and 40% are shown in Figure 5.14. All values of combustion efficiency were between 92% and 98%, with the lowest value of about 92% given by SA30% and EA0% and the highest value of about 97.8% produced at SA20% and EA20%. The highest overall combustion efficiency was generated at SA20% and EA20% and SA10% at EA40%. The final combustion efficiency values at EA 60% showed that the smallest value was experienced by SA40% and the highest value was resulted from SA10%. It was important to note that almost all SA show increasing combustion efficiency, except SA40%. In addition, the SA0%, SA20% and SA30% show their peak combustion efficiency values at EA20%. The EA affected to decrease bed temperature, and the lower bed temperature affected to loss thermal efficiency.

The experimental results of combustion efficiency with respect to the increase of the SA from 0% to 40% for various EA (EA) ratios of 0%, 20%, 40% and 60% are shown in Figure 5.15. All values of combustion efficiency were between 92.2% and 97.8%, in which the lowest was produced at EA0% and SA30% and the highest was produced at EA20% and SA20%. For SA0%, the lowest efficiency was 95% (EA0%) and the highest was 97.5% (EA20%). While for SA40%l, lowest efficiency was 93% (EA60%) and the highest was 97.2% (EA0%). It was important to note that almost all combustion efficiency show a decreasing trend, except EA0%,

in which the combustion efficiency was initially decreasing from SA0% to SA30% and increasing again at SA40%. By injection SA, it resulted in low CO emission and high combustion efficiency [168]. Thus, the air staging affected to increase the combustion efficiency.

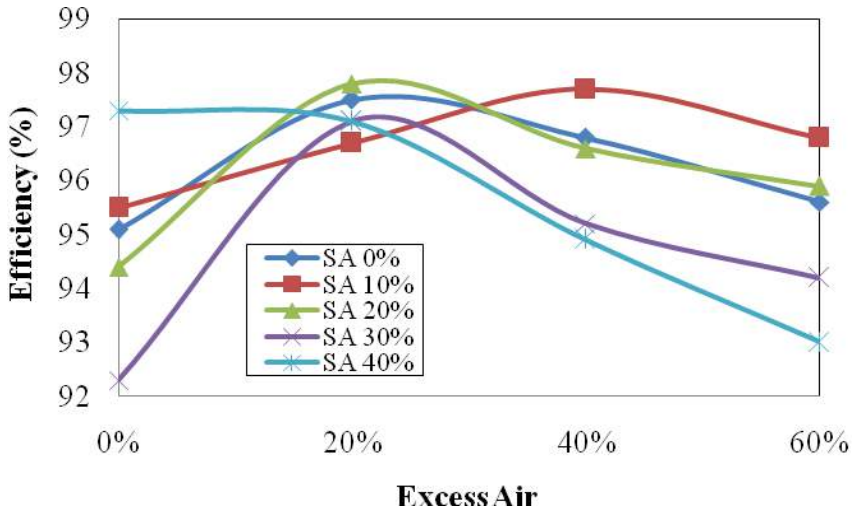

Figure 5.14 Effect of EA on combustion efficiency at different SA

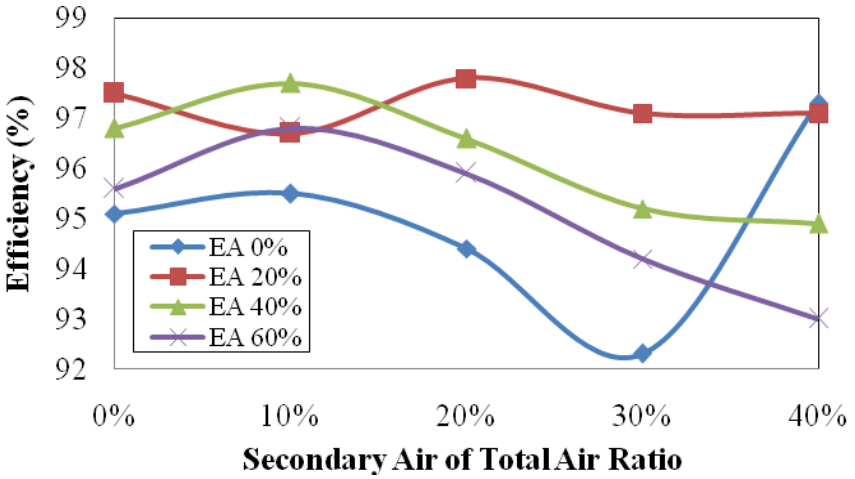

Figure 5.15 Effect of SA ratio on combustion efficiency at different EA

In addition, the highest combustion efficiency of 98% was produced at EA20% and SA20%. The combustion efficiency was higher than the sawdust for 96.48% and the rice husk for 83.24% [59]. It showed that palm shell was better than sawdust and rice husk, in term of combustion efficiency.

5.2 Experimental Test Result and Discussion at Fuel Feed Rate 98.5g/min

5.2.1 Effect on Chamber Temperature Profile

The experimental results for an increase in fuel flow rate to 98.5g/min produced almost about the same trend as that of 87.9g/min. However, the values of temperatures and gaseous concentration vary slightly.

The experimental results of temperature distributions measured at 11-different locations are shown in Figures 5.16 to 5.19. Generally, for all EA conditions, the results showed that temperatures affected by all SA ratios had similar trends which were gradually decreasing from the starting values between 900ºC to 1070ºC to the final values between 450ºC to 600ºC. For this case fuel feed rate 98.5kg/min, higher fuel feed rate resulted in higher temperature profile due to higher heating rate in the combustion chamber, it compared to the fuel feed rate 87.9kg/min. In addition, for this case, the bed temperature started to decrease at location4, meanwhile for the first case fuel feed rate 87.9kg/min the bed temperature started to decrease at location5.

Regardless of EA conditions, the increases for SA caused the decrease in the axial temperature distributions along the FBC height. The highest axial temperature of initial location of about 1070ºC was produced at SA0% and EA0%, while the lowest one, of about 900ºC, was produced by SA0% and EA0%. SA 0% (EA 0%) achieved the maximum temperature of 1070 º C. For all EA conditions, it was found that SA40% produced the lowest temperature at its final location. In addition, for all EA at all SA, it implied that the air staging affected to the temperature profile.

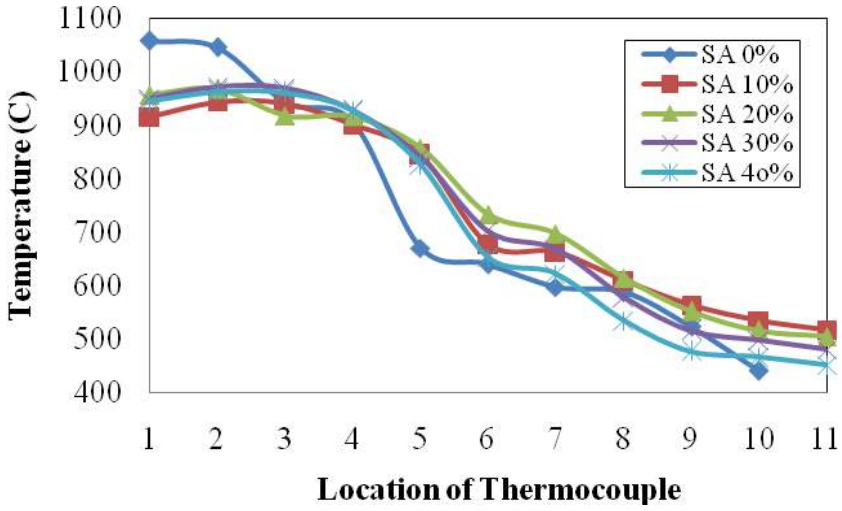

Figure 5.16 Effect of SA on temperature profile at EA0%

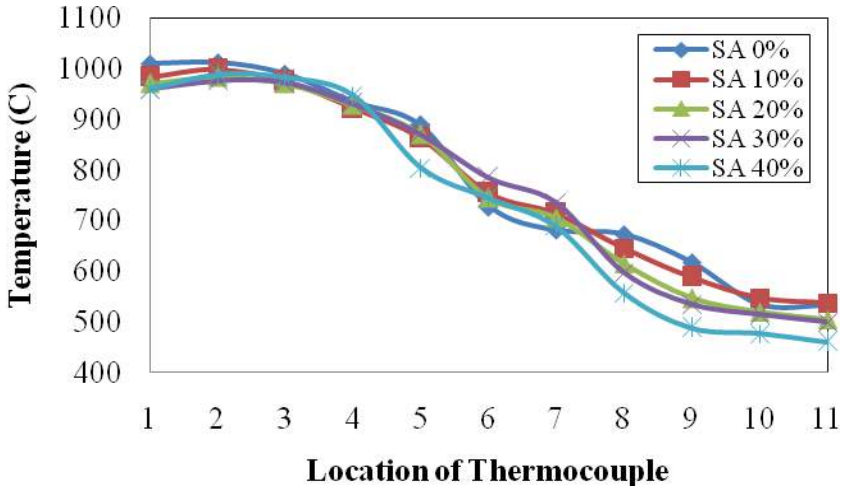

Figure 5.17 Effect of SA on temperature profile at EA20%

Introducing SA nearby location9 would decrease the freeboard temperature. It caused early condition of the freeboard below the SA injector to be in air rich (or fuel-lean) condition, and it drastically decreased the bed temperature. Due to the SA injections, there was an increase in the residence time of the volatile and the unburned carbon in the freeboard, which induced reaction to take place. However, for the position far from the SA injector, the residence time would decrease faster than the one near the SA injector. For the case of fuel feed rate 98.5kg/min the bed temperature started to decrease at location4, meanwhile for the first case fuel feed rate 87.9kg/min the bed temperature started to decrease at location5. It was caused by the increase in fuel feed rate and hence the mixing rate of fuel, sand and air

become faster and more thorough. Consequently, the rate of combustion happened faster than the first ones; however it also affected to the residence time of the flame, especially if the efficiency of air occurred.

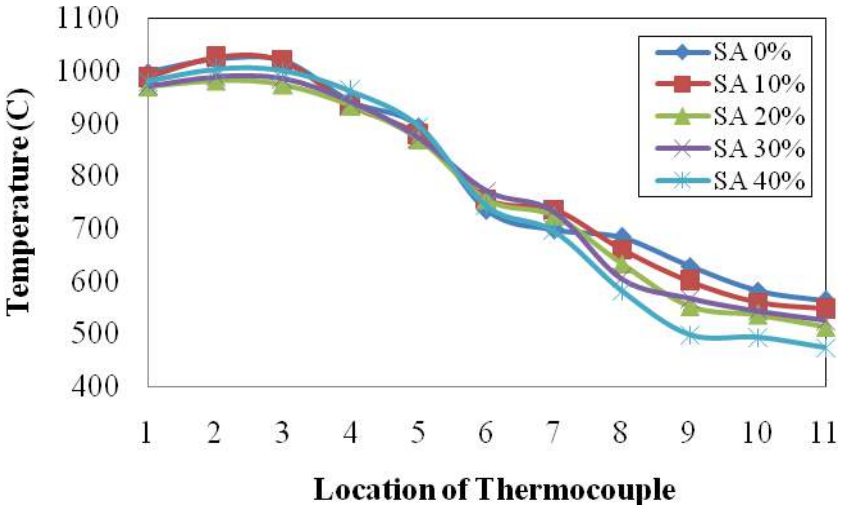

Figure 5.18 Effect of SA on temperature profile at EA40%

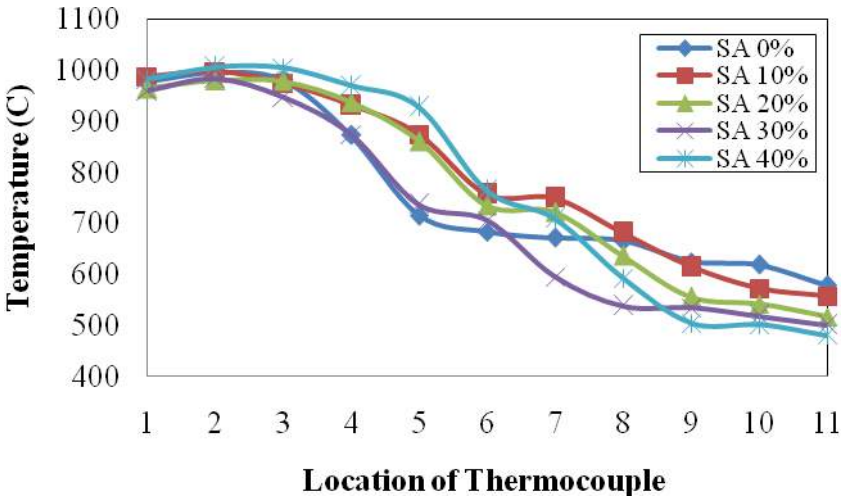

Figure 5.19 Effect of SA on temperature profile at EA60%

5.2.2 Effects of EA and SA at Location 11

The last instrumented point of the ABFBC is at location11, thus the results at this point is presented in Figure 5.20. Figure 5.20 shows the effect of secondary air ratio on temperature for all EAs at location11. At locatian11 above the position of SA introduced, the minimum temperature was achieved by EA0% and SA40% at 444ºC and the maximum temperature was achieved by EA20%SA0% at 566.9ºC. From this figure, it could be seen that increasing the amount SA of total air ratio decreased the temperature especially for EA40% and EA60%. For EA0% and EA20%, the temperatures increased from SA0% to SA10% and then decreased. For all SAs, increasing EA resulted in an increasing the temperature with a range varied from 12ºC to 139ºC.

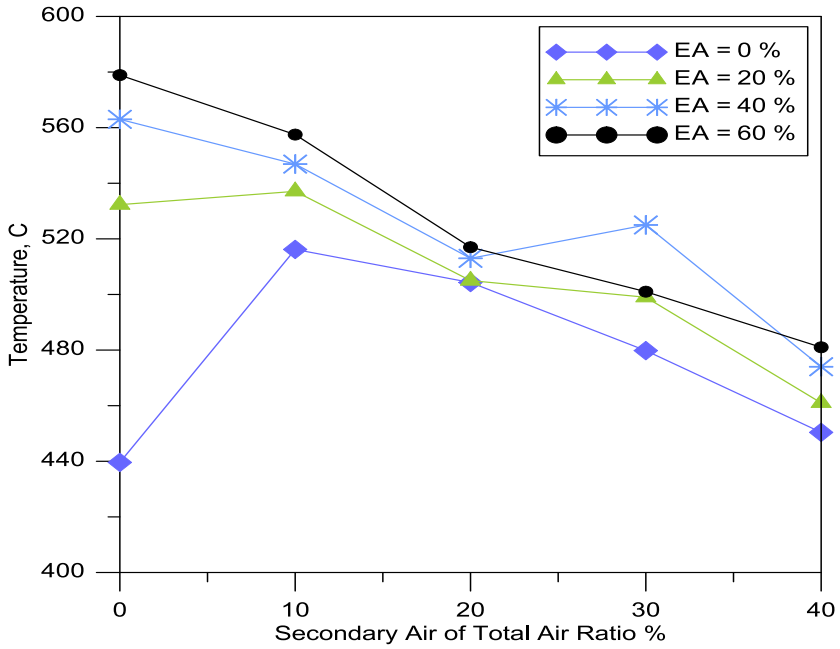

Figure 5.20 Effect of SA on temperature profile at location11 for all EA

5.2.3 Effect on O_2 Concentration

The experimental results of O_2 concentration with respect to the increase of the EA (EA) from 0% to 60% for various SA (SA) ratios of 0%, 10%, 20%, 30% and 40% are shown in Figure 5.21. From the results, it could be seen that with the increase of EA, the O_2 concentration tended to increase. The SA0%, SA30% and SA40% had fluctuating O_2 values. The highest increase in O_2 was produced at SA 0% and EA60%, while the smallest was generated at SA0% and EA0%, although the SA10% had its peak O_2 value at EA60%. With 20% SA ratio (SA20%), the O_2 concentration almost linearly increased from about 7.5% at EA0% to 10% at EA60%, while for SA10%, the O_2 concentration almost linearly increased when the EA was between 0% and 40%.

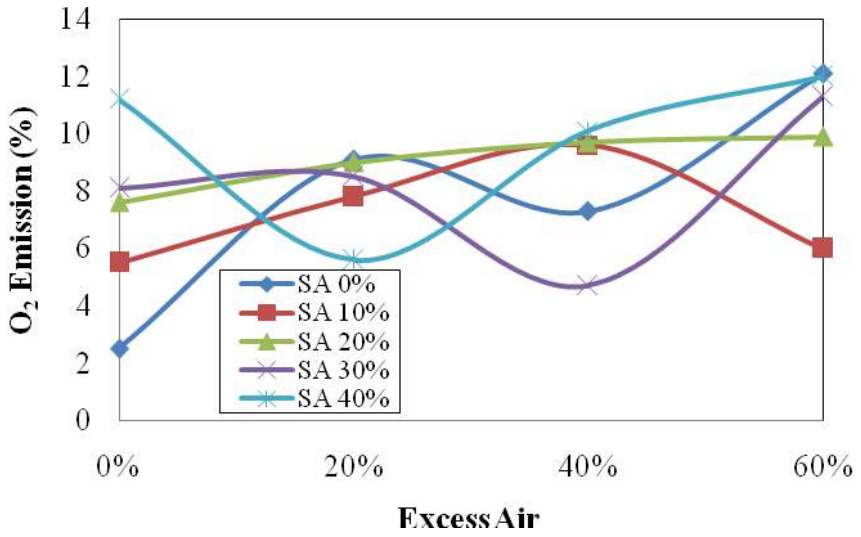

Figure 5.21 Effect of EA on O_2 concentration at different SA

The experimental results of O_2 with respect to the increase of the SA (SA) from 0% to 40% for various EA (EA) ratios are shown in Figure 5.22. The results showed that only EA0% and EA40% produced increasing O_2 measurement, in which when compared to the EA40%, the EA0% had consistendedly increased without a large fluctuation. Compared with others, under the EA of 60%, the O_2 started with the highest value of about 12% at SA0% and ended with the same highest value at SA40%, although in between SA0% and SA40%, the O_2 value decreased to 6% momentarily at SA10%.

It was worthy to note that for all EA conditions, the EA0% had the largest increase of O_2 (around 9%) and the EA20% was the only one which had a decreasing O_2. Therefore, there was correlation between air staging and O_2, in which increasing amount of air staging caused an increase of O_2 concentration.

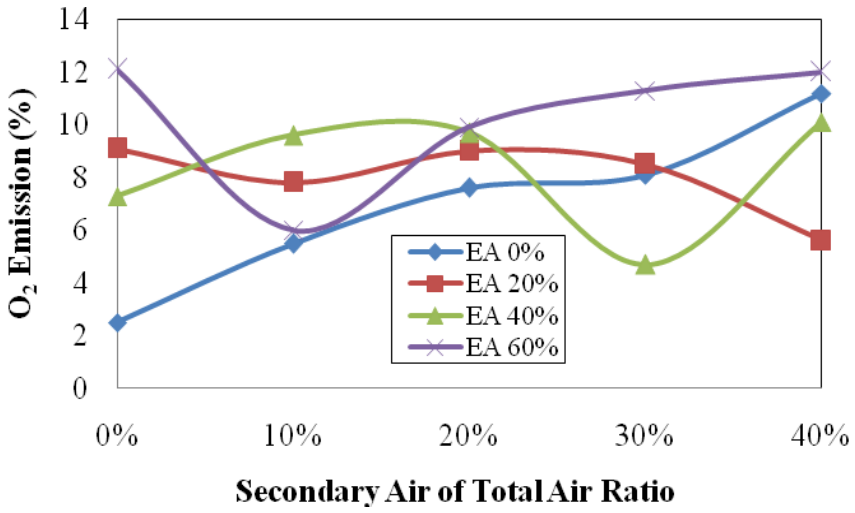

Figure 5.22 Effect of SA on O_2 concentration at different EA

For this case fuel feed rate 98.5kg/min, higher fuel feed rate resulted in lower value of O_2 due to higher heating rate in the combustion chamber, compared to the fuel feed rate 87.9kg/min.

5.2.4 Effect on CO Emission Concentration

The experimental results of CO emission with respect to the increase of the EA from 0% to 60% for various SA ratios of are shown in Figure 5.23. The results showed that at EA0%, the SA0% had generated the highest CO emission of about 5000ppm, while the SA 40% had the lowest one of about 1100ppm. Most of EA show a decreasing trend, except for the SA40% which produced an increasing CO emission from about 1100 to 1750ppm. The biggest CO emission decreasing was experienced by SA0%, while the SA10%, SA20% and SA30% produce small decrease in CO emission. The CO emission formation was limited by lower EA,

restricted residence time, lower temperature and diffusion controlled reactions due to fuel composition (high ash contended). By injection of SA into the bed, that results in low emission of CO. The fluctuating trend was experienced by SA0% and SA10%.

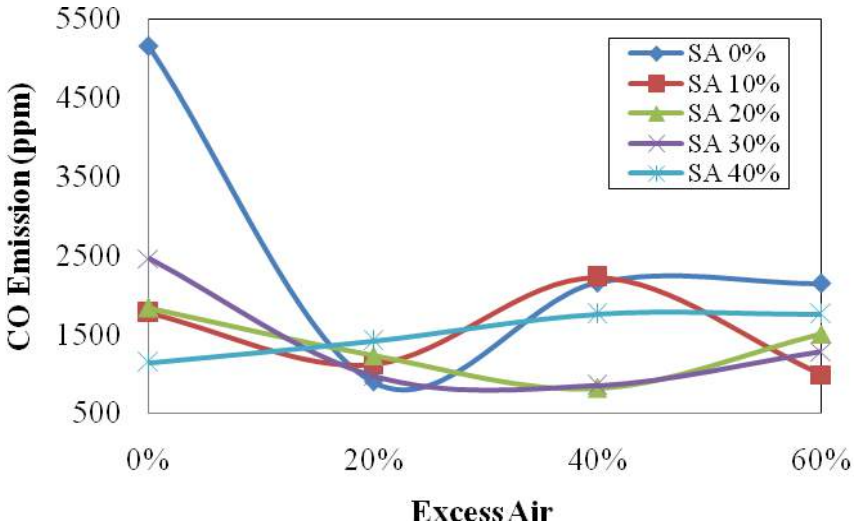

Figure 5.23 Effect of EA on CO emission concentration at different SA

The experimental results of oxygen emission with respect to the increase of the SA (SA) from 0% to 40% for various EA (EA) ratios are shown in Figure 5.24. Compared with others, under the EA of 60%, the O_2 concentration started with the highest value of about 12ppm at SA10% and ended also with the highest value of about 20ppm at SA40%, although in between SA 10% and SA 40%, the value of O_2 decreased momentarily at SA20%. It was worthy to note that for all EA conditions, the EA 0% caused the highest decrease in O_2 (4000ppm), while the EA 40% and 60% produced equally small decreasing of O_2 (about 250ppm) and conversely, the EA 20% was the only one which had an increased in concentration (about 500ppm). All EA conditions, except EA 20%, had fluctuating trends.

From bed temperature profile figures, the highest temperature profile (EA40% for SA20% and SA30%) showed the lowest value of CO emission. In other word, the air staging reduced the CO emission. In addition, CO emission at fuel feed rate 98.5kg/min was lower than at fuel feed rated 87.9kg/min. The increase in fuel

feed rate resulted in the lower CO emission. This is due to the faster the fuel feed rate resulted in higher bed temperature and faster combustion resulted in a lower CO emission.

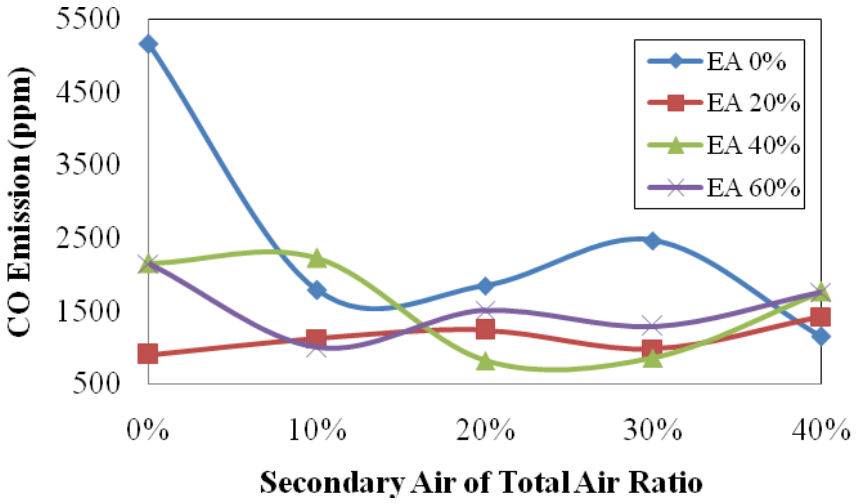

Figure 5.24 Effect of SA on CO emission concentration at different EA

5.2.5 Effect on CO_2 Emission Concentration

The experimental results of CO_2 emission with respect to the increase of the EA (EA) from 0% to 60% for various SA (SA) ratios are shown in Figure 5.25. From the figure, it could be seen that all SA conditions had decreasing trends in which the SA 0% gave the biggest decreasing (about 6.5 %). The SA 20% produced CO_2 emission decreasing at a slightly constant rate from about 10% at EA0% to 8% at EA 60%, while the SA10% produced a decreasing CO_2 emission from 11.5% at EA0% to about 8% at EA 40%, then an increasing again to 11% at EA60%. The SA40% produced the smallest decreasing of CO_2 emission, although the CO_2 emission reached peaks value to 11.5% at EA20%. Similarly, the SA 30% had a fluctuating trend of CO_2 emission and a peak CO_2 emission of 12% at EA 40%.

The experimental results of CO_2 emission with respect to the increase of the SA (SA) from 0% to 40% for various EA (EA) ratios are shown in Figure 5.26. It could be seen from the figure that the largest initial value of CO_2 emission was

13.6% (EA0%) and the smallest was 6.6% (EA60%), while the highest final value of CO_2 emission was 11% (EA20%) and the smallest was 6.5% (EA60%). The EA 0% and EA 40% produced decreasing CO_2 emission, but the EA 0% showed a gradual decreasing rate from 13.5 % at SA0% to 7% at SA40%, while the EA40% displayed a fluctuating trend with a peak CO_2 emission of 12 % at SA30% and final CO_2 emission of 8%. The EA20% produced an increasing CO_2 emission from 8.5% at EA0% to about 11% at SA20% with a small fluctuating about 9.8% at SA10%. The EA60% reached highest CO_2 emission (11%) at SA10%, and decreased to 6.5% at SA60%.

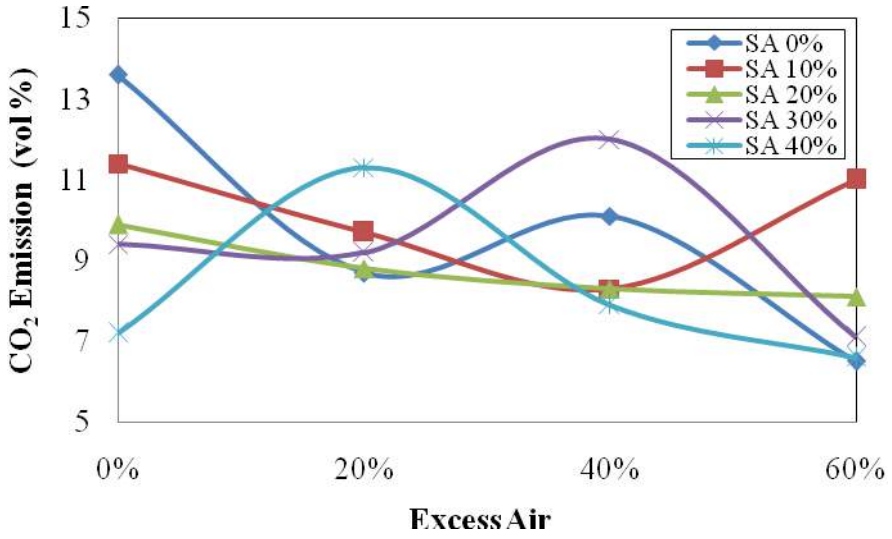

Figure 5.25 Effect of EA on CO_2 emission concentration at different SA

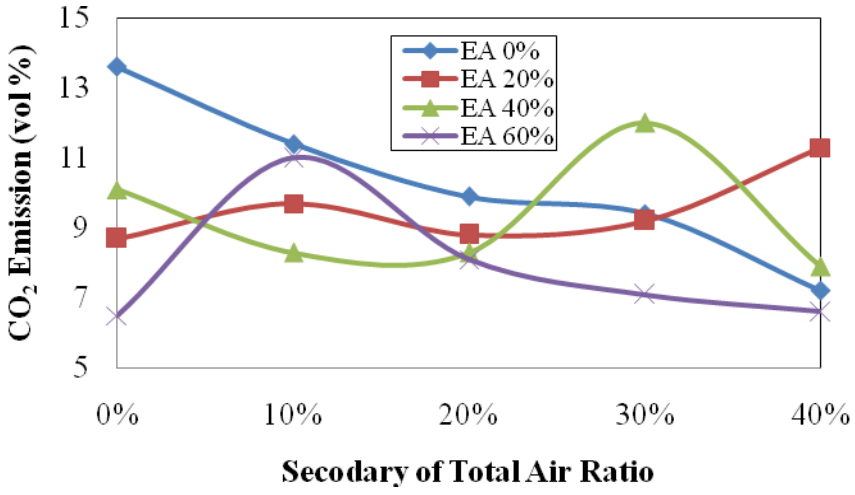

Figure 5.26 Effect of SA on CO_2 emission concentration at different EA

From these figures, it could be seen that air staging affected to the CO_2 emission. Decreasing CO emission was accompanied with increasing O_2 concentration level. The presence of air staging can greatly help in completing the oxidation of carbon monoxide (CO) to be carbon dioxide (CO_2). It could see from those figures, the highest EA and SA (EA60% and SA40%) exhibited the lowest CO_2 emission of 11%vol.

In addition, CO_2 emission at fuel feed rate 98.5kg/min was lower than at fuel feed rated 87.9kg/min. The faster of fuel feed resulted in the lower CO_2 emission. Because the faster of fuel feed rate resulted in higher bed temperature, faster complete combustion.

5.2.6 Effect on NO_x Emission Concentration

The experimental results of NO_x emission with respect to the increase of the EA from 0% to 60% for various SA (SA) ratios of 0%, 10%, 20%, 30% and 40% are shown in Figure 5.27. From the figure, it could be seen that the biggest initial value of NO_x emission was 220ppm (EA10%) and the smallest was 120ppm (EA0%), while the biggest final value of NO_x emission was 180ppm (EA0%, EA10%, EA30%) and the smallest was 150ppm (EA20%). The overall biggest NO_x emission (260ppm) took place for SA30% at EA40%.

The EA10%, 20% and 30% had decreasing NO_x emission, but the EA0% had a gradual decreasing rate from about 220ppm at EA0% to about 180ppm at EA 60%. Meanwhile, the EA20% had a fluctuating trend with a peak NO_x emission of 220ppm at SA20% and final NO_x emission of 150ppm. In addition, the EA30% had a fluctuating trend with a peak NO_x emission of 260ppm at SA40% and final NO_x emission of 180ppm. Conversely, the EA0% and EA40% had increasing NO_x emission, the EA0% had a fluctuating trend with a peak NO_x emission of 220ppm at SA20% and final NO_x emission of 180ppm, and the EA40% had a fluctuating trend with a peak NO_x emission of 220ppm at SA 0% and final NO_x emission of 170ppm.

It was worthy to note that all EA's had almost the same values NO_x emission of 220ppm at SA20%, and except EA30%, they had their peak values at SA20%.

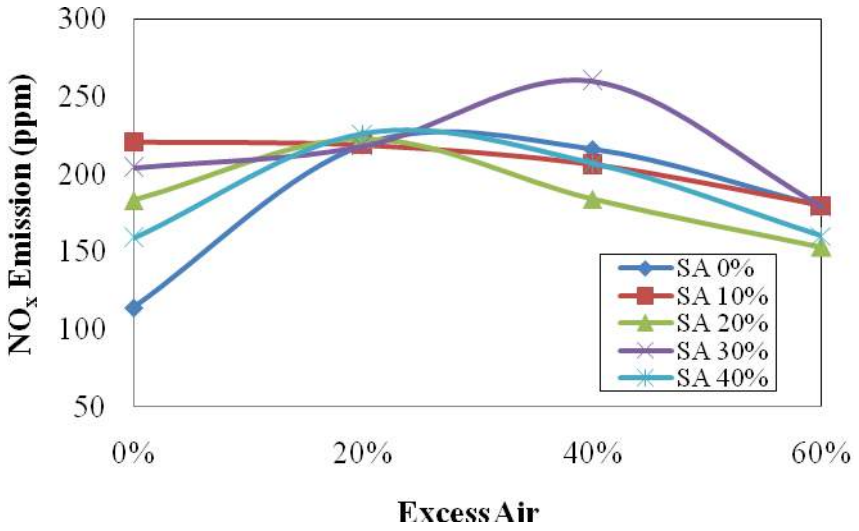

Figure 5.27 Effect of EA on NO_x emission concentration at different SA

From Figure 5.21 and Figure 5.27, it could be seen that when the value of O_2 concentration tended to decrease, so the value of NO_x emission tended to increase. Conversely, when the value of O_2 tended to increase, the value of NO_x emission tended to decrease. Therefore, the present trend values of O_2, as the impact of air staging, affected to the trend values of NO_x emission.

The experimental results of NO_x emission with respect to the increase of the SA from 0% to 40% for various EA (EA) ratios of 0%, 20%, 40% and 60% are shown in Figure 5.28. From the figure, it could be seen that EA40% and EA60% had fluctuating and small decreasing trends of NO_x emission, in which the EA40% had NO_x emission fluctuating peak of 260% at SA30% and the EA60% had a small NO_x emission tumbling of 150% at SA20%.

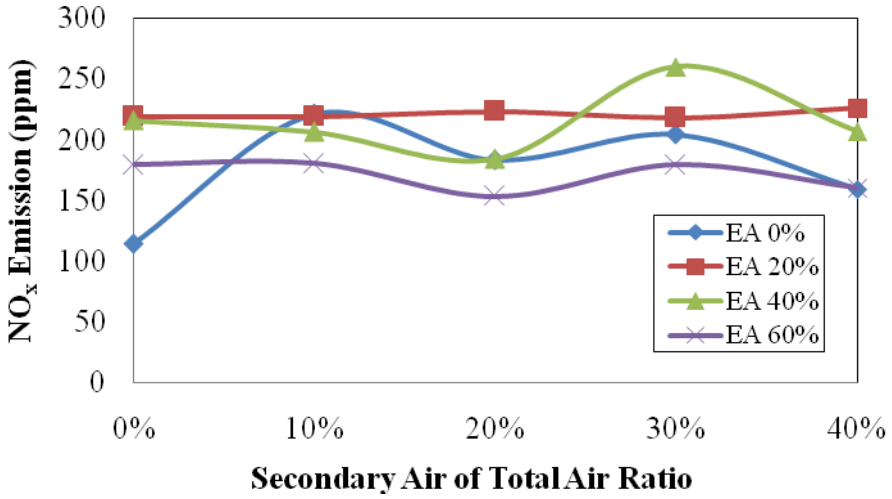

Figure 5.28 Effect of SA on NO_x emission concentration at different EA

Conversely, the EA20% had a small increasing trend of NO_x emission from 220% at SA0% to about 230% at SA20%. While the EA0% had a fluctuating and increasing trend of NO_x emission from 110% at SA0% to about 160% at SA40%, with its first peak of 220% at SA10%, tumbling of about 190% at SA20% and second peak of 200% at SA30%.

From Figure 5.22 and Figure 5.28 it could be seen when the value of O_2 tended to decrease, so the value of NO_x emission tended to increase. Conversely, when the value of O_2 emission tended to increase, the value of NO_x emission tended to decrease. Therefore, the presence trend values of O_2, as the impact of air staging, affected to the trend values of NO_x emission.

Besides that, the bed temperature also had effect to the NO_x emission. For the EA0% and EA60% (Figure 5.16 and Figure 5.19), trend of that temperatures were lower than the other temperature conditions, it made for the same conditions, the NO_x emission also tended to decreases.

From Figure 5.27 and Figure 5.28, the average values of NO_x emission were still within acceptable level, except for SA30%, at EA40%, whereas the Environmental Protection agency (EPA) requires it to be less than 250ppm. In

addition, NO_x emission at fuel feed rate 98.5kg/min was lower than at fuel feed rate 87.9kg/min.

5.2.7 Effect on Combustion Efficiency

The experimental results of combustion efficiency with respect to the increase of the EA from 0% to 60% for various SA (SA) ratios of 0%, 10%, 20%, 30% and 40% are shown in Figure 5.29. All values of combustion efficiency were between 98.1% and 99.3%, with the lowest initial efficiency of about 97.6% given by SA0% and the biggest initial efficiency of about 99.3% produced by SA10%. The biggest overall efficiency (99.3%) was generated by SA30% at EA40%. The final efficiency values at EA 60% showed that the smallest efficiency (about 97.6%) was produced by SA0% and the biggest efficiency (99.3%) was resulted from SA10%. It was important to note that the SA10% and 30% had increasing efficiency, while others had decreasing efficiency. It could see, for all SA, increasing EA tended to decrease combustion efficiency, except for EA60% and SA10%. Thus, the EA affected to decrease bed temperature, and the lower temperature gave the lower combustion efficiency.

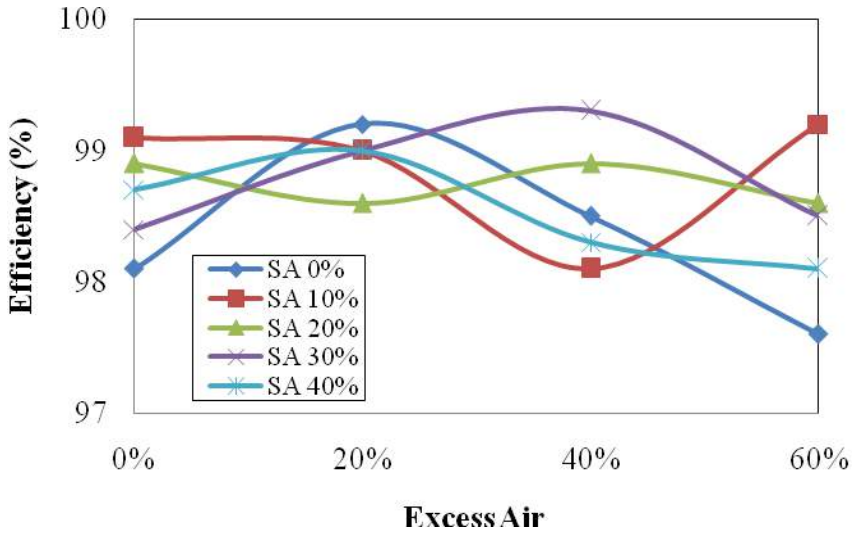

Figure 5.29 Effect of EA on combustion efficiency at different SA

The maximum efficiency of the EA0% (99.2%) and EA40% (99.3%) were located at SA 30% and the EA30% (about 99.3%) at SA40%. The minimum efficiency of the EA10% (98.1%) was located at SA40%. All values of combustion efficiency in MPR2 (fuel feed rate 98.5kg/min) are around 98.1% - 99.3%, which were higher than combustion efficiency of MPR1 (fuel feed rate 87.9kg/min). It meant that higher fuel feed rates resulted in higher combustion efficiency.

The experimental results of combustion efficiency with respect to the increase of the SA from 0% to 40% for various EA (EA) ratios of 0%, 20%, 40% and 60% are shown in Figure 5.30. All values of combustion efficiency were between 97.6% and 99.2%, in which the lowest was given by EA 60% at SA 0% and the biggest values were produced by EA40% at SA30%. For initial efficiency values, the smallest was 97.6% (EA60%) and the biggest was 99.1% (EA20%). While for the final efficiency values at SA40%, the smallest was 98.1 % (EA60%) and the biggest was 99% (EA20%). It was important to note that almost all SA have increasing efficiency, except SA20%, in which the efficiency was slightly decreasing from EA0% to EA20%, increasing again at EA30% and constant at EA40%. Thus, air staging had effect to increase the combustion efficiency.

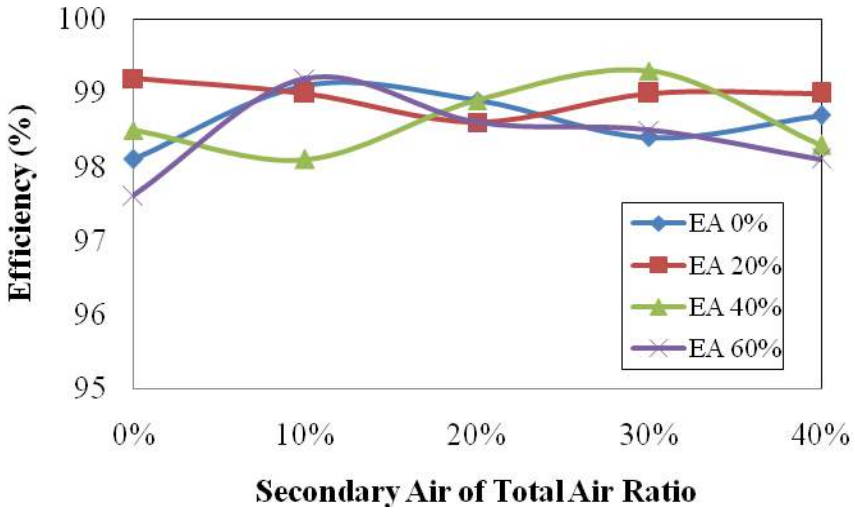

Figure 5.30 Effect of SA on combustion efficiency at different EA

5.3 Numerical Modelling of Turbulent Multiphase Reacting Flow

Considerable progress has been made in recent years in the mathematical modelling of turbulent multiphase reacting flow. The particular aspect of the modelling that was given special attention was the selection of suitable mathematical formulation. For single-phase turbulent reacting flows the central problem is the turbulence-chemistry interaction. For reacting two-phase flows the main problem is the particle reaction-dispersion interaction. This interaction between the gas and solid phases is a crucial factor, in fact, it determines turbulence intensity, mixing rates, and mass and heat transfer. The existing turbulence-chemistry models still need improvement and are still computationally very expensive.

In the present study, numerical modelling of multiphase turbulent reacting flow was carried out using commercial CFD codes, ANSYS FLUENT 13.0. The reacting flow simulation domain has the same geometry as the lab-scale experimental combustion rig as shown in Figure 3.9 and schematically in Figure 3.13. The simulation was done in Eulerian-Eulerian (EE) multiphase model kinetic theory of granular flow approach with species transport. The turbulent flow field was modeled with a two equation standard k-ε models as this is one of the most common turbulence models and is widely used. This model is known not to perform well in cases of large adverse pressure gradients. However, for initial FBC study before a more complex model is employed, k-ε model is reasonable as it can save computing time. The default values as provide by ANSYS FLUENT was employed for the kinetics of combustion reaction. Other aspects of the present study such as the geometry and grid set-up, numerical discretization and solution algorithm were discussed in section 3.4.

5.3.1 Numerical Result and Discussion at Fuel Feed Rate 98.5g/min

ANSYS FLUENT 13.0 was used to run the simulation at fuel feed rate of 98.5g/min with no SA and EA (SA0% and EA0%). The CFD study simulated the

palm shell combustion in the lab-scale fluidized-bed reactor, using the experimental operating conditions. The CFD model of the palm shell combustion for EA0% and SA0%was validated in the lab-scale fluidized-bed combustor. The results of the experiment are shown in Figure 5.1 and the comparison of the CFD results with the experiment are show in Figure 5.31.

Figure 5.1 shows that the temperatures in and near the bed areas from the experiment are significantly higher than the CFD results. This was caused by the fact that the oil palm waste had high volatile matter. The volatile matter were released and tended to burn easily in the bed or near the bed of the combustor. Secondly, the fiber components in the oil palm waste were light thus during the combustion process, these fibers were blown out got burnt easier in the bed, resulting in higher temperatures compared to the prediction by CFD. Thirdly, for the simulation cases, the multiphase flow structure near and around the air distributor is quit complex. Some reverse flow phenomena occurred in this area and also high flow curvature also existed close to the wall. In this case, the turbulent fluctuation in this area was anisotropic and k-ε turbulent model which is only good for isotropic turbulent was not able to properly simulate the flow. Better turbulent model have to be used in areas of reverse and high curvature flow. Lastly, for the CFD simulation domain, the outlet boundary condition was at the top of the freeboard where the pressure was set to atmospheric. However, for the experimental case, the atmospheric pressure condition was at the exhaust outlet.

At far distances from the bed, the temperatures from CFD and experiment agreed very well. This shows that the simulation model is reasonably valid for the combustion in ABFBC.

Figure 5.31 shows that the temperatures in and near the bed areas from the experiment are significantly higher than the CFD results. This was caused by the fact that the oil palm waste had high volatile matter. The volatile matter was released and tended to burn easily in the bed or near the bed of the combustor. Secondly, there was fiber component in the oil palm waste which burns easier than

the shell material, thus got burnt in or near the bed. The two reasons explained the higher temperatures from the experiment compared to the prediction by CFD.

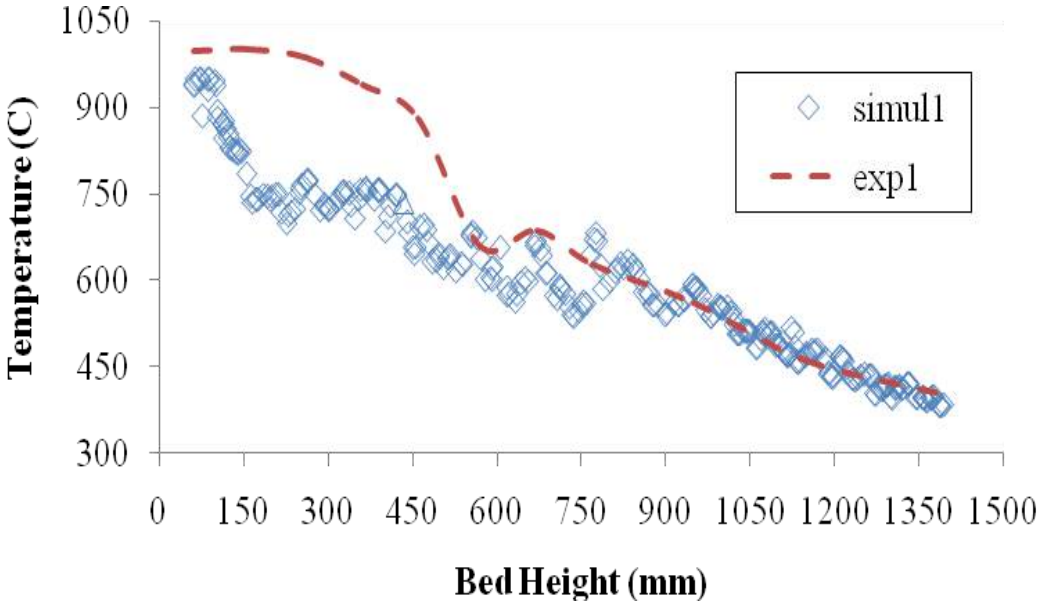

Figure 5.31 Numerical and experimental temperature data distribution at different heights above the bed of the ABFBC for EA0% and SA0%

Thirdly, for the simulation cases, the multiphase flow structure near and around the air distributor is quite complex. Some reverse flow phenomena occurred in this area and high flow curvature also existed close to the wall. In this case, the turbulent fluctuation in this area was anisotropic and the k-ε turbulent model which is only good for isotropic turbulence was not able to properly simulate the flow. Better turbulent model have to be used in areas of reverse and high curvature flow. Lastly, for the CFD simulation domain, the outlet boundary condition was at the top of the freeboard where the pressure was set to atmospheric. However, for the experiment, the atmospheric pressure condition was at the exhaust outlet.

The results at further distances from the bed, the temperatures of the CFD and experiment agreed very well. This shows that the simulation model is reasonably valid for the combustion in ABFBC.

CHAPTER 6

CONCLUSION AND RECOMMENDATIONS

6.1 Cold Flow

Experiments on solid-gas multiphase system using PIV and numerical modeling using ANSYS FLUENT 13.0 were performed. The numerical model was validated by the experimental data. From these two works, the following conclusions can be drawn:

i) According to the experiments, clusters appeared at various positions, and its shape and velocity varied with time. The visual images of various clusters were captured.

ii) The signals of the PIV were analyzed; hence, it could determine the axial velocity profiles and the axial solid concentration.

iii) At all cross-sections, velocities of particles were measured-which in the core region the velocities were higher than near the wall region.

iv) The comparison between the developed numerical model and experimental data on velocity profiles at all axial distance showed very close agreement.

6.2 Hot Flow

Experimental study to investigate the effects of staged air on the combustion of palm shell in a laboratory scale ABFBC and the numerical model using ANSYS FLUENT 13.0 was performed. The combustion performance is characterized by axial profiles of temperature, pollutant emissions (NO_X, CO, and CO_2), O_2 concentration and combustion efficiency. The following conclusions can be drawn.

i) Increasing of SA ratio will increase the in bed temperature but decrease the freeboard temperature for all percentages of EA.

ii) The use of air staging reduces NO_x emission and CO emission significantly from ABFBC as the proportion of SA is increased at 0% and 60% EA.

iii) The 0% and 60%EA at 40%SA is the optimum condition for CO emission reduction purposes.

iv) For fuel feed rate 87.9kg/min, the 0% and 60%EA at 30%SA can be used for NO_x emission reduction purposes.

v) For fuel feed rate 98.5kg/min, the 0% and 60%EA at 20% and 40%SA can be used for NO_x emission reduction purposes.

vi) Increasing of air staging level will decrease CO_2 concentration at 60%EA. Introduction of SA could assist in completing the oxidation of CO in the flue gas.

vii) The combustion efficiency increases with increasing SA for 60%EA at 20% and 40%SA

viii) Increasing of fuel feed rates will decrease the CO, NO_x and CO_2 concentrations.

ix) The combustion efficiency increases with increasing fuel feed rates.

x) The comparison between the developed numerical model and experimental data on temperature profiles along the height of the ABFBC showed very close agreements. Thus the experiment validated the developed numerical model.

6.3 Recommendations

To overcome the shortcomings from the research conducted, the following recommendations should be taken into consideration.

i) For the PIV experiment, the sand particles should be replaced with glass beads as they are transparent in nature. This will enable the laser light to go through the glass beads (solid phase) and hence the whole flow field could be better-analyzed.

ii) Obtain suitable technique to achieve simultaneous imaging for the whole height of the long Perspex (combustion chamber) so that the whole flow field can be visualized at the same time.

iii) The effect of fuel feeder system slope on the combustion performance should be studied at different slope angles from horizontal position.

REFERENCES

1. Varun, Prakash, R. and Bhat, I. K. Energy, Economics and Environmental Impacts of Renewable Energy Systems. *Renewable and Sustainable Energy Reviews.* 2009. 13(9):2716-2721.
2. Jappe Frandsen, F. Utilizing Biomass and Waste for Power Production--a Decade of Contributing to the Understanding, Interpretation and Analysis of Deposits and Corrosion Products. *Fuel.* 2005. 84(10):1277-1294.
3. Gross, R., Leach, M. and Bauen, A. Progress in Renewable Energy. *Environment International.* 2003. 29(1):105-122.
4. Shrestha, R. M., Malla, S. and Liyanage, M. H. Scenario-Based Analyses of Energy System Development and Its Environmental Implications in Thailand. *Energy Policy.* 2007. 35(6):3179-3193.
5. Koh, S. L. and Lim, Y. S. Meeting Energy Demand in a Developing Economy without Damaging the Environment--a Case Study in Sabah, Malaysia, from Technical, Environmental and Economic Perspectives. *Energy Policy.* 2010. 38(8):4719-4728.
6. Karki, S. K., Mann, M. D. and Salehfar, H. Energy and Environment in the Asean: Challenges and Opportunities. *Energy Policy.* 2005. 33(4):499-509.
7. Duic, N., Guzovic, Z. and Lund, H. Sustainable Development of Energy, Water and Environment Systems. *Energy.* 2011. 36(4):1839-1841.
8. Abdullah, K. Renewable Energy Conversion and Utilization in Asean Countries. *Energy.* 30(2-4):119-128.
9. Wahlund, B. Rational Bioenergy Utilisation in Energy Systems and Impacts on Co2 Emissions. *Doctorial thesis, Department of Chemical engineering and Technology, Energy proceses, Royal Institute of Technology, Stockholm, Sweden.* 2003.

10. Liu, D. C., Mi, T., Shen, B. X., Feng, B. and Franz, W. Reducing N2o Emission by Co-Combustion of Coal and Biomass. *Energy and Fuels.* 2002. 16(2):525-526.
11. Bhattacharya, S. C., Abdul Salam, P. and Sharma, M. Emissions from Biomass Energy Use in Some Selected Asian Countries. *Energy.* 2000. 25(2):169-188.
12. Omer, A. M. Green Energies and the Environment. *Renewable and Sustainable Energy Reviews.* 2008. 12(7):1789-1821.
13. Abbasi, T. and Abbasi, S. A. Biomass Energy and the Environmental Impacts Associated with Its Production and Utilization. *Renewable and Sustainable Energy Reviews.* 2010. 14(3):919-937.
14. Tillman, D. A. Biomass Cofiring: The Technology, the Experience, the Combustion Consequences. *Biomass and Bioenergy.* 2000. 19(6):365-384.
15. Zhou, X., Wang, F., Hu, H., Yang, L., Guo, P. and Xiao, B. Assessment of Sustainable Biomass Resource for Energy Use in China. *Biomass and Bioenergy.* 2011. 35(1):1-11.
16. Yin, C., Rosendahl, L. A. and Kær, S. K. Grate-Firing of Biomass for Heat and Power Production. *Progress in Energy and Combustion Science.* 2008. 34(6):725-754.
17. Trebbi, G. Power-Production Options from Biomass: The Vision of a Southern European Utility. *Bioresource Technology.* 1993. 46(1-2):23-29.
18. Suppes, G. J. and Storvick, T. S. Energy Reserves and Renewable Energy Sources. *In* Galen, JS and Truman, SS, eds. Sustainable Nuclear Power Academic Press, Burlington. 2007.
19. Sta, hl, K. and Neergaard, M. Igcc Power Plant for Biomass Utilisation, Värnamo, Sweden. *Biomass and Bioenergy.* 1998. 15(3):205-211.
20. Baratieri, M., Baggio, P., Fiori, L. and Grigiante, M. Biomass as an Energy Source: Thermodynamic Constraints on the Performance of the Conversion Process. *Bioresource Technology.* 2008. 99(15):7063-7073.
21. Dowaki, K. and Mori, S. Biomass Energy Used in a Sawmill. *Applied Energy.* 2005. 80(3):327-339.
22. Balat, H. and Kirtay, E. Hydrogen from Biomass - Present Scenario and Future Prospects. *International Journal of Hydrogen Energy.* 2010. 35(14):7416-7426.

23. Gokcol, C., Dursun, B., Alboyaci, B. and Sunan, E. Importance of Biomass Energy as Alternative to Other Sources in Turkey. *Energy Policy*. 2009. 37(2):424-431.
24. Demirbas, A. H. and Demirbas, I. Importance of Rural Bioenergy for Developing Countries. *Energy Conversion and Management*. 2007. 48(8):2386-2398.
25. Sulaiman, F., Abdullah, N., Gerhauser, H. and Shariff, A. An Outlook of Malaysian Energy, Oil Palm Industry and Its Utilization of Wastes as Useful Resources. *Biomass and Bioenergy*. In Press, Corrected Proof.
26. Demirbas, A. Potential Applications of Renewable Energy Sources, Biomass Combustion Problems in Boiler Power Systems and Combustion Related Environmental Issues. *Progress in Energy and Combustion Science*. 2005. 31(2):171-192.
27. Demirbas, M. F., Balat, M. and Balat, H. Potential Contribution of Biomass to the Sustainable Energy Development. *Energy Conversion and Management*. 2009. 50(7):1746-1760.
28. Kelly-Yong, T. L., Lee, K. T., Mohamed, A. R. and Bhatia, S. Potential of Hydrogen from Oil Palm Biomass as a Source of Renewable Energy Worldwide. *Energy Policy*. 2007. 35(11):5692-5701.
29. Chen, L., Xing, L. and Han, L. Renewable Energy from Agro-Residues in China: Solid Biofuels and Biomass Briquetting Technology. *Renewable and Sustainable Energy Reviews*. 2009. 13(9):2689-2695.
30. Kaltschmitt, M., Thrän, D. and Smith, K. R. Renewable Energy from Biomass. *In* Robert, AM, ed. Encyclopedia of Physical Science and Technology Academic Press, New York. 2001.
31. Yusoff, S. Renewable Energy from Palm Oil - Innovation on Effective Utilization of Waste. *Journal of Cleaner Production*. 2006. 14(1):87-93.
32. Saidur, R., Abdelaziz, E. A., Demirbas, A., Hossain, M. S. and Mekhilef, S. A Review on Biomass as a Fuel for Boilers. *Renewable and Sustainable Energy Reviews*. 2011. 15(5):2262-2289.
33. Arena, U., Di Gregorio, F. and Santonastasi, M. A Techno-Economic Comparison between Two Design Configurations for a Small Scale, Biomass-to-Energy Gasification Based System. *Chemical Engineering Journal*. 2010. 162(2):580-590.

34. Abnisa, F., Daud, W. M. A. W., Husin, W. N. W. and Sahu, J. N. Utilization Possibilities of Palm Shell as a Source of Biomass Energy in Malaysia by Producing Bio-Oil in Pyrolysis Process. *Biomass and Bioenergy.* In Press, Corrected Proof.
35. Hall, D. O. Biomass Energy in Industrialised Countries--a View of the Future. *Forest Ecology and Management.* 1997. 91(1):17-45.
36. Chuah, T. G., Wan Azlina, A. G. K., Robiah, Y. and Omar, R. Biomass as the Renewable Energy Sources in Malaysia: An Overview. *International Journal of Green Energy.* 2006. 3(3):323-346.
37. Chaturvedi, P. Biomass--the Fuel of the Rural Poor in Developing Countries. *In* Ralph, EHS, ed. Bioenergy Options for a Cleaner Environment Elsevier, Oxford. 2004.
38. Carlos, R. M. and Ba Khang, D. Characterization of Biomass Energy Projects in Southeast Asia. *Biomass and Bioenergy.* 2008. 32(6):525-532.
39. Zhang, L., Xu, C. and Champagne, P. Overview of Recent Advances in Thermo-Chemical Conversion of Biomass. *Energy Conversion and Management.* 2010. 51(5):969-982.
40. Abbas, T., Costen, P. G. and Lockwood, F. C. Solid Fuel Utilization: From Coal to Biomass. *Symposium (International) on Combustion.* 1996. 26(2):3041-3058.
41. Keong, W. K. Soft Energy from Palm Oil and Its Wastes. *Agricultural Wastes.* 1981. 3(3):191-200.
42. Basu, P. Biomass Characteristics. Biomass Gasification Design Handbook Academic Press, Boston. 2010.
43. Prasertsan, S. and Prasertsan, P. Biomass Residues from Palm Oil Mills in Thailand: An Overview on Quantity and Potential Usage. *Biomass and Bioenergy.* 1996. 11(5):387-395.
44. Prasertsan, S. and Sajjakulnukit, B. Biomass and Biogas Energy in Thailand: Potential, Opportunity and Barriers. *Renewable Energy.* 2006. 31(5):599-610.
45. Barlow, C., Zen, Z. and Gondowarsito, R. The Indonesian Oil Palm Industry. *Oil Palm Industry Economic Journal.* 2003. 3(1):8-15.
46. Shuit, S. H., Tan, K. T., Lee, K. T. and Kamaruddin, A. H. Oil Palm Biomass as a Sustainable Energy Source: A Malaysian Case Study. *Energy.* 2009. 34(9):1225-1235.

47. Sumathi, S., Chai, S. P. and Mohamed, A. R. Utilization of Oil Palm as a Source of Renewable Energy in Malaysia. *Renewable and Sustainable Energy Reviews.* 2008. 12(9):2404-2421.

48. Mahlia, T. M. I., Abdulmuin, M. Z., Alamsyah, T. M. I. and Mukhlishien, D. An Alternative Energy Source from Palm Wastes Industry for Malaysia and Indonesia. *Energy Conversion and Management.* 2001. 42(18):2109-2118.

49. Armesto, L., Boerrigter, H., Bahillo, A. and Otero, J. N2o Emissions from Fluidised Bed Combustion. The Effect of Fuel Characteristics and Operating Conditions* 1. *Fuel.* 2003. 82(15-17):1845-1850.

50. Winter, F., Wartha, C., Löffler, G. and Hofbauer, H. The No and N2o Formation Mechanism During Devolatilization and Char Combustion under Fluidized-Bed Conditions. *Symposium (International) on Combustion.* 1996. 26(2):3325-3334.

51. Valentim, B., Lemos de Sousa, M. J., Abelha, P., Boavida, D. and Gulyurtlu, I. Combustion Studies in a Fluidised Bed--the Link between Temperature, Nox and N2o Formation, Char Morphology and Coal Type. *International Journal of Coal Geology.* 2006. 67(3):191-201.

52. Tourunen, A., Saastamoinen, J. and Nevalainen, H. Experimental Trends of No in Circulating Fluidized Bed Combustion. *Fuel.* 2009. 88(7):1333-1341.

53. Suzuki, Y., Moritomi, H. and Tanaka, H. Reduction of N2o Emissions from Circulating Fluidized Bed Combustors by Injection of Fuel Gases and Changing of Coal Feed Point. *Energy Conversion and Management.* 37(6-8):1285-1290.

54. Loeffler, G., Wartha, C., Winter, F. and Hofbauer, H. Study on No and N2o Formation and Destruction Mechanisms in a Laboratory-Scale Fluidized Bed. *Energy and Fuels.* 2002. 16(5):1024-1032.

55. Mann, M. D., Collings, M. E. and Botros, P. E. Nitrous-Oxide Emissions in Fluidized-Bed Combustion - Fundamental Chemistry and Combustion Testing. *Progress in Energy and Combustion Science.* 1992. 18(5):447-461.

56. Shen, B. X., Mi, T., Liu, D. C., Feng, B., Yao, Q. and Winter, F. N2o Emission under Fluidized Bed Combustion Condition. *Fuel Processing Technology.* 2003. 84(1-3):13-21.

57. Bonn, B., Pelz, G. and Baumann, H. Formation and Decomposition of N2o in Fluidized Bed Boilers. *Fuel.* 1995. 74(2):165-171.

58. Qian, F. P., Chyang, C. S., Huang, K. S. and Tso, J. Combustion and No Emission of High Nitrogen Content Biomass in a Pilot-Scale Vortexing Fluidized Bed Combustor. *Bioresource Technology.* 2011. 102(2):1892-1898.

59. Permchart, W. and Kouprianov, V. I. Emission Performance and Combustion Efficiency of a Conical Fluidized-Bed Combustor Firing Various Biomass Fuels. *Bioresource Technology.* 2004. 92(1):83-91.

60. Nordin, A., Eriksson, L. and Öhman, M. No Reduction in a Fluidized Bed Combustor with Primary Measures and Selective Non-Catalytic Reduction : A Screening Study Using Statistical Experimental Designs. *Fuel.* 1995. 74(1):128-135.

61. Mahmoudi, S., Baeyens, J. and Seville, J. P. K. Nox Formation and Selective Non-Catalytic Reduction (Sncr) in a Fluidized Bed Combustor of Biomass. *Biomass and Bioenergy.* 2010. 34(9):1393-1409.

62. Leckner, B. Fluidized Bed Combustion: Mixing and Pollutant Limitation. *Progress in Energy and Combustion Science.* 1998. 24(1):31-61.

63. Leckner, B., Ã…mand, L. E., LÃ¼cke, K. and Werther, J. Gaseous Emissions from Co-Combustion of Sewage Sludge and Coal/Wood in a Fluidized Bed. *Fuel.* 2004. 83(4-5):477-486.

64. Leckner, B. and Karlsson, M. Gaseous Emissions from Circulating Fluidized Bed Combustion of Wood. *Biomass and Bioenergy.* 1993. 4(5):379-389.

65. Li, Y. H., Lu, G. Q. and Rudolph, V. The Kinetics of No and N2o Reduction over Coal Chars in Fluidised-Bed Combustion. *Chemical Engineering Science.* 1998. 53(1):1-26.

66. Löffler, G., Wargadalam, V. J. and Winter, F. Catalytic Effect of Biomass Ash on Co, Ch4 and Hcn Oxidation under Fluidised Bed Combustor Conditions. *Fuel.* 2002. 81(6):711-717.

67. Kouprianov, V. I. and Permchart, W. Emissions from a Conical Fbc Fired with a Biomass Fuel. *Applied Energy.* 74(3-4):383-392.

68. Johansson, L. S., Tullin, C., Leckner, B. and Sjövall, P. Particle Emissions from Biomass Combustion in Small Combustors. *Biomass and Bioenergy.* 2003. 25(4):435-446.

69. Janvijitsakul, K. and Kuprianov, V. I. Major Gaseous and Pah Emissions from a Fluidized-Bed Combustor Firing Rice Husk with High Combustion Efficiency. *Fuel Processing Technology.* 2008. 89(8):777-787.

70. Grass, S. W. and Jenkins, B. M. Biomass Fueled Fluidized Bed Combustion: Atmospheric Emissions, Emission Control Devices and Environmental Regulations. *Biomass and Bioenergy.* 1994. 6(4):243-260.

71. Chyang, C.-S., Wu, K.-T. and Lin, C.-S. Emission of Nitrogen Oxides in a Vortexing Fluidized Bed Combustor. *Fuel.* 2007. 86(1-2):234-243.

72. Armesto, L., Boerrigter, H., Bahillo, A. and Otero, J. N2o Emissions from Fluidised Bed Combustion. The Effect of Fuel Characteristics and Operating Conditions. *Fuel.* 82(15-17):1845-1850.

73. Gungor, A. and Eskin, N. Effects of Operational Parameters on Emission Performance and Combustion Efficiency in Small-Scale Cfbcs. *Journal of the Chinese Institute of Chemical Engineers.* 2008. 39(6):541-556.

74. Okasha, F. Modeling Combustion of Straw-Bitumen Pellets in a Fluidized Bed. *Fuel Processing Technology.* 2007. 88(3):281-293.

75. Yang, Y. B., Newman, R., Sharifi, V., Swithenbank, J. and Ariss, J. Mathematical Modelling of Straw Combustion in a 38 mwe Power Plant Furnace and Effect of Operating Conditions. *Fuel.* 2007. 86(1-2):129-142.

76. Scala, F. and Salatino, P. Modelling Fluidized Bed Combustion of High-Volatile Solid Fuels. *Chemical Engineering Science.* 2002. 57(7):1175-1196.

77. Krzywanski, J., Czakiert, T., Muskala, W. and Nowak, W. Modelling of Co2, Co, So2, O2 and Nox Emissions from the Oxy-Fuel Combustion in a Circulating Fluidized Bed. *Fuel Processing Technology.* 2011. 92(3):590-596.

78. Rozainee, M., Ngo, S. P., Salema, A. A. and Tan, K. G. Computational Fluid Dynamics Modeling of Rice Husk Combustion in a Fluidised Bed Combustor. *Powder Technology.* 2010. 203(2):331-347.

79. Gungor, A. Two-Dimensional Biomass Combustion Modeling of Cfb. *Fuel.* 2008. 87(8-9):1453-1468.

80. Agraniotis, M., Stamatis, D., Grammelis, P. and Kakaras, E. Numerical Investigation on the Combustion Behaviour of Pre-Dried Greek Lignite. *Fuel.* 2009. 88(12):2385-2391.

81. Gorostiza, L. G. and Rodrigues, E. R. A Stochastic Model for Transport of Particulate Matter in Air: An Asymptotic Analysis. *Acta Applicandae Mathematicae.* 1999. 59(1):21-43.

82. Steingart, D. A. and Evans, J. W. Measurements of Granular Flows in Two-Dimensional Hoppers by Particle Image Velocimetry. Part I: Experimental Method and Results. *Chemical Engineering Science.* 2005. 60(4):1043-1051.

83. Lueptow, R., Akonur, A. and Shinbrot, T. Piv for Granular Flows. *Experiments in Fluids.* 2000. 28(2):183-186.

84. Kompenhans, J. and Kähler, C. Particle Image Velocimetry--an Advanced Experimental Tool for the Investigation of Turbulent Flow Fields. *In* Rodi, W and Fueyo, N, eds. Engineering Turbulence Modelling and Experiments 5 Elsevier Science Ltd, Oxford. 2002.

85. Leckner, B. Fluidized Bed Combustion: Simeon N. Oka, Marcel Decker Inc., 2004, Isbn 0-8247-4699-6. *Energy.* 2005. 30(1):97-99.

86. Jiradilok, V., Gidaspow, D., Damronglerd, S., Koves, W. J. and Mostofi, R. Kinetic Theory Based Cfd Simulation of Turbulent Fluidization of Fcc Particles in a Riser. *Chemical Engineering Science.* 2006. 61(17):5544-5559.

87. Ahuja, G. N. and Patwardhan, A. W. Cfd and Experimental Studies of Solids Hold-up Distribution and Circulation Patterns in Gas-Solid Fluidized Beds. *Chemical Engineering Journal.* 2008. 143(1-3):147-160.

88. Hosseini, S. H., Ahmadi, G., Rahimi, R., Zivdar, M. and Esfahany, M. N. Cfd Studies of Solids Hold-up Distribution and Circulation Patterns in Gas-Solid Fluidized Beds. *Powder Technology.* 2010. 200(3):202-215.

89. Abdullah, H., Ani, F. N., Jaafar, M. and Nazri, M. Combustion Characteristics Study of Biomass in a Fluidized Bed Combustor. 2005.

90. Koornneef, J., Junginger, M. and Faaij, A. Development of Fluidized Bed Combustion--an Overview of Trends, Performance and Cost. *Progress in Energy and Combustion Science.* 2007. 33(1):19-55.

91. Anthony, E. J. Fluidized Bed Combustion of Alternative Solid Fuels; Status, Successes and Problems of the Technology. *Progress in Energy and Combustion Science.* 1995. 21(3):239-268.

92. Scala, F. and Chirone, R. Fluidized Bed Combustion of Alternative Solid Fuels. *Experimental Thermal and Fluid Science.* 2004. 28(7):691-699.

93. Khan, A. A., de Jong, W., Jansens, P. J. and Spliethoff, H. Biomass Combustion in Fluidized Bed Boilers: Potential Problems and Remedies. *Fuel Processing Technology*. 2009. 90(1):21-50.

94. Hupa, M. Current Status and Challenges within Fluidized Bed Combustion. *Advanced Combustion and Aerothermal Technologies: Environmental Protection and Pollution Reductions.* 2007:87-101.

95. Kovacs, J. What Are the Main Characteristics of Fluidised Bed Combustors? *Combustion File*. 2001. 87(1).

96. Williams, A., Jones, J. M., Ma, L. and Pourkashanian, M. Pollutants from the Combustion of Solid Biomass Fuels. *Progress in Energy and Combustion Science.* 2012. 38(2):113-137.

97. Vassilev, S. V., Baxter, D., Andersen, L. K. and Vassileva, C. G. An Overview of the Chemical Composition of Biomass. *Fuel.* 2010. 89(5):913-933.

98. Ayhan, D. Combustion Characteristics of Different Biomass Fuels. *Progress in Energy and Combustion Science.* 2004. 30(2):219-230.

99. Demirbas, A. Combustion Characteristics of Different Biomass Fuels. *Progress in Energy and Combustion Science.* 2004. 30(2):219-230.

100. Plunkett, J. W. *Plunkett's Energy Industry Almanac 2008*. Plunkett Research, Ltd. 2007.

101. Srinivasa Rao, K. and Venkat Reddy, G. Effect of Secondary Air Injection on the Combustion Efficiency of Sawdust in a Fluidized Bed Combustor. *Brazilian Journal of Chemical Engineering.* 2008. 25(1):129-141.

102. Varol, M. and Atimtay, A. T. Combustion of Olive Cake and Coal in a Bubbling Fluidized Bed with Secondary Air Injection. *Fuel.* 2007. 86(10-11):1430-1438.

103. Atimtay, A. T. and Varol, M. Investigation of Co-Combustion of Coal and Olive Cake in a Bubbling Fluidized Bed with Secondary Air Injection. *Fuel.* 2009. 88(6):1000-1008.

104. Munir, S., Nimmo, W. and Gibbs, B. M. The Effect of Air Staged, Co-Combustion of Pulverised Coal and Biomass Blends on Nox Emissions and Combustion Efficiency. *Fuel.* 2011. 90(1):126-135.

105. Yang, Y. B., Ryu, C., Khor, A., Yates, N. E., Sharifi, V. N. and Swithenbank, J. Effect of Fuel Properties on Biomass Combustion. Part Ii.

Modelling Approach--Identification of the Controlling Factors. *Fuel.* 2005. 84(16):2116-2130.

106. Kuprianov, V. I., Kaewklum, R. and Chakritthakul, S. Effects of Operating Conditions and Fuel Properties on Emission Performance and Combustion Efficiency of a Swirling Fluidized-Bed Combustor Fired with a Biomass Fuel. *Energy.* In Press, Corrected Proof.
107. Sirisomboon, K., Kuprianov, V. I. and Arromdee, P. Effects of Design Features on Combustion Efficiency and Emission Performance of a Biomass-Fuelled Fluidized-Bed Combustor. *Chemical Engineering and Processing: Process Intensification.* 2010. 49(3):270-277.
108. Winter, F., Wartha, C. and Hofbauer, H. No and N2o Formation During the Combustion of Wood, Straw, Malt Waste and Peat. *Bioresource Technology.* 1999. 70(1):39-49.
109. Nussbaumer, T. Combustion and Co-Combustion of Biomass: Fundamentals, Technologies, and Primary Measures for Emission Reduction. *Energy and Fuels.* 2003. 17(6):1510-1521.
110. Gungor, A. Prediction of So2 and Nox Emissions for Low-Grade Turkish Lignites in Cfb Combustors. *Chemical Engineering Journal.* 2009. 146(3):388-400.
111. Sun, Z., Jin, B., Zhang, M. and Liu, R. Cotton Stalk Combustion in a Circulating Fluidized Bed. *Chemical Engineering and Technology.* 2008. 31(11):1605-1614.
112. Sun, Z., Jin, B., Zhang, M., Liu, R. and Zhang, Y. Experimental Studies on Cotton Stalk Combustion in a Fluidized Bed. *Energy.* 2008. 33(8):1224-1232.
113. Sulaiman, F., Abdullah, N., Gerhauser, H. and Shariff, A. An Outlook of Malaysian Energy, Oil Palm Industry and Its Utilization of Wastes as Useful Resources. *Biomass and Bioenergy.* 2011. 35(9):3775-3786.
114. Palm Oil Production to Strengthen in Malaysia, Indonesia. *Focus on Surfactants.* 2006. 2006(8):2.
115. Horio, M. Fluidization Science, Its Development and Future. *Particuology.* 2010. 8(6):514-524.
116. Werther, J. Fluidization Technology Development — the Industry/Academia Collaboration Issue. *Powder Technology.* 2000. 113(3):230-241.

117. Vun, S., Naser, J., Witt, P. J. and Yang, W. Measurements and Numerical Predictions of Gas Vortices Formed by Single Bubble Eruptions in the Freeboard of a Fluidised Bed. *Chemical Engineering Science.* 2010. 65(22):5808-5820.

118. Peng, B., Zhang, C. and Zhu, J. Theoretical and Numerical Studies on the Flow Multiplicity Phenomenon for Gas-Solids Two-Phase Flows in Cfb Risers. *International Journal of Multiphase Flow.* 2011. 37(6):660-670.

119. van Wachem, B. G. M., Schouten, J. C., Krishna, R. and van den Bleek, C. M. Validation of the Eulerian Simulated Dynamic Behaviour of Gas–Solid Fluidised Beds. *Chemical Engineering Science.* 1999. 54(13–14):2141-2149.

120. Ekambara, K., Dhotre, M. T. and Joshi, J. B. Cfd Simulations of Bubble Column Reactors: 1d, 2d and 3d Approach. *Chemical Engineering Science.* 2005. 60(23):6733-6746.

121. Wolfrum, J. Lasers in Combustion: From Basic Theory to Practical Devices. *Symposium (International) on Combustion.* 1998. 27(1):1-41.

122. Wang, X. S., Palero, V., Soria, J. and Rhodes, M. J. Laser-Based Planar Imaging of Nano-Particle Fluidization: Part I--Determination of Aggregate Size and Shape. *Chemical Engineering Science.* 2006. 61(16):5476-5486.

123. Wang, X. S., Palero, V., Soria, J. and Rhodes, M. J. Laser-Based Planar Imaging of Nano-Particle Fluidization: Part Ii--Mechanistic Analysis of Nanoparticle Aggregation. *Chemical Engineering Science.* 2006. 61(24):8040-8049.

124. Solimene, R., Marzocchella, A., Ragucci, R. and Salatino, P. Laser Diagnostics of Hydrodynamics and Gas-Mixing Induced by Bubble Bursting at the Surface of Gas-Fluidized Beds. *Chemical Engineering Science.* 2007. 62(1-2):94-108.

125. Du, L., Yao, J. Z. and Lin, W. G. Experimental Study of Particle Flow in a Gas-Solid Separator with Baffles Using Pdpa. *Chemical Engineering Journal.* 2005. 108(1-2):59-67.

126. Ibsen, C. H., Solberg, T., Hjertager, B. H. and Johnsson, F. Laser Doppler Anemometry Measurements in a Circulating Fluidized Bed of Metal Particles. *Experimental Thermal and Fluid Science.* 2002. 26(6-7):851-859.

127. Lackermeier, U., Rudnick, C., Werther, J., Bredebusch, A. and Burkhardt, H. Visualization of Flow Structures inside a Circulating Fluidized Bed by

Means of Laser Sheet and Image Processing. *Powder Technology*. 2001. 114(1-3):71-83.

128. Mudde, R. F., Groen, J. S. and Van Den Akker, H. E. A. Application of Lda to Bubbly Flows. *Nuclear Engineering and Design*. 1998. 184(2-3):329-338.
129. Busciglio, A., Grisafi, F., Scargiali, F. and Brucato, A. On the Measurement of Bubble Size Distribution in Gas-Liquid Contactors Via Light Sheet and Image Analysis. *Chemical Engineering Science*. 2010. 65(8):2558-2568.
130. Chen, R. C. and Fan, L. S. Particle Image Velocimetry for Characterizing the Flow Structure in Three-Dimensional Gas-Liquid-Solid Fluidized Beds. *Chemical Engineering Science*. 47(13-14):3615-3622.
131. Sathe, M. J., Thaker, I. H., Strand, T. E. and Joshi, J. B. Advanced Piv/Lif and Shadowgraphy System to Visualize Flow Structure in Two-Phase Bubbly Flows. *Chemical Engineering Science*. 2010. 65(8):2431-2442.
132. Armstrong, L. M., Gu, S. and Luo, K. H. Three-Dimensional Modelling on the Hydrodynamics of a Circulating Fluidised Bed. 2009.
133. Bertrand, F., Leclaire, L. A. and Levecque, G. Dem-Based Models for the Mixing of Granular Materials. *Chemical Engineering Science*. 60(8-9):2517-2531.
134. Buwa, V. V., Deo, D. S. and Ranade, V. V. Eulerian-Lagrangian Simulations of Unsteady Gas-Liquid Flows in Bubble Columns. *International Journal of Multiphase Flow*. 2006. 32(7):864-885.
135. Chaikittisilp, W., Taenumtrakul, T., Boonsuwan, P., Tanthapanichakoon, W. and Charinpanitkul, T. Analysis of Solid Particle Mixing in Inclined Fluidized Beds Using Dem Simulation. *Chemical Engineering Journal*. 2006. 122(1-2):21-29.
136. Chen, X.-Z., Shi, D.-P., Gao, X. and Luo, Z.-H. A Fundamental Cfd Study of the Gas-Solid Flow Field in Fluidized Bed Polymerization Reactors. *Powder Technology*. 2011. 205(1-3):276-288.
137. Cheng, Y. and Zhu, J. Hydrodynamics and Scale-up of Liquid-Solid Circulating Fluidized Beds: Similitude Method Vs. Cfd. *Chemical Engineering Science*. 2008. 63(12):3201-3211.
138. Cornelissen, J. T., Taghipour, F., Escudié, R., Ellis, N. and Grace, J. R. Cfd Modelling of a Liquid-Solid Fluidized Bed. *Chemical Engineering Science*. 2007. 62(22):6334-6348.

139. Das, A. K., De Wilde, J., Heynderickx, G. J., Marin, G. B., Vierendeels, J. and Dick, E. Cfd Simulation of Dilute Phase Gas-Solid Riser Reactors: Part I--a New Solution Method and Flow Model Validation. *Chemical Engineering Science.* 2004. 59(1):167-186.

140. He, Y. and Rudolph, V. Gas-Solids Flow in the Riser of a Circulating Fluidized Bed. *Chemical Engineering Science.* 1995. 50(21):3443-3453.

141. Huilin, L., Yunhua, Z., Ding, J., Gidaspow, D. and Wei, L. Investigation of Mixing/Segregation of Mixture Particles in Gas-Solid Fluidized Beds. *Chemical Engineering Science.* 2007. 62(1-2):301-317.

142. Koenigsdorff, R. and Werther, J. Gas-Solids Mixing and Flow Structure Modeling of the Upper Dilute Zone of a Circulating Fluidized Bed. *Powder Technology.* 1995. 82(3):317-329.

143. Bai, D., Shibuya, E., Masuda, Y., Nakagawa, N. and Kato, K. Flow Structure in a Fast Fluidized Bed. *Chemical Engineering Science.* 1996. 51(6):957-966.

144. Ellis, N., Bi, H. T., Lim, C. J. and Grace, J. R. Hydrodynamics of Turbulent Fluidized Beds of Different Diameters. *Powder Technology.* 2004. 141(1-2):124-136.

145. Jun, L., Changqing, D., Junjiao, Z. and Yongping, Y. Experimental Research on Gas-Solid Flow in a Dual Fluidized Bed. *Sustainable Power Generation and Supply, 2009. SUPERGEN '09. International Conference on.* 6-7 April 2009. 2009. 1-6.

146. Lijie, Y., Shuyan, W., Huilin, L., Shuai, W., Pengfei, X., Lixing, W. and Yurong, H. Flow of Gas and Particles in a Bubbling Fluidized Bed with a Filtered Two-Fluid Model. *Chemical Engineering Science.* 2010. 65(9):2664-2679.

147. Fan, X., Yang, Z., Parker, D. J. and Armstrong, B. Prediction of Bubble Behaviour in Fluidised Beds Based on Solid Motion and Flow Structure. *Chemical Engineering Journal.* 2008. 140(1–3):358-369.

148. Chok, V. S., Gorin, A. and Chua, H. B. Minimum and Complete Fluidization Velocity for Sand-Palm Shell Mixtures, Part Ii: Characteristic Velocity Profiles, Critical Loading and Binary Correlations. *American Journal of Applied Sciences.* 2010. 7(6):773-779.

149. Kaewklum, R., Kuprianov, V. I. and Douglas, P. L. Hydrodynamics of Air-Sand Flow in a Conical Swirling Fluidized Bed: A Comparative Study between Tangential and Axial Air Entries. *Energy Conversion and Management.* 2009. 50(12):2999-3006.

150. Abdullah, M. Z., Husain, Z. and Yin Pong, S. L. Analysis of Cold Flow Fluidization Test Results for Various Biomass Fuels. *Biomass and Bioenergy.* 2003. 24(6):487-494.

151. Cui, H. and Grace, J. R. Fluidization of Biomass Particles: A Review of Experimental Multiphase Flow Aspects. *Chemical Engineering Science.* 2007. 62(1-2):45-55.

152. Hongbo, L., Feng, Z. and Guangyu, Z. Experimental Study on Fluidization Characteristics of Mixture of Biomass and Coal in a Fluidized Bed. *Power and Energy Engineering Conference (APPEEC), 2010 Asia-Pacific.* 28-31 March 2010. 2010. 1-4.

153. Miao, Q., Wang, C., Wu, C., Yin, X. and Zhu, J. Fluidization of Sawdust in a Cold Model Circulating Fluidized Bed: Experimental Study. *Chemical Engineering Journal.* 2011. 167(1):335-341.

154. Zhou, W., Zhao, C. S., Duan, L. B., Chen, X. P. and Liang, C. Two-Dimensional Computational Fluid Dynamics Simulation of Nitrogen and Sulfur Oxides Emissions in a Circulating Fluidized Bed Combustor. *Chemical Engineering Journal.* 2011. 173(2):564-573.

155. Zhou, H., Flamant, G. and Gauthier, D. Dem-Les of Coal Combustion in a Bubbling Fluidized Bed. Part I: Gas-Particle Turbulent Flow Structure. *Chemical Engineering Science.* 2004. 59(20):4193-4203.

156. Zhou, H., Flamant, G. and Gauthier, D. Dem-Les Simulation of Coal Combustion in a Bubbling Fluidized Bed Part Ii: Coal Combustion at the Particle Level. *Chemical Engineering Science.* 2004. 59(20):4205-4215.

157. Gungor, A. Two-Dimensional Biomass Combustion Modeling of Cfb. *Fuel.* 2008. 87(8–9):1453-1468.

158. Zhou, W., Zhao, C. S., Duan, L. B., Qu, C. R. and Chen, X. P. Two-Dimensional Computational Fluid Dynamics Simulation of Coal Combustion in a Circulating Fluidized Bed Combustor. *Chemical Engineering Journal.* 2011. 166(1):306-314.

159. Afsin, G. Simulation of Emission Performance and Combustion Efficiency in Biomass Fired Circulating Fluidized Bed Combustors. *Biomass and Bioenergy.* 2010. 34(4):506-514.

160. Versteeg, H. K. and Malalasekera, W. *An Introduction to Computational Fluid Dynamics: The Finite Volume Method*. Prentice Hall 2007.

161. Tu, J., Yeoh, G. H. and Liu, C. *Computational Fluid Dynamics: A Practical Approach*. Butterworth Heinemann 2008.

162. Shah, S., Klajny, M., Myöhänen, K. and Hyppänen, T. Improvement of Cfd Methods for Modeling Full Scale Circulating Fluidized Bed Combustion Systems. *Proceedings of the 20th International Conference on Fluidized Bed Combustion.* Springer. 2010. 792-798.

163. Kumar, R. and Pandey, K. Cfd Analysis of Circulating Fluidized Bed Combustion.

164. Fluent, A. 13.0. *Theory Guide. ANSYS Inc.* 2010.

165. Chiesa, M., Mathiesen, V., Melheim, J. A. and Halvorsen, B. Numerical Simulation of Particulate Flow by the Eulerian–Lagrangian and the Eulerian–Eulerian Approach with Application to a Fluidized Bed. *Computers & Chemical Engineering.* 2005. 29(2):291-304.

166. Singh, R. I., Brink, A. and Hupa, M. Cfd Modelling to Study Fluidized Bed Combustion and Gasification. *Applied Thermal Engineering.* (0).

167. Zhang, N., Lu, B., Wang, W. and Li, J. 3d Cfd Simulation of Hydrodynamics of a 150 Mwe Circulating Fluidized Bed Boiler. *Chemical Engineering Journal.* 2010. 162(2):821-828.

168. Kuprianov, V. I., Kaewklum, R. and Chakritthakul, S. Effects of Operating Conditions and Fuel Properties on Emission Performance and Combustion Efficiency of a Swirling Fluidized-Bed Combustor Fired with a Biomass Fuel. *Energy.* 2011. 36(4):2038-2048.

APPENDIX A

LIST OF PUBLICATIONS

A.1 Journal

1. Mohd Jaafar, Mohammad Nazri; Permatasari, Rosyida; Mohd Sobree, Mohd Nazar Yakin. Pengurangan Pelepasan Emisi dari Pembakar Lapisan Terbendalir Menggunakan Tempurung Kelapa Sawit Sebagai Bahan Api. *Jurnal Teknologi*, 2012. 59:07-11.

A.2 Proceedings

1. Rosyida Permatasari; Mohd Jaafar, M.N.; Tholudin Mat Lazim; Mohammad Sayuthy. Flow Characterization of Gas - Solid Mixture in Fluidized Bed Combustion. 1st Engineering Conference on Energy & Environment. Kuching, Sarawak, Malaysia, December 27-28, 2007.
2. Rosyida Permatasari; Mohd Jaafar, M.N.; Mohammad Nazar Yakin. Combustion Characteristics of Fluidized Bed Combustion Using Palm Shell Fuel. 7th High Temperature Air Combustion and Gasification International Symposium. Phuket, Thailand, January 13-16, 2008.
3. Rosyida Permatasari; Mohd Jaafar, M.N. Combustion Characteristics of Palm Shell Fuel in Fluidized Bed Combustion. Proceedings of the International Graduate on Engineering and Science. UTM Skudai, Malaysia, December 23-24, 2008.

4. Rosyida Permatasari; Kang Kin Hui; Mohd Jaafar, M.N. Combustion Characteristice of Palm Wastes in Fluidized Bed Combustor. 8th EEEIC International Conference on Environment and Electrical Engineering. Karpacz, Poland, May 10-13, 2009.
5. Rosyida Permatasari; Mohd Jaafar, M.N. Emission Characteristics of Palm Shell Fuel in Fluidized Bed Combustion. 2nd International Conference on Mechanical and Electronics Engineering, ICMEE 2010. Kyoto, Japan. August 1-3, 2010.

APPENDIX B

THERMOCOUPLE & TYPE ACCORDING TO ANSI STANDARD

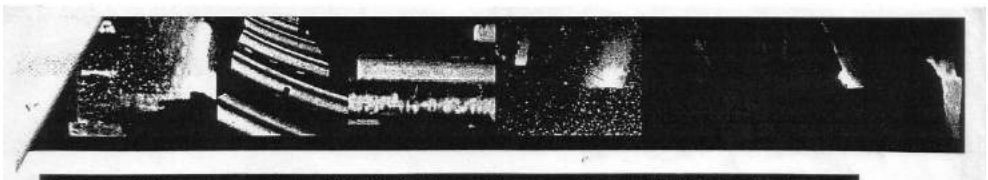

Types of Thermocouple and its limitation with according to ANSI standard

ANSI CODE	CONDUCTOR COMBINATIONS POSITIVE + LEG	CONDUCTOR COMBINATIONS NEGATIVE − LEG	TEMP. RANGE	LIMITS OF ERROR RANGE (°F)	LIMITS OF ERROR STANDARD	LIMITS OF ERROR SPECIAL	APPLICATION INFORMATION
TYPE J	IRON (magnetic) WHITE +	CONSTANTAN RED −	32 to 1400°F (0 to 760°C)	0 to 530 530 to 1400	±4°F ±0.75%	+2°F ±.4%	Suitable for vacuum, reducing, or inert atmospheres. Reduced life in oxidizing atmosphere. Iron oxidizes rapidly above 1000°F (538°C) so only heavy gauge wire is recommended for high temperature. Bare elements should not be exposed to sulfurous atmospheres above 1000°F (538°C).
TYPE K	CHROMEL YELLOW +	ALUMEL (magnetic) RED −	32 to 2300°F (0 to 1260°C)	0 to 530 530 to 2300	±4°F ±0.75%	±2°F ±.4%	Recommended for continuous oxidizing or neutral atmospheres. Mostly used above 1000°F (530°C). Subject to failure if exposed to sulfur. Preferential oxidation of chromium in positive leg at certain low oxygen concentrations causes "green rot" and large negative calibration drifts most serious in the 1500-1900°F range.
TYPE T	COPPER BLUE +	CONSTANTAN RED −	-300 to 700°F (-184 to +371°C)	-75 to 200 200 to 700	±1 1/2% ±0.75%	±.4% ±.4%	Useable in oxidizing, reducing, or inert atmospheres, as well as vacuum. Not subject to corrosion in moist atmospheres.
TYPE E	CHROMEL PURPLE +	CONSTANTAN RED −	32 to 1600°F (0 to 871°C)	0 to 600 600 to 1600	±3°F ±0.5%		Recommended for continuously oxidizing or inert atmospheres. Highest thermoelectric output of common calibration.
TYPE S	PLATINUM-10% Rhodium +	PLATINUM −	1000 to 2700°F (538 to 1482°C)	0 to 1000 1000 to 2700	±3°F ±0.25%	±1 1/2°F ±.1%	Recommended for high temperature. Must be protected with non-metallic protection tube and ceramic insulators. Continued high temperature usage causes grain growth which can lead to mechanical failure. Negative calibration drift caused by rhodium diffusion to pure leg as well as from rhodium volatilization.
TYPE R	PLATINUM-13% Rhodium +	PLATINUM −					
TYPE B	PLATINUM-30% Rhodium +	PLATINUM 6% Rhodium −	1600 to 3100°F (871 to 1705°C)	1000 to 3100	±0.5%		Same as S & R but output is lower. Also less susceptible to grain growth and drift.
TYPE N	NICROSIL +	NISIL (magnetic) −	32 to 2282°F (0 to 1250°C)	32 to 530 530 to 2300	±4°F ±0.75%	±2°F ±0.4%	Nicrosil/Nisil nickel-based thermocouple alloy used primarily at high temperature (up to 2300°F). While not a direct replacement for Type K, Type N provides better resistance to oxidation at high temperature and longer life in applications where sulfur is present.
TYPE C	TUNGSTEN 5% Rhenium +	TUNGSTEN 26% Rhenium −	32 to 4200°F (0 to 2330°C)	32 to 800 800 to 4200	±8°F ±1.0%		This refractory metal thermocouple may be used at temperatures up to 4200°F (2315°C). As it has no oxidation resistance its use is restricted to vacuum, hydrogen or inert atmospheres.

Most common and highly recommended used sensors Temperature chart

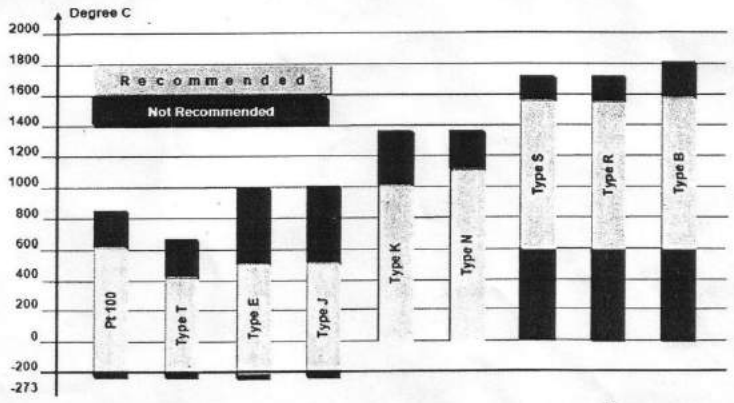

APPENDIX C

MIKI PULLEY'S DATA AND SPECIFICATION

PDS-□ BELT UNIT

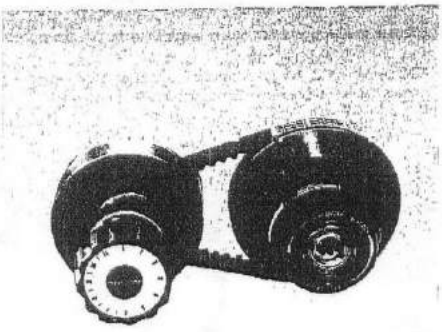

Large speed change ratio
Two types of speed change pulleys (types AK and PE) are combined to obtain a large speed change ratio.

One-touch speed change operation
A detent is contained for easy speed change operation. Rotate the handle clockwise to obtain a low speed, counterclockwise a high speed.

Easy-to-read handle scale
Read the scale indicated by the indicator needle as a main scale and the rotating dial on the handle as a vernier.

Specification

Model			PDS-02	PDS-04	PDS-07	PDS-15	PDS-22	PDS-37
Motor [kW] (4P)			0.2	0.4	0.75	1.5	2.2	3.7
Speed Change Ratio			1:4	1:3.5	1:4	1:4	1:4.5	1:3
Output Rotation Speed (r/min)	50Hz		500~2000	720~2520	600~2400	500~2000	500~2250	780~2350
	60Hz		600~2400	870~3060	720~2880	600~2400	600~2700	940~2820
Speed Change Drive	Motor	Model	AK-90	AK-124	AK-140	AK-155	AK-185	AK-215
		Mass [kg]	1.3	2.4	2.8	3.7	5.4	6.9
	Machine	Model	PE-106	PE-124	PE-156	PE-186	PE-216	PE-216
		Mass [kg]	1.6	2.2	4.0	6.0	10	10

※Use at an input rotation speed 1800r/min or less.
※The output rotation speed is that when a 3-phase, 4-pole motor is installed.
※Consult Miki Pulley or its agent in your country if the motor capacity is 5.5kw or higher.

Ordering Information: Specify PDS-□-□
Model
Option
No mark: Standard
SD : Indicator of Handle Rotation Speed
TH : With square bore bushing for adjustment in machine stoppage

Belt No. and Center distance between shafts

Model	PDS-02	PDS-04	PDS-07	PDS-15	PDS-22	PDS-37
Center Distance	163	200	172	182	230	247
Belt No.	1022V 220	1422V 270	1422V 270	1822V 296	2322V 364	2322V 396
Center Distance	172	242	214	211	275	279
Belt No.	1022V 223	1422V 300	1422V 300	1822V 331	2322V 396	2322V 421
Center Distance	200	278	252	235	304	304
Belt No.	1022V 247	1422V 330	1422V 330	1822V 338	2322V 421	2322V 441

※The center distance is Dimension C in the design type diagram shown on the right page.

APPENDIX D

CALCULATION OF PRE-EXPERIMENT DATA

Properties of Ultimate analysis (% by mass)

Constituent		Combustion Equations	Oxygen required per kg of palm shell	Product per kg of palm shell
C	0.5794	C + O2 ----> CO2		
		12 kg + 32 kg ----> 44kg	1.5451	2.1244667
H	0.0565	2H2 + O2 ---> 2H2O		
		4 kg + 32 kg ---> 36 kg	0.4520	0.5085
O	0.3138	-	-0.3138	-
N	0.0065	2N + O2 ---> 2NO		
		28 kg + 32 kg ---> 60 kg	0.007428571	0.0065
S	0.0006	S + O2 ---> SO2		
		32 kg + 32 kg ---> 64 kg	0.0006	-
Total			1.6913	

Air contain oxygen by mass (assumption)	23.30%	
Mini. Air required for complete combustion of 1 kg of palm shell (kg)	7.2588	
Air fuel ratio (AFR) stoichiometric	7.2588	(kg air/kg palm shell)

Untuk putaran miki pulley 1 (fuel feed rate 87.9kg/min)

ffr, kg/min	AFR stoic	afr, kg/min	air dencity, kg/m3	AFR, LPM	EA	EA+1	udara prima, LPM	udara prima, m3/s	udara prima, m/s	udara prima, CFM
0.0879	7.2588	0.6380	1.15	554.823	0%	100%	554.823	0.009	4.912	19.594
				554.823	20%	120%	665.788	0.011	5.894	23.512
				554.823	40%	140%	776.752	0.013	6.876	27.431
				554.823	60%	160%	887.717	0.015	7.858	31.350

EA	Primary Air (LPM) : Secondary Air (LPM)									
	100%	0%	90%	10%	80%	20%	70%	30%	60%	40%
0%	554.823	0	499.341	55.482	443.858	110.965	388.376	166.447	332.894	221.929
20%	665.788	0	599.209	66.579	532.630	133.158	466.051	199.736	399.473	266.315
40%	776.752	0	699.077	77.675	621.402	155.350	543.727	233.026	466.051	310.701
60%	887.717	0	798.945	88.772	710.174	177.543	621.402	266.315	532.630	355.087

Untuk putaran miki pulley2(fuel feed rate 98.5kg/min)

ffr, kg/min	AFR stoic	afr, kg/min	air dencity, kg/m3	AFR, LPM	EA	EA+1	udara prima, LPM	udara prima, m3/s	udara prima, m/s	udara prima, CFM
0.0985	7.2588	0.7150	1.15	621.730	0%	100%	621.730	0.010	5.504	21.956
				621.730	20%	120%	746.076	0.012	6.605	26.348
				621.730	40%	140%	870.422	0.015	7.705	30.739
				621.730	60%	160%	994.768	0.017	8.806	35.130

EA	Primary Air (LPM) : Secondary Air (LPM)									
	100%	0%	90%	10%	80%	20%	70%	30%	60%	40%
0%	621.730	0	559.557	62.173	497.384	124.346	435.211	186.519	373.038	248.692
20%	746.076	0	671.469	74.608	596.861	149.215	522.253	223.823	447.646	298.430
40%	870.422	0	783.380	87.042	696.338	174.084	609.296	261.127	522.253	348.169
60%	994.768	0	895.291	99.477	795.815	198.954	696.338	298.430	596.861	397.907

APPENDIX E

bp_drag.c

```
/* This is a routine for customizing default Syamlal drag law in Fluent 6.
   The default drag law uses 0.8 (for void<=0.85) and 2.65 (void>0.85) for
   bfac. This is for a min fluid vel of 25 cm/s. The current drag law has been
   tuned for a min fluid vel of 8 cm/s and uses 0.28 and 9.07 for these
   parameters. */

#include "udf.h"
#include "sg_mphase.h"

# define pi 4.*atan(1.)
#define diam2 3.e-4

DEFINE_EXCHANGE_PROPERTY(custom_drag_syam, cell, mix_thread, s_col,
f_col)
{
 Thread *thread_g, *thread_s;
 real x_vel_g, x_vel_s, y_vel_g, y_vel_s, abs_v, slip_x, slip_y,
      rho_g, rho_s, mu_g, reyp, afac,
      bfac, void_g, vfac, fdrgs, taup, k_g_s;

 /* find the threads for the gas (primary) and solids (secondary phases).
These phases appear in columns 2 and 1 in the Interphase panel respectively*/

 thread_g = THREAD_SUB_THREAD(mix_thread, s_col);/*gas phase*/
 thread_s = THREAD_SUB_THREAD(mix_thread, f_col);/* solid phase*/
```

```
/* find phase velocities and properties*/

x_vel_g = C_U(cell, thread_g);
y_vel_g = C_V(cell, thread_g);

x_vel_s = C_U(cell, thread_s);
y_vel_s = C_V(cell, thread_s);

slip_x = x_vel_g - x_vel_s;
slip_y = y_vel_g - y_vel_s;

rho_g = C_R(cell, thread_g);
rho_s = C_R(cell, thread_s);

mu_g = C_MU_L(cell, thread_g);

/*compute slip*/
abs_v = sqrt(slip_x*slip_x + slip_y*slip_y);

/*compute reynolds number*/

reyp = rho_g*abs_v*diam2/mu_g;

/* compute particle relaxation time */

taup = rho_s*diam2*diam2/18./mu_g;

void_g = C_VOF(cell, thread_g);/* gas vol frac*/

/*compute drag and return drag coeff, k_g_s*/

afac = pow(void_g,4.14);
```

```
if(void_g<=0.85)
 bfac = 0.281632*pow(void_g, 1.28);
else
 bfac = pow(void_g, 9.076960);

vfac = 0.5*(afac-0.06*reyp+sqrt(0.0036*reyp*reyp+0.12*reyp*(2.*bfac-
          afac)+afac*afac));
fdrgs = void_g*(pow((0.63*sqrt(reyp)/vfac+4.8*sqrt(vfac)/vfac),2))/24.0;

k_g_s = (1.-void_g)*rho_s*fdrgs/taup;

return k_g_s;

}

DEFINE_EXCHANGE_PROPERTY(custom_drag_ihme, cell, mix_thread, s_col,
f_col)

{

 Thread *thread_g, *thread_s;
 real x_vel_g, x_vel_s, y_vel_g, y_vel_s, abs_v, slip_x, slip_y,
     rho_g, rho_s, mu_g, reyp, cd, eg,
     void_g, k_g_s;

 /* find the threads for the gas (primary) and solids (secondary phases).
These phases appear in columns 2 and 1 in the Interphase panel respectively*/

 thread_g = THREAD_SUB_THREAD(mix_thread, s_col);/*gas phase*/
 thread_s = THREAD_SUB_THREAD(mix_thread, f_col);/* solid phase*/

 /* find phase velocities and properties*/

 x_vel_g = C_U(cell, thread_g);
```

```
y_vel_g = C_V(cell, thread_g);

x_vel_s = C_U(cell, thread_s);
y_vel_s = C_V(cell, thread_s);

slip_x = x_vel_g - x_vel_s;
slip_y = y_vel_g - y_vel_s;

rho_g = C_R(cell, thread_g);
rho_s = C_R(cell, thread_s);

mu_g = C_MU_L(cell, thread_g);

/*compute slip*/
abs_v = sqrt(slip_x*slip_x + slip_y*slip_y);

/*compute reynolds number*/

reyp = rho_g*abs_v*diam2/mu_g;

cd = (24./(reyp+SMALL)) + 5.48*pow((reyp+SMALL),-0.573) + 0.36;

void_g = C_VOF(cell, thread_g);/* gas vol frac*/

eg = pow(void_g,-2.65);

k_g_s = (3./4.)*(cd*(1.-void_g)*abs_v*rho_g*eg)/diam2;

return k_g_s;

}
```